POLITECNICO DI TORINO

Collegio di Ingegneria Chimica e dei Materiali

Corso di Laurea Magistrale

in Ingegneria Chimica e dei Processi Sostenibili

Tesi di Laurea Magistrale

3D printing of polymeric composites with cellulose micro-fibrils

Relatore/i

Prof. Roberta Bongiovanni

Ing. Davide Beneventi

Ing. Sara Dalle Vacche

Ing. Alessandra Vitale

firma del relatore (dei relatori)

Candidato

Giulia Iannello

firma del candidato

Ottobre 2020

Sommario

Questa tesi di laurea magistrale scaturisce da un'attività sperimentale di ricerca interamente svolta presso i laboratori dell'Institute Politecnique di Grenoble (INP – Pagora, LG2P). La sua stesura è stata pertanto eseguita in lingua inglese.

Lo scopo del lavoro è la produzione e caratterizzazione di un bio-composito costituito da una resina termoindurente a base di alcol poli-furfurilico (PFA), con agente di rinforzo a base di cellulosa, ovvero micro-fibrille di canapa (MFC). La matrice polimerica di PFA è il risultato della polimerizzazione dell'alcool furfurilico (FA), che può essere ottenuto dal furfurale, un'aldeide derivata dall'idrolisi degli zuccheri pentosi contenuti nelle fonti ricche di emicellulosa, ad esempio i residui agricoli di canna da zucchero e mais (Guigo et al. , 2010). Il ciclo produttivo della matrice polimerica è presentato in Figura 1.

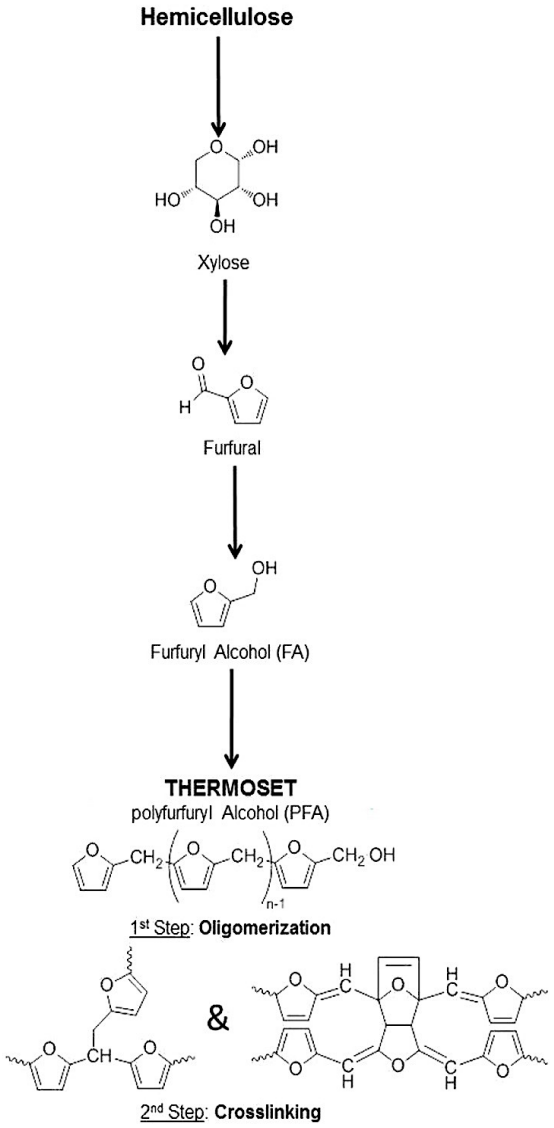

Figura 1: Dall'emicellulosa ad una resina solida (immagine originale tratta da Pin et al. (2014) modificata e adattata per lo scopo di questo lavoro; ogni altro permesso dovrebbe essere diretto da ACS).

Il PFA possiede ottime proprietà, essendo termicamente resistente e chimicamente resistente alla corrosione e ai solventi (Machado et al., 2016); il suo difetto principale risiede nelle scarse proprietà meccaniche che presenta (modulo di Young sui 2 GPa (Deka et al., 2013; Linganiso et al., 2014)), motivo per cui risulta interessante la possibilità di rinforzare la matrice (Pin et al., 2014).

Le micro-fibrille di cellulosa sono descritte come un filamento altamente cristallino di cellulosa con spessore di 2-10 nm e lunghezza di decine di micrometri, circondato da una parte amorfa (emicellulosa, lignina) che lo separa dalle altre (Siqueira et al., 2010). Le micro-fibrille sono presenti all'interno delle fibre delle piante vegetali e possono essere estratte con trattamenti meccanici di "fibrillazione", che "aprono" sostanzialmente le fibre di partenza (Fig. 2). L'interesse per l'MFC nasce dalle notevoli proprietà meccaniche che caratterizzano le micro-fibrille, le quali possiedono una superficie specifica di gran lunga superiore alle fibre originali e di conseguenza anche un maggior numero di gruppi idrossilici (che sono disposti proprio sulla superficie esterna): il fatto di poter formare più legami idrogeno tra di loro rispetto alle macro-fibre, unito all'alto grado di cristallinità, fa sì che la resistenza dei materiali rinforzati con le micro-fibrille di cellulosa possa aumentare in modo significativo (Berto and Arantes, 2019; Ho et al., 2015).

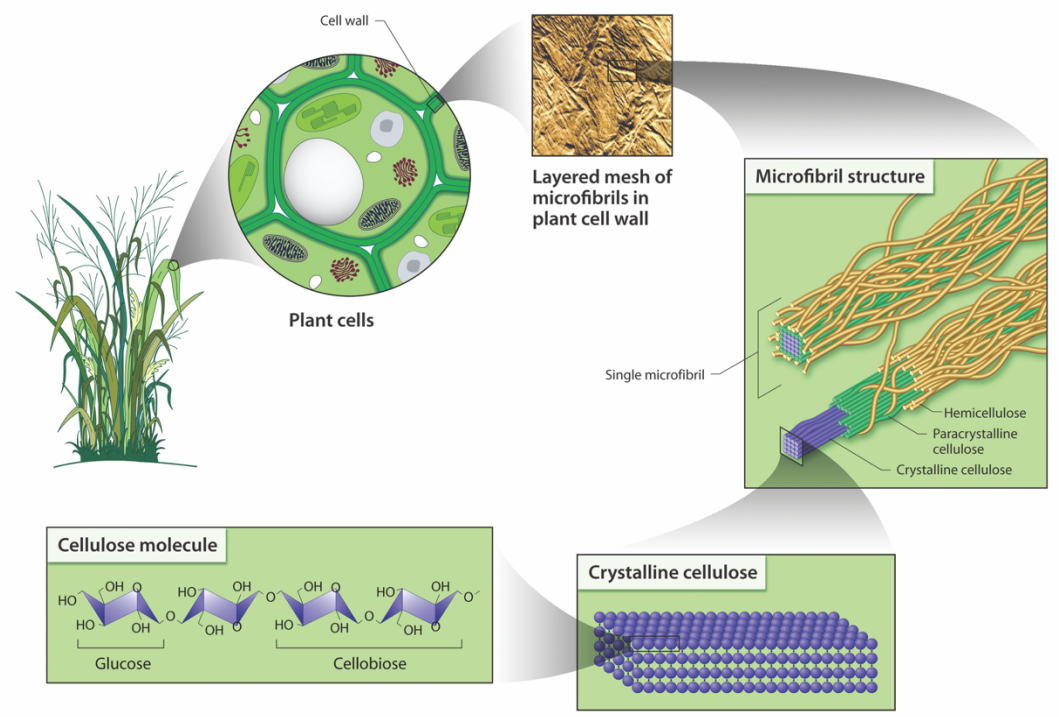

Figura 2: La struttura delle microfibrille all'interno delle piante vegetali (riprodotta da US DOE. 2005. Genomics:GTL Roadmap, DOE/SC-0090, U.S. Department of Energy Office of Science. (p. 204), website: https://genomicscience.energy.gov.)

L'uso della resina PFA come matrice e dell'MFC come filler/rinforzo consente di ottenere un composito definibile 100% bio-based.

Il composito è utilizzato per la produzione di un oggetto tridimensionale tramite stampa 3D.

La scelta della stampa 3D è giustificata dai numerosi vantaggi che stanno rendendo questa tecnologia sempre più popolare negli ultimi anni. Il processo consente di fabbricare oggetti direttamente da un modello virtuale tridimensionale, attraverso la deposizione della materia strato per strato. Questo metodo offre un alto livello di automazione e riproducibilità, inoltre garantisce un'elevata accuratezza, per cui è possibile produrre strutture di elevata complessità con ottima definizione e in modo relativamente rapido, evitando inoltre sprechi di materiale connessi all'uso di stampi che avrebbero impatto negativo sui costi di produzione (Wang et al., 2018).

Le MFC modificano il comportamento reologico della resina, che, senza l'aggiunta di un altro componente, sarebbe inutilizzabile nel processo di stampa 3D. Infatti, la stampa 3D effettuata attraverso l'estrusione e deposizione di una pasta o inchiostro (processo "Direct Ink Writing" (DIW)) richiede che questi abbiano due caratteristiche fondamentali: un comportamento pseudoplastico, che garantisce una buona estrudibilità attraverso un ugello, e una viscosità intrinseca (a riposo) abbastanza elevata da consentire agli strati stampati di mantenere la propria struttura (Wang et al., 2018; Xu et al., 2018).

Nonostante l'utilizzo dell'MFC come rinforzo di matrici polimeriche sia davvero promettente, ciò è limitato dall'elevato consumo di energia che richiedono i processi di produzione comunemente utilizzati (Rol et al., 2017).

Per questo motivo, un obiettivo secondario di questo lavoro è la produzione di MFC tramite il processo di estrusione bi-vite, già recentemente testato da Rol et al. (2017) per la fibrillazione di polpa di eucalipto. L'estrusione associata a un trattamento enzimatico di raffinazione, ha dimostrato di consumare fino al 63% in meno di energia rispetto ad uno dei metodi di estrazione più comuni che prevede l'uso di una macina (grinder). Inoltre l'estrusione permette di lavorare a concentrazioni più elevate di solido rispetto al suddetto metodo, il che è molto interessante dal punto di vista industriale, poiché riduce di conseguenza i costi di trasporto e recupero del prodotto (Ho et al., 2015). Ciò è ancor più rilevante nella prospettiva di incorporare l'MFC nel PFA, essendo la resina non totalmente idrofila (Pranger e Tannenbaum, 2008).

Infine, l'uso della canapa come fibra vegetale di partenza risulta interessante non solo per la sostenibilità della coltivazione di questa pianta (Pacaphol and Aht-Ong, 2017), ma anche per l'ottima resistenza delle sue fibre. Esse possiedono un grado di cristallinità superiore a quello di piante simili (e pur di produzione sostenibile) come il lino (Alila et al., 2013), contenendo infatti tra il 55% e l'80% del componente cristallino, la cellulosa, e minor quantità di emicellulosa e lignina, che costituiscono invece la parte amorfa delle fibre (Marrot et al., 2013). Il modulo di Young della cellulosa è difatti circa 30 volte quello degli altri due componenti e ciò sicuramente ha influenza sulle buone proprietà meccaniche proprie della fibra di canapa.

1. Produzione dell'MFC

Per la prima parte del lavoro, concernente la produzione di MFC, è stata utilizzata della polpa di canapa sbiancata e pre-raffinata (contenuto medio di acqua: 8% wt). Prima della fase di fibrillazione vera e propria, questa è stata sottoposta ad un pre-trattamento in due steps:

- Preparazione di una sospensione al 2% wt di polpa in acqua, ridotta in piccoli pezzi grazie all'utilizzo di un pulper; successiva raffinazione della polpa fino ad un grado Schopper-Reigler di 80 tramite l'utilizzo di un raffinatore di tipo "Valley Beater" (22 L);

- Idrolisi enzimatica della sospensione raffinata (sempre al 2% wt) a T=50°C e pH=5 in reattore batch incamiciato da 15 L, grazie all'aggiunta di endoglucanasi (e soluzione buffer).

Affinché potesse essere processata nell'estrusore, la sospensione è stata poi concentrata tramite centrifugazione a 10000 rpm per 10-15 min, trattamento che l'ha portata al 30% wt circa.

L'estrusione è stata condotta in un estrusore bi-vite (Twin-Screw Extruder, TSE) con camera cilindrica di 16 mm di diametro e un rapporto lunghezza/diametro (L/D) di 45, testando due diversi profili di estrusione delle viti con due diversi gradi di aggressività (Fig. 3 e 4).

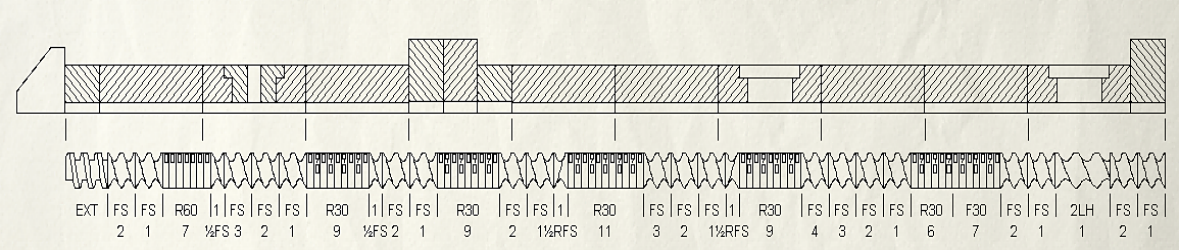

Figura 3: Profilo di estrusione A, 6 zone di taglio.

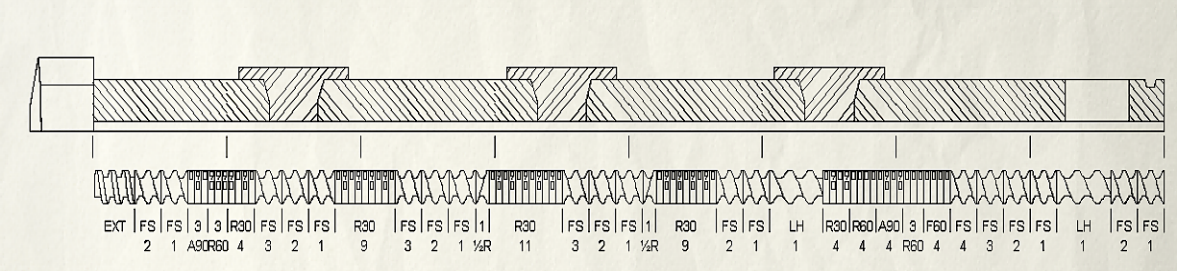

Figura 4: Profilo di estrusione B, meno aggressivo, 5 zone di taglio.

Tre diversi batch di polpa pre-trattata sono stati sottoposti ad estrusione (vedi Tab. 1), imponendo una certa velocità di rotazione delle viti e misurando il momento richiesto per estrudere la relativa polpa. I due parametri sono collegati: una velocità di rotazione più alta permette di abbassare il valore del momento richiesto, il quale comunque aumenta all'aumentare della concentrazione della polpa. Pertanto, per ogni batch di polpa, si è cercato un valore di velocità tale da garantire un momento non superiore agli 80 Nm e tale velocità è stata mantenuta costante per tutta l'estrusione.

I valori dei parametri di processo utilizzati sono riportati in Tab. 1, insieme al consumo specifico di energia su peso secco di MFC prodotta (SME_D) calcolato, per ogni estrusione eseguita, con la formula 1:

$$SME_D = \frac{n \cdot T \cdot P_{max}}{Q_D \cdot n_{max} \cdot T_{max}} \quad (1)$$

in cui T è il momento misurato dal software del TSE (in Nm), T_{max} è il massimo momento esercitabile (130 Nm), n è la velocità di rotazione imposta alle viti (rpm), n_{max} è la

massima velocità di rotazione applicabile alle viti (1100 rpm), P_{max} è la potenza del motore (7 kW) e Q_D è la portata di MFC prodotta (peso secco, in kg/h).

Tabella 1: Parametri chiave del processo di estrusione; i dati sono forniti per ogni estrusione eseguita.

	35% - 1p (A)	**29,2% - 1p (B)**	**29,2% - 2p (B)**	**32,5% - 1p (B)**	**32,5% - 2p (B)**
n (rpm)	1000	700	700	700	700
$T_{average}$ (Nm)	78	70	70	75	78
Q_D (Kg/h)	0,11	0,41	0,86	0,44	0,44
SME_D (Kwh/Kg)	34,6	5,82	2,80	5,89	6,17
Tot SME_D (Kwh/Kg)			**8,62**		**12,06**
Dry content after extrusion	35 %	-	29,75 %	33,85%	34,5%

Il profilo A (Fig. 3, recentemente sviluppato da Rol et al. (2020) per polpa di eucalipto al 20% wt circa) si è rivelato essere troppo aggressivo ed inutilizzabile con polpa di canapa ad una concentrazione attorno al 30% wt, verificandosi sistematicamente il blocco del sistema per raggiungimento di un valore troppo alto (>100 Nm) del momento di rotazione richiesto per estrudere. Il profilo B invece (Fig. 4), sviluppato durante questa attività di ricerca, ha dato dei buoni risultati in termini di continuità e stabilità del processo, tanto che è stato possibile passare una seconda volta attraverso l'estrusore parte della polpa con l'intento di incrementarne il grado di fibrillazione (vedi Tab. 1, 32,5% - 2p (B)).

L'estrusione eseguita con il profilo B è stata soddisfacente anche dal punto di vista del consumo energetico (SME_D), il cui valore più alto è stato circa di 12 kWh per ogni kg (peso secco) di MFC, prodotta passando per due volte attraverso l'estrusore una polpa di canapa a concentrazione iniziale del 32,5% wt e finale del 34,5% wt. Nel caso del profilo A invece si è calcolato un consumo superiore a 34 kWh/kg per una polpa inizialmente concentrata al 35% wt (un solo passaggio attraverso l'estrusore).

Si è inoltre riscontrato che l'energia richiesta per l'estrusione si abbassa in modo significativo al diminuire della concentrazione della polpa in ingresso, poiché certamente, a parità di velocità di rotazione delle viti, il momento che è necessario applicare per mantenere tale velocità risulta minore (vedi Tab. 1). Occorre poi precisare che la comune fibrillazione tramite macina (grinder) richiede circa 15 kWh per kg (secco) di MFC, prodotta tra l'altro in forma di sospensione acquosa al 2% wt (Rol et al., 2017); il processo qui implementato permette dunque una minor spesa energetica, con in più il vantaggio di ottenere un prodotto molto più concentrato.

La temperatura, che tende a crescere durante l'estrusione, soprattutto in corrispondenza delle zone in cui la polpa viene sottoposta a più alto sforzo (shearing zones), è stata

mantenuta sotto controllo tramite circolazione di acqua fredda all'interno di una camicia che avvolge la camera cilindrica dell'estrusore. Nonostante l'imposizione di un set-point di 10°C, la temperatura ha raggiunto i 65°C nella parte centrale dell'estrusore, rivelando la non completa efficacia di questo sistema di raffreddamento (nelle condizioni operative applicate). Ad ogni modo, è possibile affermare che non si sia verificata alcuna degradazione della polpa, dato che questa non dovrebbe avvenire in modo significativo prima dei 200°C (Pacaphol and Aht-Ong, 2017). È importante comunque sottolineare che un ulteriore aumento di temperatura potrebbe causare un'eccessiva concentrazione del materiale con conseguente intasamento dell'apparato (Ho et al., 2015).

Varie analisi e test sono stati effettuati per valutare la qualità dell'MFC prodotta.

Preparando delle sospensioni acquose allo 0,5% wt, filtrandole sottovuoto e asciugando (sempre sottovuoto) a temperatura tra i 60 e gli 80 °C , è stato possibile realizzare dei film sia con l'MFC ("nanopapers", tipico risultato in Fig. 5) che con la polpa post trattamento enzimatico.

Si è registrato un aumento del tempo necessario alla filtrazione con il migliorare della qualità dell'MFC, essendo le micro-fibrille più idrofile delle fibre di partenza (maggior superficie specifica, maggior numero di -OH). Inoltre, la trasparenza di questi film (misurata tramite trasmittanza, vedi risultati in Tab. 3.4) è un buon indice del grado di fibrillazione del materiale poiché i nano-elementi non diffrangono la luce (Chinga-Carrasco, 2013; Rol et al., 2018); i nanopapers ottenuti con la polpa più concentrata passata due volte attraverso il profilo B sono risultati essere i più trasparenti.

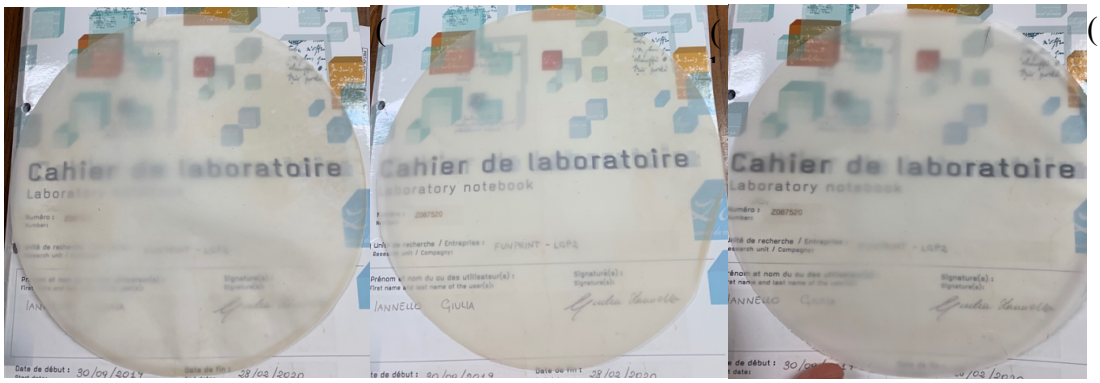

Figura 5: Nanopapers ottenuti dall'MFC prodotta utilizzando il profile di estrusione B – (a): 29,2% - 2p; (b): 32,5% - 1p; (c): 32,5% - 2p.

Le principali proprietà dei film prodotti sono raccolte in Tab. 2.

Tabella 2: Proprietà dei film prodotti.

	Ref-Enz	**35% - 1p (A)**	**29,2% - 2p (B)**	**32,5% - 1p (B)**	**32,5% - 2p (B)**
Transmittance (%)	0,61 ± 0,05	11,52 ± 0,14	4,62 ± 0,19	7,83 ± 0,18	12,3 ± 0,5
Grammage (g/mm^2)	64,8 ± 4,1	58,2 ± 0,7	67,7 ± 6,2	66,3 ± 0,4	70 ± 1
Thickness (µm)	96 ± 6	64 ± 4	76 ± 0,005	64 ± 3	72 ± 5
Young's Modulus (GPa)	4,44 ± 0,25	3,99 ± 1,1	5,87 ± 0,24	6,65 ± 0,24	?
Elongation at break (%)	0,77 ± 0,19	0,458 ± 0,07	0,61 ± 0,12	0,28 ± 0,07	?
Tensile strength (MPa)	19,8 ± 1,33	14 ± 2,3	29 ± 6,8	15,6 ± 2,94	?

Testando a trazione delle strisce ritagliate dai vari film (Fig. 2.9) è stato possibile stimare le proprietà meccaniche dell'MFC prodotta, confrontandole con quelle della polpa post trattamento enzimatico. Si è notato che il modulo di Young dei film prodotti con l'MFC (usando il profilo B) è in generale più alto rispetto a quello dei film prodotti con la polpa pre-estrusione. Inoltre, i nanopapers ottenuti da polpa inizialmente più concentrata passata una sola volta attraverso l'estrusore sono più rigidi e resistenti rispetto a quelli ottenuti passando due volte una polpa inizialmente meno concentrata (Tab. 2, Fig. 3.6).

Le MFC che si è riusciti a produrre con il profilo A sono l'unico materiale a presentare un modulo elastico addirittura inferiore a quello della polpa non estrusa, nonostante la buona trasmittanza del relativo nanopaper (Tab. 2).

Dalla misura della torbidità di sospensioni acquose allo 0,1 % wt di MFC, accoppiate all'analisi morfologica tramite apparato MorFi®, si sono ricavate ulteriori informazioni sulla quantità di fibre residue e di conseguenza sul grado di fibrillazione (Tab. 3.5, 3.6).

Le sospensioni a maggior presenza di fibre sono infatti più torbide: i valori di torbidità ottenuti rispecchiano i diversi gradi di qualità dell'MFC prodotta già suggeriti dalle caratterizzazioni dei nanopaper. Così come la trasmittanza, anche la torbidità dell'MFC ottenuta con il profilo A dimostra un buon grado di fibrillazione; dalle analisi dell'indice di cristallinità (CI) (Tab. 3.3) si evince che le scarse proprietà meccaniche di questa MFC dipendono dunque dall'eccessiva aggressività del profilo di estrusione, che, accoppiato ad una concentrazione iniziale della polpa del 35% wt, ha ridotto di più del 22% il CI della canapa trattata enzimaticamente.

Dal confronto con una polpa di eucalipto sottoposta agli stessi processi (Tab. 3.3) si nota come la canapa abbia un CI iniziale maggiore, il quale cresce ancor di più dopo il trattamento enzimatico con endoglucanasi (che attaccano la parte amorfa delle fibre);

l'MFC di canapa dovrebbe di conseguenza avere proprietà meccaniche superiori rispetto a quella di eucalipto. Tuttavia, il modulo di Young ottenuto da Rol et al. (2020) per un MFC di eucalipto prodotta (al 20% wt) usando il profilo A risulta essere superiore a quello dell'MFC di canapa di questo lavoro: se ne deduce che non si è ancora raggiunto lo stesso grado di fibrillazione conseguito dai suddetti autori.

L'analisi morfologica effettuata sull'MFC prodotta con il profilo B ha dimostrato come l'MFC con le migliori proprietà (32,5% - 2p, Tab. 2) contenga il minor numero di fibre residue e il maggior numero di "fini", elementi fibrosi del diametro massimo di 76 μm che si generano durante i vari processi di raffinazione della polpa (Fischer et al., 2017; Odabas et al., 2016). I fini, pur non essendo micro-fibrille (la risoluzione del MorFi® non è sufficiente a rilevare quest'ultime), sono un buon indice del grado di lavorazione del prodotto; la loro presenza nell'MFC aumenta con il migliorare della qualità, così come, allo stesso tempo, la presenza di fibre residue diminuisce. Tutti i risultati della prova MorFi® sono illustrati in Tab. 3.6 e Fig. 3.7.

Diverse immagini (Fig. 3.8, 3.11) sono state scattate al microscopio ottico al fine di mostrare l'effetto dei pre-trattamenti e della fibrillazione sulla morfologia delle fibre, nonché di confrontare le varie MFC prodotte anche dal punto di vista visivo. Il risultato dell'analisi al microscopio è perfettamente in accordo con quanto già discusso, confermando oltretutto il buon grado di fibrillazione dell'MFC prodotta con il profilo A e dunque il fatto che le sue scarse proprietà meccaniche siano dovute all'eccessiva aggressività del profilo.

Si evince infine dai vari risultati che più passaggi della stessa polpa (stessa concentrazione iniziale) attraverso l'estrusore (profilo B) migliorano effettivamente la fibrillazione. Inoltre, a parità di numero di passaggi, la polpa inizialmente più concentrata risulta in un'MFC più fibrillata e quindi con migliori proprietà; ciò si spiega perché, come già fatto notare, la maggior concentrazione richiede un momento applicato più alto, che si traduce in una maggior energia trasferita alle fibre (oltre che consumata) per la loro fibrillazione (Rol et al., 2020).

3. Produzione del composito

Si è scelto di unire alla resina le MFC della miglior qualità ottenute, ovvero quelle prodotte a partire da una polpa a concentrazione del 32,5% wt, passandola due volte attraverso il profilo di estrusione B. Sono state preparate varie formulazioni a diversa percentuale (wt) di MFC, mantenendo costante e pari al 5 % wt il contenuto di catalizzatore ($C_2H_8N_2O_4$, necessario per il cross-linking finale) (Tab. 2.1).

Una prima miscelazione dei due componenti è stata effettuata utilizzando una planetaria alla sua massima potenza. Per rompere gli agglomerati di MFC e disperdere bene le micro-fibrille all'interno della resina è stato poi necessario un ulteriore step, diverso a seconda della % di MFC: fino al 20% wt l'utilizzo di un mixer Ultra-Turrax® ha dato dei buoni risultati, ma per la pasta al 25 e 35% wt si è dovuto utilizzare una macchina a tre rulli attraverso cui la pasta è stata fatta passare fino a 6 volte.

L'effetto di quest'ultimo processo di dispersione è stato esaminato sia ad occhio nudo che tramite ingranditore binoculare: in Fig. 6 e 3.13 è possibile notare come la dispersione degli agglomerati di MFC migliori gradualmente dopo diversi passaggi della pasta attraverso i rulli. La rottura degli agglomerati consente inoltre di liberare le micro-fibrille, che possono così formare un network dentro la resina grazie ai i propri gruppi idrossilici;

la conseguenza di ciò è un aumento significativo della viscosità della pasta, maggiore ovviamente per la formulazione a maggior contenuto di MFC (35% wt).

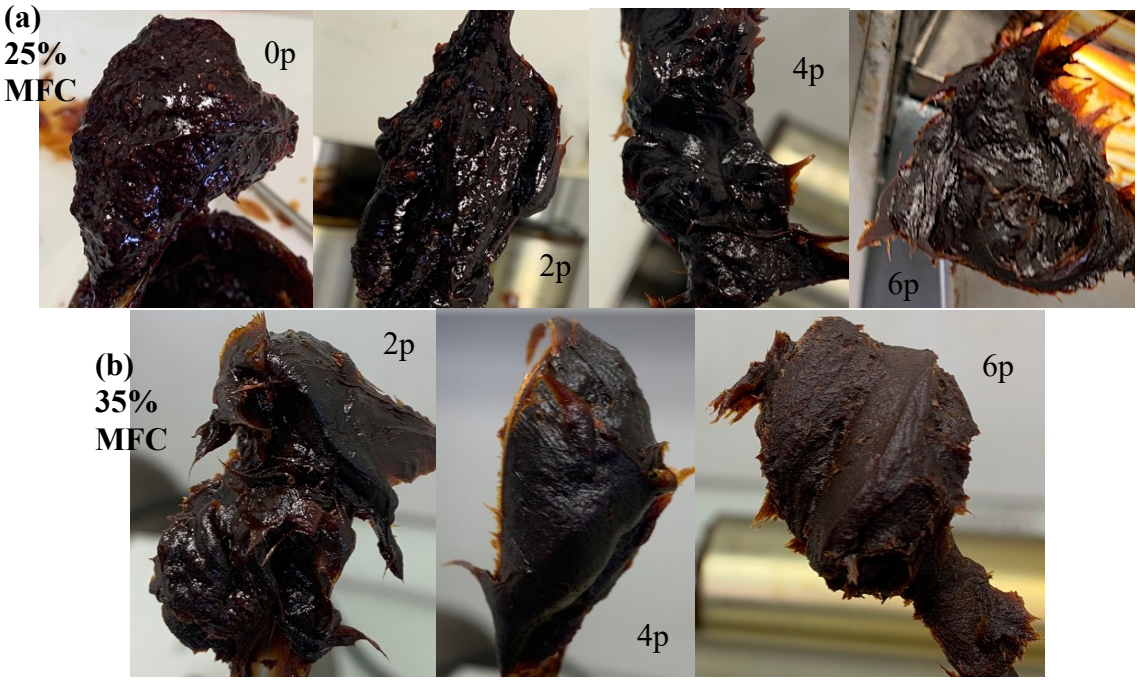

Figura 6: Aspetto ad occhio nudo delle due paste ad alta concentrazione di MFC dopo diversi numeri di passaggi attraverso la macchina a tre rulli.

Il comportamento reologico della pasta è stato poi esaminato tramite l'utilizzo di un reometro a piatti paralleli, confrontandolo con quello della resina pura. La viscosità dei campioni è stata misurata al variare del gradiente di velocità imposto, ed è stato applicato il modello della legge di potenza (Ostwald-de Waele, formula 3.2) ad ogni curva sperimentale trovata (Fig. 7): è stato possibile quindi evidenziare come il comportamento Newtoniano della resina diventi pseudoplastico quando anche solo il 5% wt dell'MFC prodotta viene aggiunto ad essa. Come auspicato, la pseudoplasticità della pasta composita si accentua all'aumentare della quantità di MFC dispersa al suo interno (indice di potenza n decrescente, Tab. 3.7) e il modello utilizzato diventa sempre più idoneo a descriverne il comportamento reologico (vedi valori R^2 tendenti all'unità, Fig. 7 e Tab. 3.7).

In Fig. 7 è anche possibile notare come effettivamente la viscosità a taglio zero aumenti al crescere del contenuto di MFC, e come essa venga perfettamente recuperata quando il gradiente di velocità viene riportato al valore di partenza.

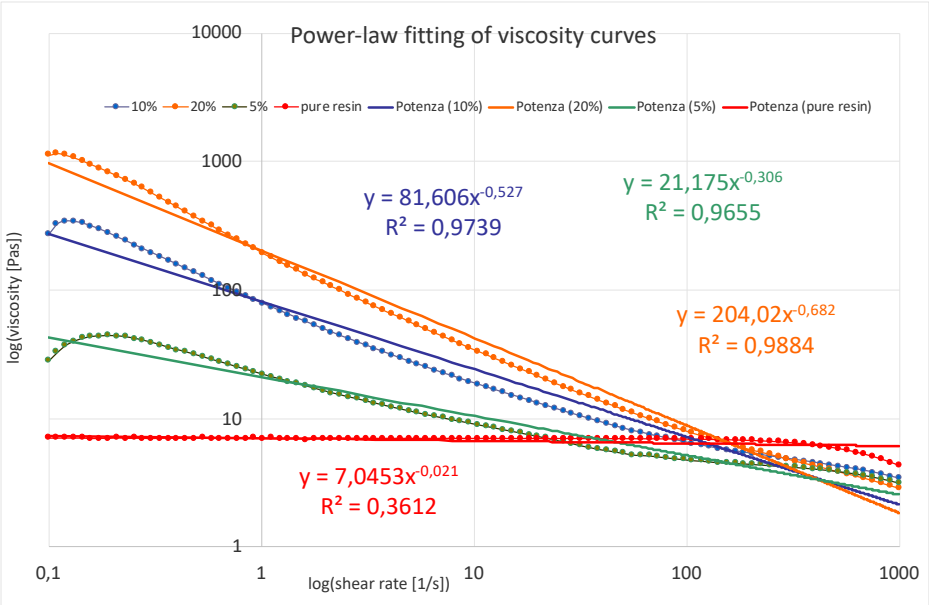

Figura 7: Comportamento reologico delle paste composite a diverse % wt di MFC: fitting tramite legge di potenza delle curve di viscosità.

Un particolare test reologico (Fig. 8) è stato effettuato proprio al fine di valutare la capacità di recupero della viscosità a taglio zero da parte delle due formulazioni più concentrate (25% e 35% MFC), imponendo e rimuovendo ciclicamente un gradiente di velocità di 500 s^{-1}. Tuttavia il test in questione, che aveva lo scopo di simulare l'estrusione della pasta attraverso l'ugello della stampante 3D, ha dato dei risultati poco affidabili: gli intervalli a gradiente di velocità costante si sono rivelati essere troppo brevi per consentire alla pasta di raggiungere un plateau di viscosità. Nondimeno, è stato dimostrato che l'applicazione di alti gradienti di velocità alle sospensioni di MFC può indurre una sorta di flocculazione delle micro-fibrille con formazione di clusters e parti vuote (cioè senza MFC) all'interno della matrice. Sia i fiocchi che i vuoti crescono all'aumentare del gradiente applicato fino a una dimensione massima, dopodiché i vuoti cominciano ad essere riempiti di nuovo (Schenker et al., 2018). Inoltre, non è da escludere che si sia verificata una separazione di fase in prossimità dei piatti del reometro, con la formazione di due zone costituite prevalentemente da PFA, fenomeno che potrebbe aver celato il reale comportamento della resina.

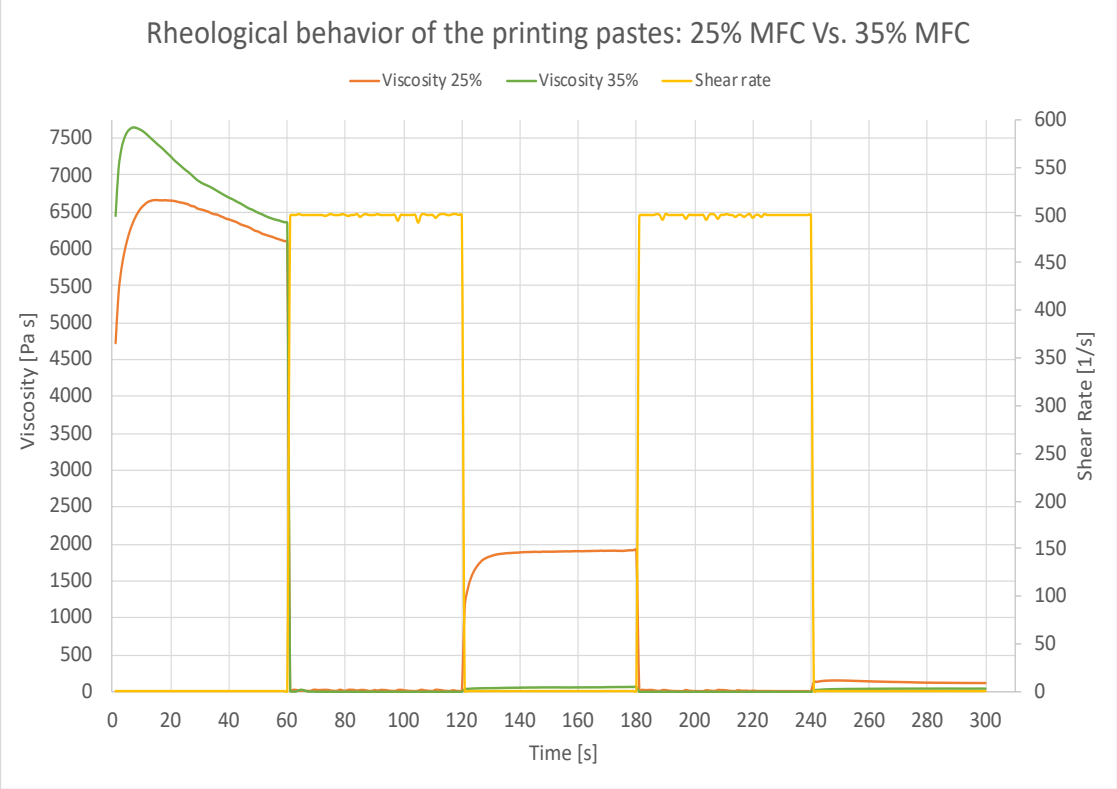

Figura 8: Test della capacità delle paste composite di recuperare la propria viscosità dopo essere state sottoposte ad uno sforzo di taglio.

È stata eseguita un'unica prova di stampa 3D utilizzando la formulazione con il più alto contenuto di MFC, 35% wt. È stato selezionato un ugello di 0,76 mm di diametro e la pasta è stata spinta attraverso una siringa ad esso collegato grazie ad una pressione pneumatica tra i 2 e i 4 bar. Il fatto che non si sia verificata alcuna ostruzione dell'ugello, suggerisce un buon grado di dispersione dell'MFC nella resina, con nessun agglomerato rimasto in grado di provocare il blocco dello strumento. La pasta si è rivelata essere stampabile, e non è stato riscontrato alcuna deformazione/rigonfiamento del singolo filamento estruso (Fig. 9), segno che la tensione di snervamento dello stesso non è stata raggiunta durante l'estrusione attraverso l'ugello. Il test è stato eseguito provando a stampare un cubo di 2 x 2 cm (Fig. 2.13, 2.14) con un infill del 100% e una velocità di stampa di 500 mm/min; strati di 0,5 mm sono stati stampati alternativamente in direzione orizzontale e verticale.

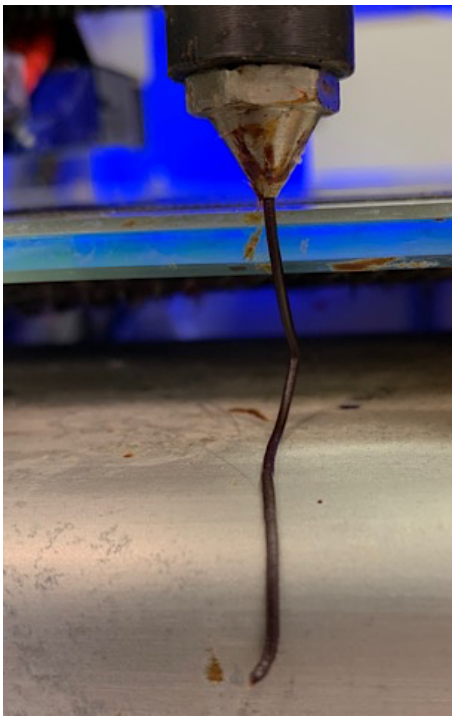

Figura 9: Stampa di un filamento di pasta contenente il 35% wt di MFC.

Durante la prova si è riscontrato come una pressione pneumatica di 4 bar abbia causato l'estrusione di un'eccessiva quantità di materiale, motivo per cui si nota che il cubo ottenuto non ha una forma ben definita, soprattutto guardando ai primi strati stampati (Fig. 10a). Tuttavia, diminuire la pressione fino a 2 bar, pur avendo migliorato l'aspetto degli ultimi strati, può essere stata la ragione della rottura del filamento verificatasi (Fig. 10b). Si rileva poi una non sufficiente distanza del piano di stampa dall'ugello: questo tocca i filamenti adiacenti a quello che sta stampando, schiacciando tra l'altro quest'ultimo sullo strato sottostante (Fig. 10). Inoltre, la velocità di stampa imposta può non essere stata sufficiente a consentire un buon assestamento dei filamenti estrusi e una buona aderenza con lo strato sottostante.

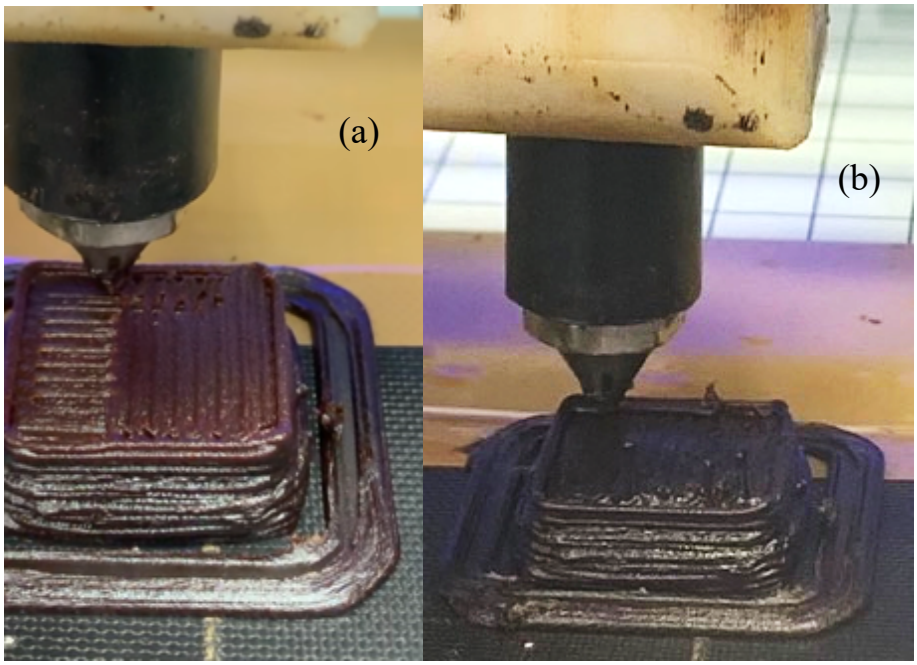

Figura 10: Stampa di un cubo di 2cm x 2cm, sono illustrate le problematiche principali: deformazione degli strati causata dall'ugello troppo vicino al piano di lavoro (a) e rottura di un filamento durante la stampa (b).

A causa di problemi logistici (chiusura laboratori per emergenza sanitaria Covid-19) non è stato possibile far avvenire la reticolazione dell'oggetto prodotto e quindi neanche testarne le proprietà meccaniche. Tuttavia, le prove di trazione eseguite sui nanopapers prodotti restituiscono dei valori di modulo elastico (Tab. 2) più alti rispetto ai 2 GPa riportati in letteratura per il PFA (Deka et al., 2013; Linganiso et al., 2014), per cui è ragionevole supporre che l'aggiunta di MFC alla resina produca un aumento del modulo di Young di quest'ultima. Oltretutto è da sottolineare il fatto che il modulo elastico delle singole micro-fibrille è in generale di gran lunga superiore a quello dei film che possono essere prodotti con essa, superando normalmente i 100 GPa (Biron, 2017; Iwamoto et al., 2009). Pertanto, per effettuare una predizione teorica del possibile modulo elastico del composito, occorrerebbe valutare tramite altre tecniche le proprietà meccaniche delle singole micro-fibrille prodotte (Iwamoto et al., 2009).

Ad ogni modo, la resistenza reale del composito potrebbe discostarsi da quella teorica: il grado raggiunto di dispersione dell'MFC nella resina potrebbe non essere effettivamente adeguato e potrebbe non esserci una sufficiente adesione interfacciale tra le micro-fibrille e la matrice. In quest'ultimo caso, il composito cederebbe all'interfaccia tra i due componenti, prima ancora che lo sforzo sia trasferito alle micro-fibrille. Infine bisogna considerare che l'estrusione attraverso l'ugello provoca un allineamento delle fibrille (Wang et al., 2018), per cui un'eventuale prova di trazione in direzione parallela alla loro orientazione fornirebbe una resistenza superiore rispetto a quella teorica (Ramamoorthy et al., 2019).

4. Conclusioni

Anche se non è stato possibile raggiungere l'obiettivo finale del lavoro (i.e. caratterizzazione meccanica del composito), diversi risultati sono stati conseguiti durante questo studio.

MFC di buona qualità ed altamente concentrate sono state ottenute tramite un processo innovativo e a basso consumo energetico; ciò costituisce un passo in avanti verso la produzione di cellulosa micro-fibrillata su scala industriale, che non si è ancora diffusa. Inoltre, l'uso della canapa come polpa vegetale di partenza è interessante non solo per le proprietà meccaniche che l'MFC da essa ottenuta può potenzialmente avere, ma anche sul piano della sostenibilità/costo della coltivazione di questa pianta.

Tuttavia, ulteriori studi sono necessari per valutare l'energia che bisogna fornire al tipo di polpa selezionata durante l'estrusione per avvicinarsi al massimo grado di fibrillazione senza danneggiare la cristallinità delle fibre. A tal proposito, sarebbe di grande utilità l'utilizzo di un software di simulazione che permetta di trovare il profilo delle viti di estrusione e i parametri di processo più adeguati per conseguire questo obiettivo con un solo passaggio della polpa attraverso l'estrusore. In questo modo, si spererebbe di ottenere l'MFC della miglior qualità possibile al tempo stesso incrementando la produttività e diminuendo la spesa energetica (che cresce ovviamente con più passaggi attraverso l'estrusore).

Sul piano della preparazione della pasta composita, nonostante il processo di dispersione tramite macchina a tre rulli abbia dato apparentemente dei buoni risultati, sarebbe interessante poter evitare questo ulteriore step iniettando direttamente la resina all'interno dell'estrusore. L'apparato utilizzato in questo lavoro permetterebbe infatti tale iniezione, che dovrebbe probabilmente essere effettuata vicino alla parte finale del profilo, in modo da non incidere sulla fibrillazione della polpa, ma da garantire una buona miscelazione dei due componenti.

La capacità della pasta di recuperare la propria viscosità quando lo sforzo di taglio viene rimosso dovrebbe essere testata diversamente da quanto fatto, allungando sicuramente gli intervalli in cui il gradiente di velocità viene mantenuto constante. Conoscere il tempo necessario alla pasta per ritornare alla viscosità a taglio zero sarebbe utile nel determinare la velocità di stampa più adeguata. Tuttavia, il fatto che i singoli filamenti stampati siano in grado di mantenere una propria forma, suggerisce che un buon valore di viscosità viene comunque recuperato dal filamento, dopo essere stato estruso attraverso l'ugello.

Nonostante siano ovviamente necessari più test di stampa per ottimizzare i parametri di processo che consentono di ottenere un oggetto 3D ben definito, la pasta composita prodotta si è rivelata essere stampabile e il grado di dispersione dell'MFC nella resina raggiunto sufficiente a non provocare l'ostruzione dell'ugello.

I risultati ottenuti finora suggeriscono che non vi sono ostacoli significativi per la produzione di un composito 100% bio-based costituito da PFA e MFC di canapa destinato alla stampa 3D.

Index

Introduction

One of the most urgent need in our society is the replacement of fossil resources, not only from an energetic point of view: most of the objects that we use every day are made of synthetic polymers which are basically derived from the oil industry. Each time we think about "plastics" we image plastic bottles and packaging, but there is a whole family of non-recyclable polymers which are the so called "thermosetting" that cannot be melted, and which could not be produced anymore when the world's oil reservoirs will be depleted. In this scenario, the production of bio-based polymers with properties similar to the petrol-based ones is becoming more and more important.

In the last years many "bio-composites" have been developed. Bio-composites are made of a polymer matrix containing wood or other natural fibers which have usually the aim of reinforcing. Bio-composites are being used for many applications, from music instruments to automotive and the demand is increasing quickly, so that they are entering new fields such as furniture's market or rigid packaging's (Partanen and Carus, 2019). This trend is well showed in Fig. 1.1, where the growth of the European production of bio-composites in the last years is evidenced and a prospective on the future is given (nova-Institut, 2019).

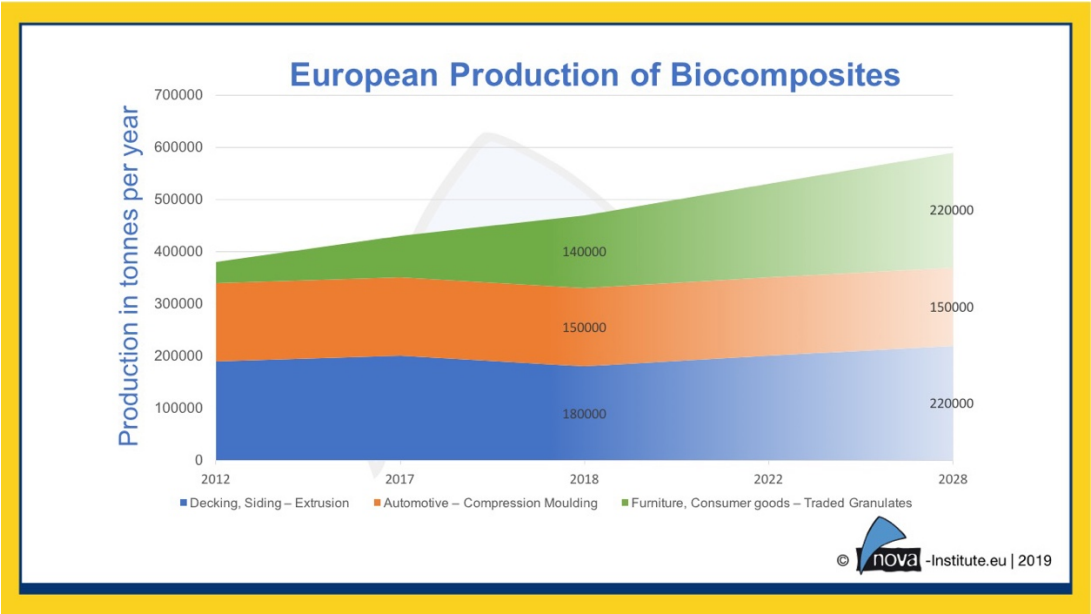

Figure 1.1: Growth of the European production of bio-composites among the last and future years (picture downloaded from the website: biobased.eu – original source: nova-Institut, (2019)).

The aim of this work is the production and characterization of a bio-composite, made of a poly-furfuryl alcohol (PFA) thermosetting resin filled and reinforced by hemp micro-fibrillated cellulose (MFC); the bio-composite is then transformed into a final object using 3D printing.

A PFA resin is the result of the polymerization of furfuryl alcohol (FA), which can be obtained from furfural, an aldehyde derived from the hydrolysis of the pentose sugars contained in hemicellulose rich sources like agricultural residues of sugarcane and corn

(Guigo et al., 2010). Using a PFA resin as matrix filled with cellulose lets us obtain a final composite which is 100% bio-based.

MFC consists of cellulose "microfibrils", fibrous cellulose structures with thickness of 2-10 nm and length of tens of micrometers (Siró and Plackett, 2010), which can be extracted from plant fibers through a mechanical treatment. MFC's use as filler, besides helping to obtain a proper rheological behavior for the paste used in 3D-printing, is expected to enhance the mechanical properties of the final composite, thanks to the microfibrils' strength and stiffness.

Despite MFC's application in polymer reinforcement is really promising, this is limited by the high energy demand required by the production process. For this reason, a secondary goal of this work is to use the innovative twin screw extrusion process already tested by Rol et al. (2017) for the production of MFC from eucalyptus pulp. This process, coupled with an enzymatic refining treatment, has been demonstrated to consume up to 63% less energy than the grinder's process. Moreover, the extrusion process allows to work at higher solid concentration, which is very interesting from the industrial point of view, reducing consequently the costs of transportation and recovery of the product (Ho et al., 2015). But this fact is even more valuable for the purpose of the present work, being the PFA resin not very hydrophilic (Pranger and Tannenbaum, 2008).

The choice of 3D-printing as the way to produce a final object is supported by the many advantages that are making this process become more and more popular in the recent years. In fact 3D-printing allows the fabrication of products directly from a 3D digital model and, thanks to the layer by layer deposition of matter, it is possible to reach an highly precise definition of shape and reproduce sophisticated geometries avoiding waste of material and so a negative impact on the costs of production (Wang et al., 2018).

It is necessary to clarify that the present work was carried out thanks to a collaboration between Politecnico di Torino (DISAT - Dipartimento di Scienza Applicata e Tecnologia) and Institut Polytechnique de Grenoble (INP Pagora - École international du papier, de la communication imprimée et des biomatériaux). The experimental part was entirely conducted in the laboratories of Grenoble INP (LGP2) during an internship gently founded by the host institution.

Because of the sanitary emergency caused by the pandemic of COVID-19, it was mandatory to stop all the experimental activities two months prior to the end of the internship. I therefore sincerely apologize for the missing data and the results of which the work is lacking, especially in its last part.

The thesis is divided into 4 chapters as follows:

- Chap. 1: the state of the art is provided analyzing some of the available studies that debate the same issues.
- Chap. 2: the experimental part of the work is showed, including the methods, materials and instrumentation used.
- Chap. 3: the main results obtained are presented and discussed.
- Chap. 4: the results are compared with the initial goals of the project and the methods used are discussed from a critical point of view. At the end, recommendations for future's studies of the same type are given.

For simplicity every chapter is divided into subchapters and sections.

1 Literature review

1.1 MFC - Micro-fibrillated cellulose

Cellulose's fibers have an ordered hierarchical structure , with larger units called "macro-fibrils" which hide inside their cell wall nano-sized elementary fibrils, so called "micro-fibrils". The process of "defibrillation" basically opens the original fibers letting the fibrils come out.

MFC consists of aggregates of microfibrils with diameters in the range of 10-100 nm and lengths in the scale of micrometers separated by less ordered regions (Alila et al., 2013; Kukle et al., 2013; Vartiainen et al., 2015); one of the most common names used to describe MFC in the literature is just "nanofibers" (Siró and Plackett, 2010). Each microfibril can be described as filaments of cellulose crystals linked one to the other by amorphous parts (Fig. 1.3) (Siqueira et al., 2010). The fibrils are characterized by a high surface area and aspect ratio and by an higher number of available -OH groups and so possibilities of forming hydrogen bonds then individual macro-fibers: this will result in higher mechanical properties such as Young's modulus and tensile strength and strain at break (Berto and Arantes, 2019; Ho et al., 2015). Moreover, the fibrils generally include more cellulose crystals within their structure then the original fibers, and this usually leads to higher elastic modulus (Kukle et al., 2013). For this reason, MFC is considered very promising as a biodegradable and sustainable reinforcement in composites materials.

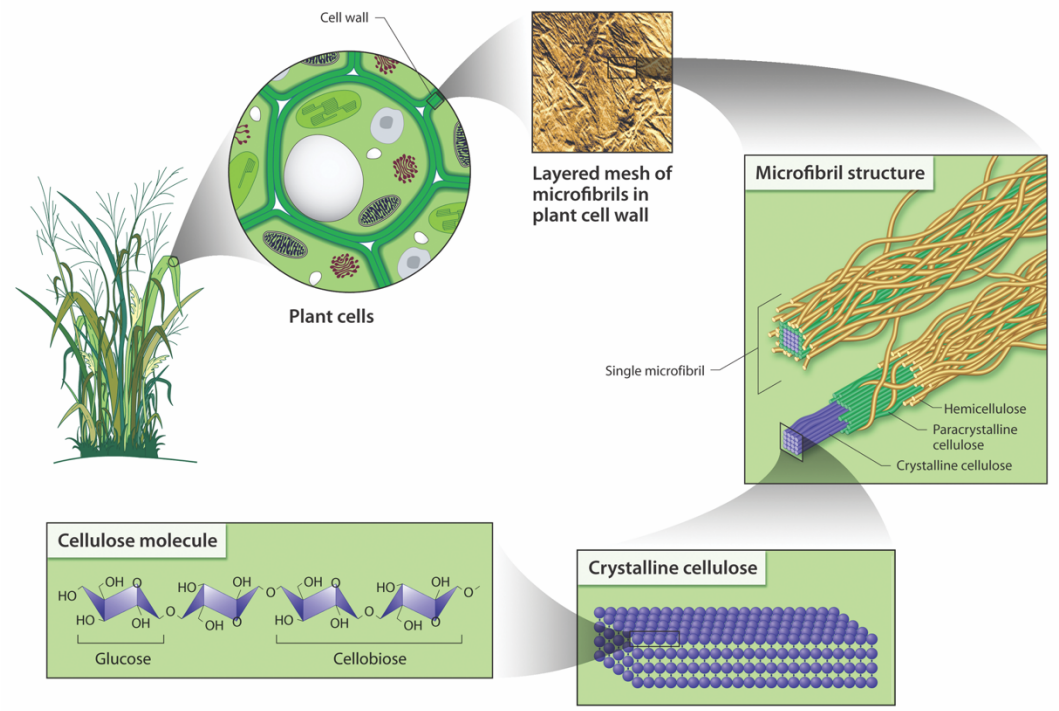

Figure 1.2: The structure of the microfibrils inside the vegetal plants (reproduced from US DOE. 2005. Genomics:GTL Roadmap, DOE/SC-0090, U.S. Department of Energy Office of Science. (p. 204), website: https://genomicscience.energy.gov.)

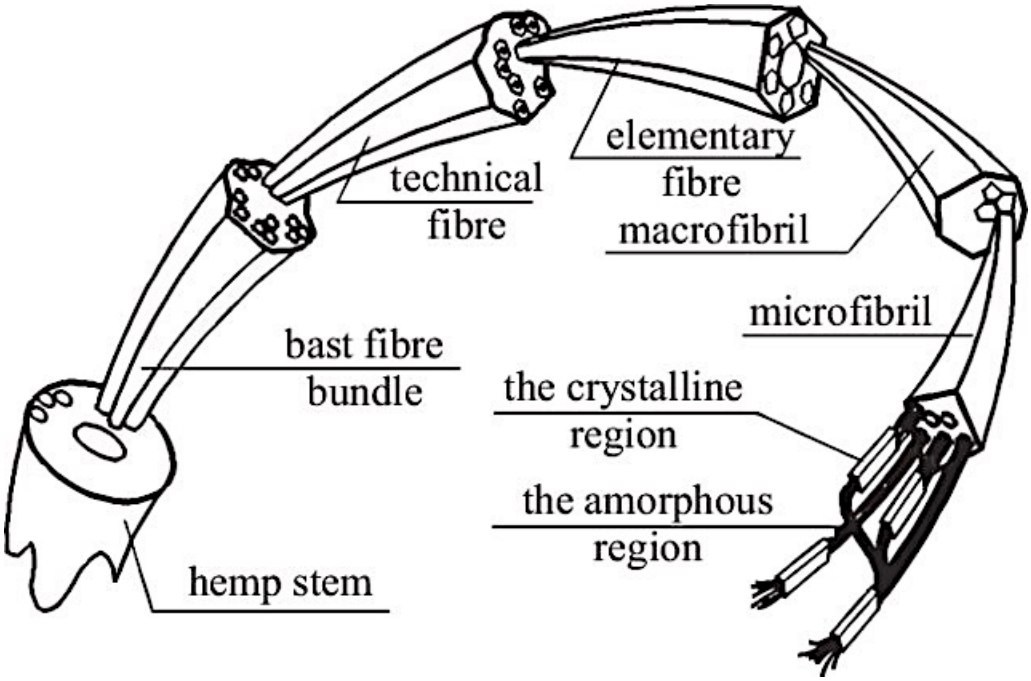

Figure 1.3: The hemp fiber structure (reproduced from Kaczmar et al., (2011)).

The first extraction of MFC reported is from 1983, when Turbak et al. had the idea of using an homogenizer: a liquid suspension of cellulose was forced to pass repeatedly through a small orifice, so the particles were subjected many times to a significant pressure drop and high velocity shearing followed by a high velocity deceleration until the suspension became stable, meaning that cellulose was converted into MFC. Indeed, one of the most noticeable features of a MFC suspension is its stability, thanks to the homogeneity, small diameter and great specific surface that the microfibrils reach (Ho et al., 2015).

As well summarized by Siró and Plackett (2010), from that first process, nanofibrils have been extracted in many mechanical ways from different kinds of raw material, like from wood pulp through grinding or from bleached potato pulp thanks to homogenization.

Every extraction process provide an intensive mechanical treatment and there are three types of equipment that are currently used: the homogenizers, the microfluidizers and the grinders. The homogenizer system first used by Turbak, et al. (1983) takes advantage of high pressure and velocity shearing, while in the microfluidizers the suspension is pumped and forced to pass through micro-channels in which, depending on those chambers' size, the fibrillation process takes place at different possible degrees. The grinder, instead, is able to break the cell wall structure using two grinding stones, a static one and a second which rotates at about 1500 rpm (Missoum et al., 2013).

Anyway, every of these three processes requires a really high amount of energy (Rol et al., 2017), but in the recent years a new method has gained attention: it was developed by Heiskanen et al. (2012b), who claimed the use of an extruder as an energy efficient way to produce MFC. They performed the process into a conical extruder, but at the same time suggested the use of any type of extruder, like the twin-screw extruder (TSE) of the present work. Nowadays, the TSE is the only device capable of producing nanofibrils at

high solid content (Rol et al., 2019), which is really important for the prospective of having an industrial scale process.

The fibrillation process through a pilot-scale TSE has then been well analyzed by Ho et al. (2015) and more recently by Rol et al. (2017), who have proved that this method, coupled with a proper pre-treatment of the pulp, is able to significantly reduce the energy usually required for fibrillation. These last authors were the first to investigate the effect of the shearing zones of the screw profile and they also calculated the energy required for the fibrillation with a TSE and compared it with the amount needed by the grinding process. They obtained very good quality MFC from bleached eucalyptus pulp, performing a mechanical refining followed by an enzymatic hydrolysis, before the fibrillation inside a TSE. These two pre-treatments steps had been already recommended by Heiskanen et al., (2012a): as the latter authors explain, the mechanical refining, besides cutting the fibers and so improving the processability at high consistency inside the TSE, opens the fibers structure making them more accessible to the enzymes. In this way the effectiveness of both the enzymatical hydrolysis and the production of MFC is enhanced.

Rol et al. (2017) also compared the effect of the enzymatic pre-treatment with the one of the TEMPO-oxidation chemical pre-treatment, showing that using the latter an higher amount of energy is then required for the extrusion.

These two just mentioned kinds of pre-treatment are the commonly used nowadays. The TEMPO-oxidation converts the C6 primary hydroxyl groups of cellulose into carboxylate groups by the use of NaClO, and so the repulsive forces of these ionized carboxylate groups overwhelm the hydrogen bonds which would hold the micro-fibrils together; in fact, the idea behind the process is to reduce the interactions between the fibrils, letting them to be separated more easily during the mechanical treatment. In the case of the enzymes, usually cello-bio-hydrolases and endoglucanases (both from the family of cellulase) are used: the first prefer to attack the crystalline region of the pulp, while the second degrade the disordered part (Missoum et al., 2013). As discussed by Heiskanen et al. (2012a), the enzymes decompose the primary layer of the fibers so that after it's easier to get in between the fibrils; these authors underlined the benefits of using enzymes affecting cellulose or hemicellulose with the goal of reducing the extension of the subsequent mechanical treatment which usually decreases the strength of the fibers. Heiskanen et al., in another already cited work (2012b), also mentioned the enzymatic treatment as a good way to pre-treat the fibers before performing an extrusion. Moreover, this pre-treatment method is considered more environmentally-friendly than TEMPO-oxidation (Missoum et al., 2013; Rol et al., 2019; Siqueira et al., 2010).

1.2 The characteristics of hemp

Hemp fibers are a sustainable and promising alternative in the field of polymer reinforcement; Pacaphol and Aht-Ong, (2017) have recently reported that the growth of this plant consumes much less water, herbicides, fertilizers, and insecticides than cotton. Moreover, like flax, hemp is easily available in Europe, but its price has been lower and more constant than the one of flax among the last years (European Industrial Hemp Association, 2017).

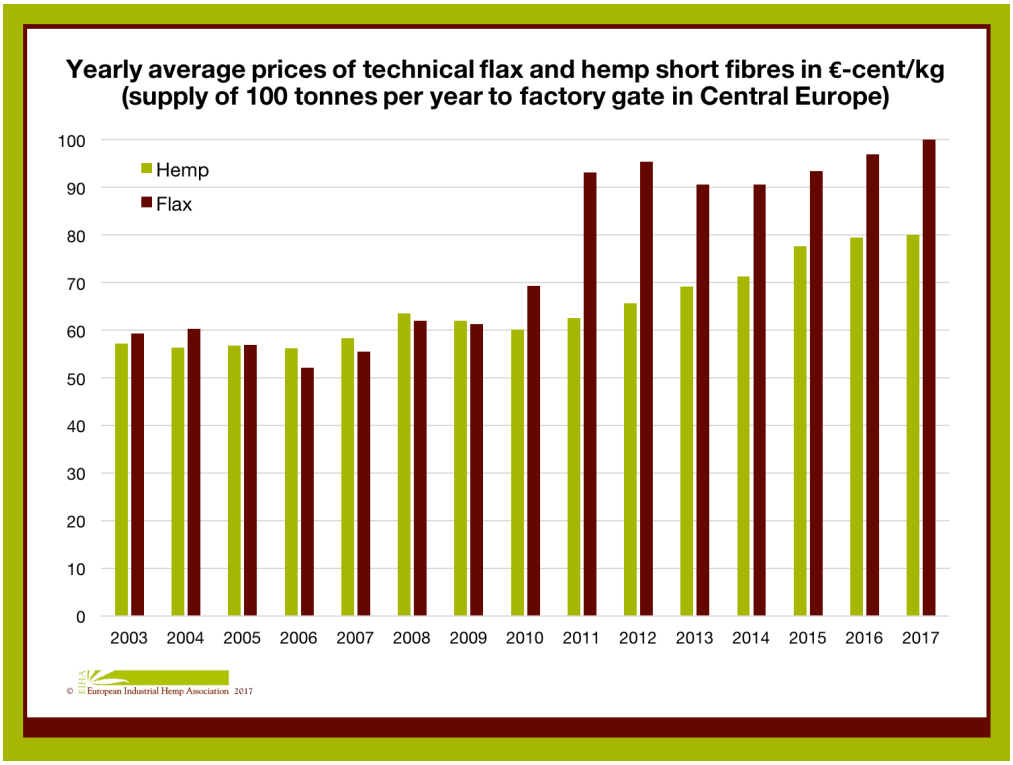

Figure 1.4: A comparison between the price of hemp and flax through the last years (picture downloaded from the website: biobased.eu – original source: European Industrial Hemp Association (2017).)

Hemp has been already used for the production of MFC and many studies can be found in the literature; the oldest found is from 2005 by Bhatnagar and Sain, who made cellulose nanofibers from different sources, including hemp, with the aim in fact of reinforcing polymer films. They reported higher values of the tensile strength and elastic modulus for the films reinforced with hemp then for the ones reinforced with flax.

The characteristics of hemp fibers are intended to give higher mechanical properties to a polymer; in fact, it has been shown that hemp fibers can have higher crystallinity degree than other non-woody plants like flax, jute, sisal and abaca (Alila et al., 2013), feature that should guarantee a good rigidity of the fibers.

Besides this, Marrot et al. (2013) underlined how the Young's modulus of cellulose is about 30 times greater than those of hemicellulose and lignin and that hemp fibers have also a good cellulose content which varies between 55% and 80% depending on the analyzed part of the stem. The same authors illustrated that the structure of hemp fibers (Fig. 1.5) is made of concentric cylinders with a thin outer primary cell wall, which surrounds a secondary one that consists of three layers; the second layer is the most abundant one (80% of the total section) and is made of highly crystalline cellulose fibrils wrapped in an amorphous matrix of hemicellulose and pectin. They also underlined that the cellulose content is higher for the fibers coming from the bottom of the stem than for the ones which come from the apical part. Finally, they reported the existence of secondary fibers, shorter (up to 2 mm vs. 5-10 mm) and thinner (6 µm vs. 15-40 µm) than the more abundant primary fibers, and representing around the 10% of the total; these can be more easily found in female plants, but are not systematically present and their proportion decreases from the bottom to the top of the stem.

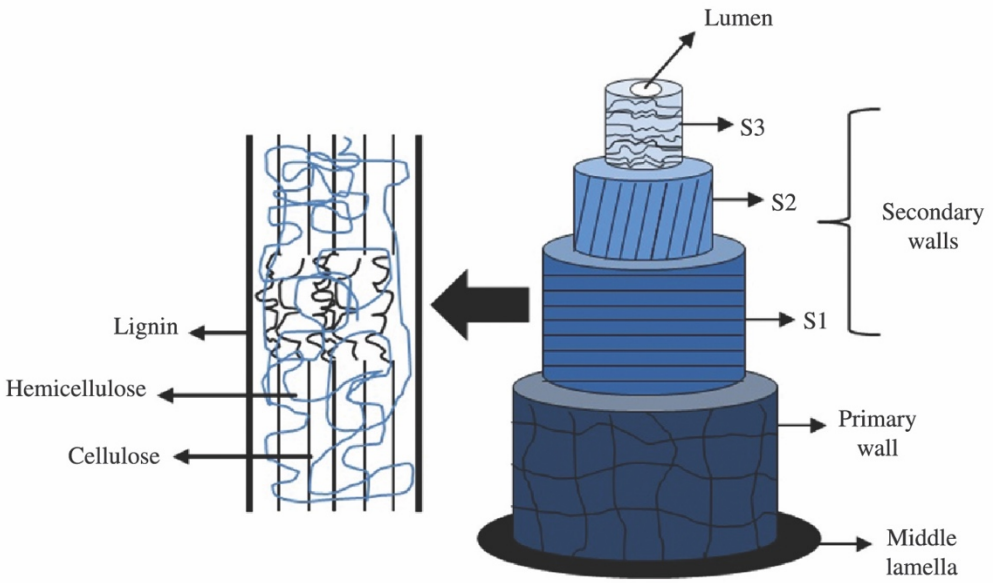

Figure 1.5: The structure of the vegetal fibers (reproduced from Pereira et al., (2015)).

The chemical composition and structural morphology of hemp was well analyzed by Wang et al. (2007), who investigated the effects of the chemical and mechanical treatments that are involved in the production of nanofibers. They used a high pressure homogenizer to produce MFC and showed how bleached nanofibers were thinner and shorter than unbleached ones, having an average diameter of 54 nm compared to the 87.5 nm of the latter and so suggesting a better reinforcing effect for a composite because of their higher surface area. They also explained how the composition of hemp changes during the entire process, being the raw fibers constituted of a not negligible amount of amorphous hemicellulose and lignin, which drastically decreased after the bleaching that is, in fact, precisely performed for this purpose. At the same time, they reported an increased crystallinity from 57.4% of raw fibers to the 71.2% of microfibrils which have only 4.3% of hemicellulose and lignin combined compared to an initial value for the untreated fibers of more than 17%; these values should ensure higher stiffness and strength for the nanofibers with respect to raw fibers.

However, Alila et al. (2013) well explained that the fibers which are supposed to have the highest mechanical properties (that means the highest amount of cellulose and crystallinity degree) like hemp and flax are not easy to be fibrillated: the role of the amorphous hemicellulose in which the microfibrils are immersed is crucial during the fibrillation process, reducing the hydrogen bonding interactions between the fibrils and so facilitating their separation by mechanical shearing. These authors underlined that the higher is the crystallinity index the lower will be the yield in MFC, being also the amorphous zones the weakest parts of the pulp through which the fibrillation occurs.

1.3 The Furanic Resin

The poly-furfuryl alcohol (PFA) resin is the result of the polymerization in acid conditions of furfuryl alcohol; this monomer derives from furfural, a bio-based chemical which is a byproduct of the production of ethanol from sugarcane. Furfural can obtained by the

hydrolysis of hemicellulose, which is the second most abundant natural polysaccharide, constituting the 25-30% of lignocellulosic material, and which is not currently used in the cellulose and paper production. Sugarcane bagasse and corncob have an high content of hemicellulose and they are available in large quantities, so more than 98% of all the furfural production derives from these two sources (Machado et al., 2016).

The 60% of the furfural produced all over the world is used in the production of furfuryl alcohol by catalytic hydrogenation; this production has increased in the last decades (Perez and Fraga, 2014). Furfuryl alcohol has an elevated tendency to self-polymerize under high temperature and acid conditions, producing poly-furfuryl alcohol, a dark viscous resin which contains water as solvent. The hydrophilicity of the FA monomer is not perfectly maintained after this first step of polymerization: most of the hydroxyl groups of the FA molecules, in fact, basically disappear after the several subsequent condensations in which they are involved (Pranger and Tannenbaum, 2008) (for a better comprehension, the two possible mechanism of reaction are synthetically showed in Fig. 1.6.).

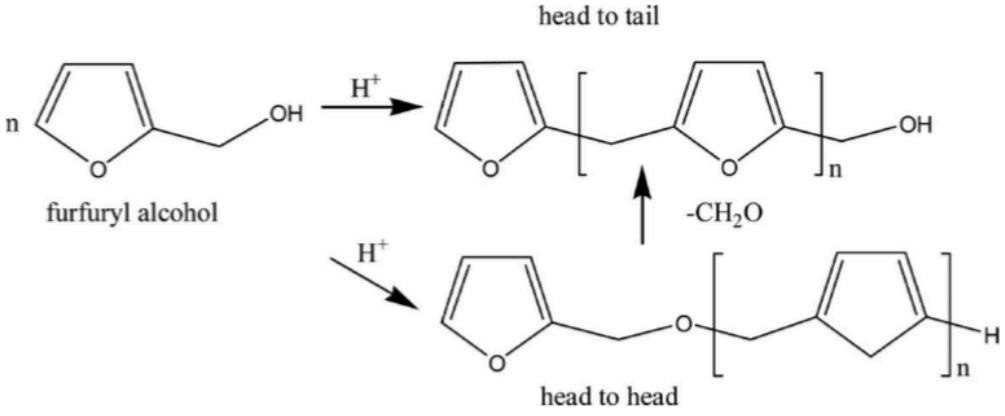

Figure 1.6: The two possible mechanisms of reaction involved in the first step of polymerization of FA (Pranger and Tannenbaum, 2008) – picture reproduced with the permission of ACS Journal, all other permissions should be directed to the ACS.

A second step of polymerization is obtained adding a catalyst and increasing again the temperature to induce the crosslinking (Fig. 1.7), which generates a solid amorphous tridimensional network (Crossley et al., 2012; Pin et al., 2014).

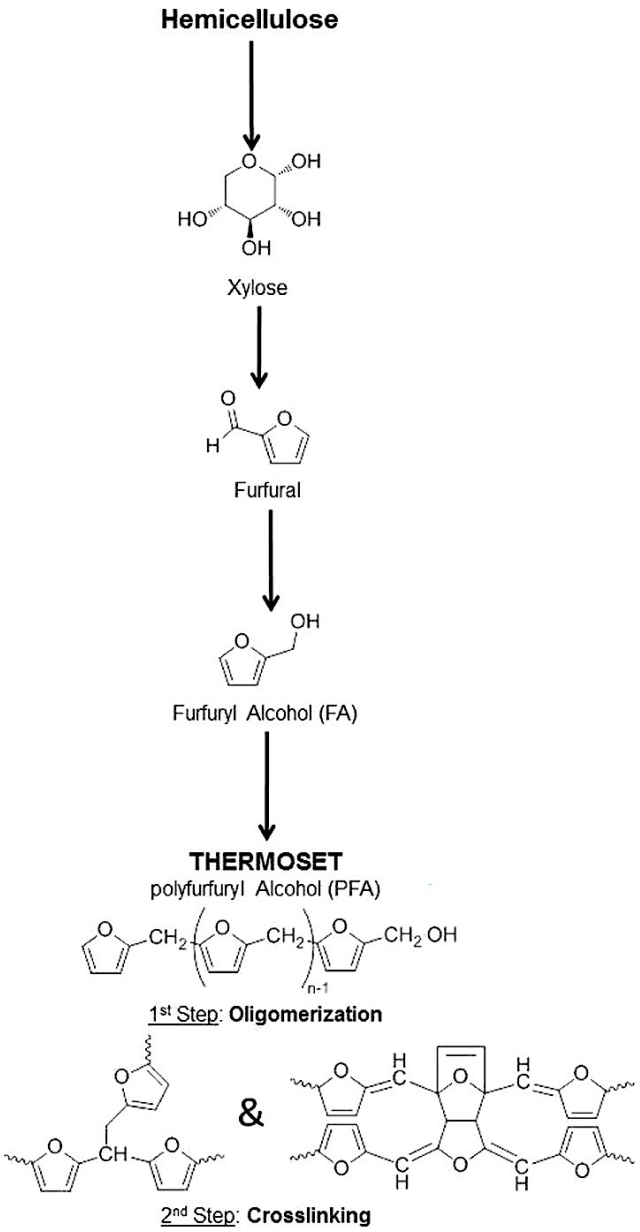

Figure 1.7: From hemicellulose to a solid resin (original picture from Pin et al. (2014) modified and adapted for the purpose of the present work; all other permissions should be directed to the ACS).

The main problem of PFA are its poor mechanical properties (it has a Young's Modulus slightly higher than 2 GPa (Deka et al., 2013; Linganiso et al., 2014)), so reinforcing it is a very interesting perspective. In fact, apart from this drawback, the resin has very good properties, being thermally resistant as well as chemically resistant against corrosion and solvents (Machado et al., 2016).

Different examples of incorporation of fibers and other bio-fillers into a PFA matrix are reported in the literature, with the aim of modifying the mechanical behavior of the thermosetting resin, obtaining at the same time a 100% bio-based final composite.

Pin et al. (2014) incorporated into the furanic resin humins, which are a byproduct of the same sugar conversion process and are nowadays mainly used as combustible to supply

power to the process itself. They successfully obtained a composite more flexible and less brittle than the pure PFA network. In fact, they reported a two times higher tensile strength for the humins/PFA composite compared with the one of the pure PFA, suggesting that some positive influencing chemical interactions occurred between the furanic network and the humins.

Two years before, Crossley et al. (2012) had tried to reinforce the PFA resin adding flax fibers, with the idea of substituting glass fibers in the task of improving the mechanical properties of the network. Suspecting that the acidity of the resin could induce a chemical degradation of the fibers, reducing the strength of the network, these authors attempted to reduce the amount of the acid catalyst necessary to the polymerization. However, in this way a temperature higher then 120°C was needed to complete the curing procedure in a reasonable period of time, and this increased the problem of foaming due to water evaporation and volatile production.

Also Pohl et al. (2011) chose flax fibers as reinforcing fillers; their work focuses on the comparison of the mechanical properties between glass fibers and flax fibers reinforced PFA matrix. They reported that the specific mechanical properties were similar for the two kinds of composites (using aligned flax fibers), except for the tensile strength. Performing the tests with different loading angles, they reported also a lower sensitivity of fiber orientation to load angle for the composite containing aligned flax fibers, suggesting that this could be due to a better adhesion between the natural fibers and the matrix. The same authors mentioned that, unlike glass fiber reinforced PFA, the flax reinforced one could be ignited, even if the burning rate was low thanks to the characteristic fire retardance of the resin.

Other authors incorporated kenaf fibers into a PFA matrix reporting a storage modulus of 5.5 GPa at 30°C for a composite containing 20% of fibers, higher than the one obtained for the pure PFA which was 2.3 GPa (Deka et al., 2013).

Anyway, to the best of my knowledge, there are not many studies about the incorporation of microfibrils into the PFA matrix. A work available at the moment is from Linganiso et al. (2014) who prepared microfibers (diameter 12-15 μm) from Agave Americana (a succulent plant from South America) and then made PFA/agave composites with different fractions of microfibers. However, the tensile modulus of these microfibers was 1.7 GPa, lower than the 2.2 GPa of the neat PFA matrix, and so the tensile modulus of the composite decreased increasing the microfibers content. The authors also reported a decrease of the hydrophobicity of the composite when the agave loading was increased; this can be clearly explained by the presence of the many hydroxyl groups characteristics of the microfibrils.

1.4 The 3D printing process

3D printing, also known as additive manufacturing, is a promising technology which allows fabricating objects directly from a tridimensional virtual model through a layer by layer deposition of matter. The advantage of the process lies not only in the fact that no mold or die is needed, but also in the automation and reproducibility that it offers. Thanks to the accuracy of the method, it is possible to produce structures of high complexity in a relatively rapid way and at with a low cost (Dai et al., 2019).

There are several techniques and systems which can be gathered under the name of 3D printing; among the most used there are extrusion based systems, in which the material goes through a nozzle and is deposited layer-by-layer. One crucial issue is that the older

layers have to maintain their shape fidelity before the deposition of the new ones. The extrusion based systems include Fused Deposition Modeling (FDM), Direct Ink Writing (DIW) and micro-extrusion 3D bio-printing. While in the FDM process there is a filament which is melted and then it passes through the nozzle (Fig. 1.8), in the DIW and the micro-extrusion process there is a paste or "ink" which is forced to pass through the nozzle thanks to a piston, a screw or just pneumatic push (Fig. 1.9) (Wang et al., 2018; Xu et al., 2018).

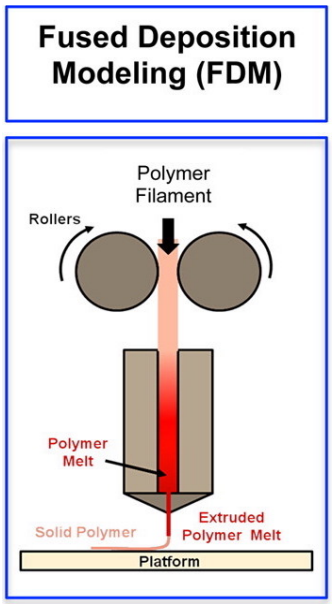

Figure 1.8: Schematic illustration of the FDM process (original picture from Guvendiren et al., (2016) modified and adapted for the purpose of the present work; all other permissions should be directed to the ACS).

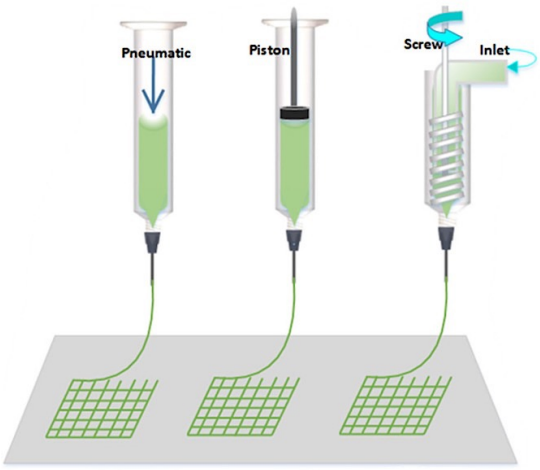

Figure 1.9: Different methods of pushing the printing paste through the nozzle in DIW or micro-extrusion processes (original picture from Xu et al., (2018), (https://pubs.acs.org/doi/10.1021/acssuschemeng.7b03924) modified and adapted for the purpose of the present work; all other permissions should be directed to the ACS).

The 3D printing technology has gained attention from many market sectors, from the automotive industry to the medical sector, and it is compatible with many different materials: gels, ceramics, polymers, metals, food etc. (Thibaut et al., 2019). However, it has been well demonstrated that the most used polymers in 3D printing, namely polylactic acid (PLA), acrylonitrile butadiene styrene (ABS) and nylon, are responsible for the emission of many volatile organic compounds (VOCs) and ultrafine particles (UFPs). In fact, these thermoplastic polymers are used in the FDM systems and necessitate high temperatures for the melting of the filaments, but during this process also some degradation of the polymer can occur, with the consequent generation of those substances. The dangerousness of the products of this decomposition depends obviously on the chemical composition of the polymer: the main substance detected is usually the related monomer, and while styrene (ABS) is a probable carcinogen and caprolactam (nylon) is toxic for eyes and lungs, lactide (PLA) is not considered really risky for health. Moreover, being the PLA nanoparticles used also in drug delivery, their inhalation should not be very dangerous. Nevertheless, also the use of this bio-based polymer can't be considered totally safe, since different toxic, irritating or carcinogen VOCs were detected during its degradation (Davis et al., 2019; Stephens et al., 2013; Unwin et al., 2013). For this reason, also in the 3D printing field, there is an increasing necessity to find new bio-based polymers; furthermore, a larger use of the DIW process instead of FDM could avoid the risks linked to the high temperature heating of the filaments.

The characteristics of the additive manufacturing process require two important features for a possible printing paste to be used in DIW: a shear thinning behavior, which guarantees a good extrudability trough a micro-sized nozzle, and a zero shear viscosity that should be high enough to let the layers maintain their structural fidelity. Moreover, usually either air or freeze-drying, or ionic, thermal or UV curing are necessary to permanently fix the structure after printing (Wang et al., 2018; Xu et al., 2018).

The hydrogels containing cellulose nanofibers have the two minimum requisites for printability cited above, even if the viscosity is determined by the cellulose concentration (Wang et al., 2018). So, also in the 3D printing field, cellulose is seen as a sustainable and cheap resource for the production of new materials, which can be employed, in its different forms, as a building block as well as a filler. Examples of 3D printing of pure cellulose nanofibers hydrogels can be found in the literature, which take advantage of the rheological properties already mentioned; on the contrary, one of the main problems is the collapse and shrinkage of the structure after air drying (Dai et al., 2019). However, Håkansson et al. (2016) demonstrated that by freeze-drying it is possible to maintain the shape of the printed structure and also to have a negligible shrinkage, even if this process is difficult to scale up because it requires too much time and energy (Dai et al., 2019).

In the field of tissue engineering and regenerative medicine, natural polymers like alginate, collagen and hyaluronic acid have been evaluated for 3D bio-printing, and the rheological properties of these can be significantly improved by the addition of cellulose nanofibers (Markstedt et al., 2015). The low zero shear viscosity of alginate was successfully increased by Markstedt et al. (2015) by adding nano-fibrillated cellulose. They were able to print scaffolds for cartilage tissue, the shape of which was fixed taking advantage of the cross-linking ability of alginate, avoiding any shrinkage linked to the drying techniques. The authors prepared bio-inks with various percentage of nanofibers at different dry content (from 2.25% to 1.5%), varying also the alginate dry content to keep the same amount of water in each ink. Noticing that all the inks had a very similar shear thinning behavior, they realized that (for the tested ratios) the viscosity was controlled by the dry content of the ink, more than by the components proportion. Therefore it was

possible to control the ionically cross-linking varying the amount of alginate without affecting the printability of the paste.

Cellulose nanofibers have been used also to increase the strength of polymer filaments to be used in FDM 3D printing: some authors incorporated them into PLA or PP producing composite filaments through extrusion, and in both cases the mechanical properties were improved (Dai et al., 2019).

Some examples can be found in the literature that report the use of crosslinkable resins in 3D printing, even if most of them are photocurable. Actually, the very first 3D printing process was developed in 1980s by Hull, who invented the stereolithography apparatus (SLA), which is based on the curing and solidification layer-by-layer of a liquid resin using an UV laser (Fig. 1.10) (Hull, 1984). This kind of process is still used nowadays among the other additive manufacturing techniques (Voet et al., 2018; Wang et al., 2018).

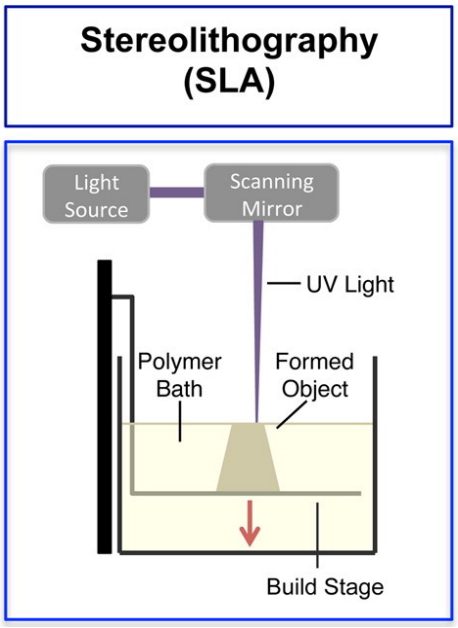

Figure 1.10: Schematic illustration of the SLA process (original picture from Guvendiren et al., (2016) modified and adapted for the purpose of the present work; all other permissions should be directed to the ACS).

One example of the use of a bio-based resin in 3D printing through the SLA was recently given by Voet et al. (2018), who successfully fabricated prototypes of complex structures from acrylate photocurable resins. The authors reported a maximum tensile strength for the printed and cured samples of 7 MPa and a good thermal stability.

The same authors underlined the scarcity of studies about the application of bio-based resins in this the SLA process; anyway, even if very few, some researches are already available (Voet et al., 2018). Instead, for the best of my knowledge, no study can be found reporting the use of bio-based resins for 3D printing through DIW or microextrusion, while various bio-based hydrogels are often employed in these processes (Xu et al., 2018).

2 Materials and Methods

2.1 Materials

Hemp bleached and pre-refined pulp (average moisture content of 8% wt) was used to prepare MFC throughout all this work. Three samples of raw (bleached), pre-treated and extruded eucalyptus pulp were used for the XRD analysis.

Poly-furfuryl alcohol (commercial name: "Furolite™") and 2-hydroxyethyl ammonium nitrate as catalyst (both supplied by TransFurans Chemicals (Belgium)) were used to prepare the Poly-furfuryl alcohol (PFA) matrix.

The following chemicals and materials were used for the enzymatic pre-treatment of the pulp: acetic acid (CH_3COOH); sodium acetate trihydrate ($CH_3COONa \cdot 3H_2O$); endoglucanase enzymes (commercial name: "FiberCare® R", supplied by Novozymes); deionized water.

2.2 Pre-treatment of the pulp

The pre-treatment of hemp pulp was performed using a protocol already employed by Rol et al. (2017) for the production of MFC from Eucalyptus.

This method consists of two steps as reported below:

2.2.1 Refining

The raw sheets of hemp pulp were made into pieces and let fully covered by water overnight; the hemp was put inside a pulper to cut finely the pulp and have a more homogeneous suspension.

Water was added in a volume necessary to have a suspension at 2% wt of solid content to be poured inside a Valley beater refiner (Fig. 2.1) with a capacity of 22 L. The working principle of the machine relies on a beater roll and a bed plate, both cogged with parallel bars, through which the pulp passes and is refined.

The desired Schopper-Riegler (SR) degree of refining was 80, the SR degree was monitored every 10 minutes until this value was reached.

Figure 2.1: A Valley beater of 22 liters of capacity fully loaded of hemp pulp at 2% wt.

The SR degree was measured in accordance with standard ISO 5267-1 (equivalent to AFNOR NF Q 50-003) using a Schopper-Riegler apparatus (see Fig. 2.2). For every measure at least two samples were taken (if the values of the SR degree differed too much a third one was taken) from the disk beater refiner using a cup which allows to take about 2 g of dry matter in the form of suspension at 2% wt. Water was added to each sample up to reach 1 L, then everything was poured into the apparatus. The water coming out from the overflow exit (visible in the front part of the apparatus, Fig. 2.2) was measured using a graduated beaker on which it is possible to read the SR degree. The disks of pulp remained from the measures inside the apparatus were taken and put inside a drier at 105°C until all the water was removed (see Fig. 2.3). Then they were weighted: if the weight differed significantly from 2 g, the SR degree corresponding to the sample was adjusted with the aid of correction curves (AFNOR NF Q 50-003, Fig. 2.4).

Figure 2.2: The Schopper-Riegler apparatus used to determine the SR degree of the pulp.

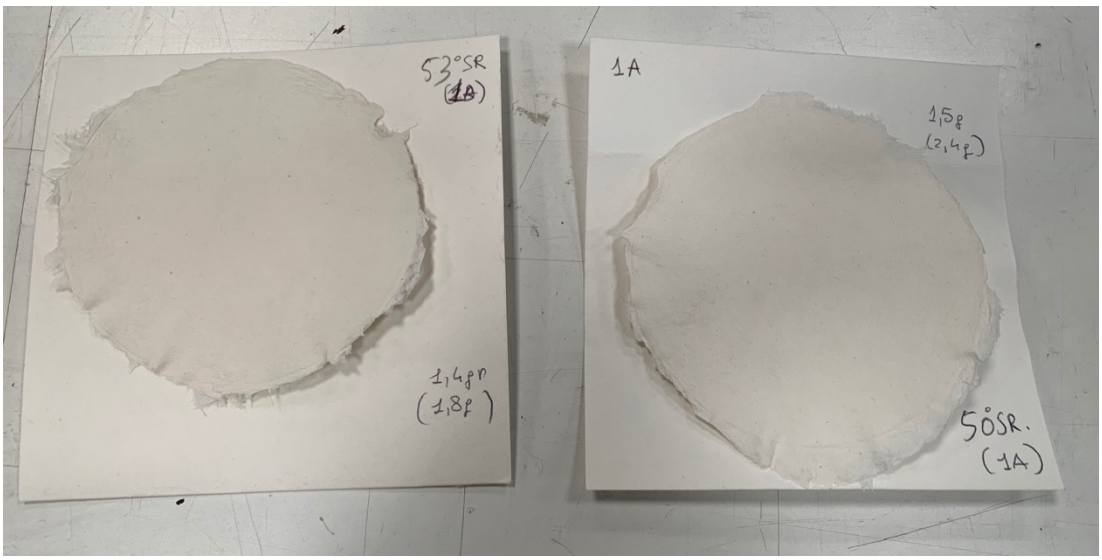

Figure 2.3: Dried disks of pulp remained inside the apparatus after the first measure of the SR degree.

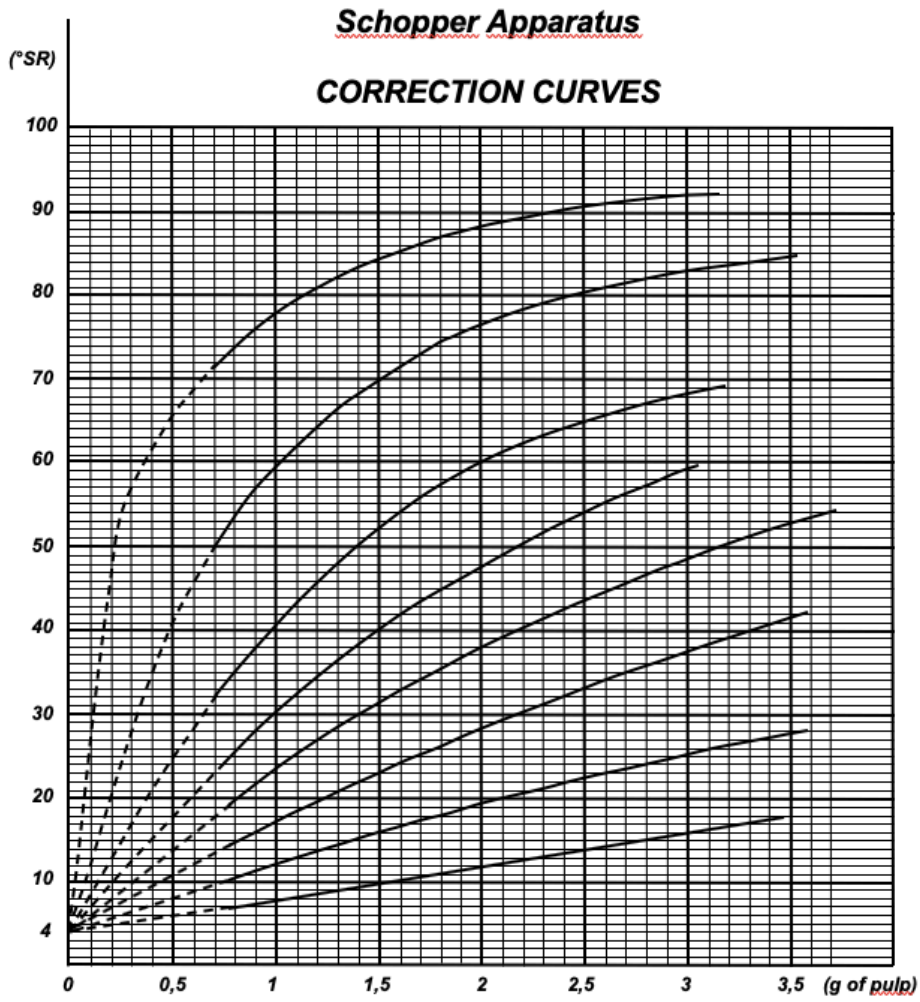

Figure 2.4: Curves of correction of the SR degree of the samples (AFNOR NF Q 50-003).

2.2.2 Enzymatic hydrolysis

The enzymes used for the enzymatic treatment were endoglucanase FiberCare® R from Novozymes in a percentage of 6,3% wt of the total dry matter. To keep the pH around the value of 5, a buffer solution was prepared mixing acetic acid and sodium acetate trihydrate, in concentrations respectively of 0,016 and 0,0339 mol/liter, in 200 ml of deionized water.

The process was carried out employing a 15 L batch jacketed reactor equipped with a 2 impellers mixer and a system for the control of the temperature (Fig. 2.5).

The hemp pulp suspension at 2% wt of dry content was poured inside the reactor, the mixer rotational velocity was set at 550 rpm and the temperature of the heating water in the jacket was set at 61°C to have a T = 50°C in the suspension. After reaching this temperature setpoint, the enzymes mixed with the buffer solution were added and the impeller velocity was set at 450 rpm.

Needing the reaction 2 hours to be completed at these operative conditions, after 90 minutes the temperature in the jacket was set at 95°C to have around 83°C in the sample

and deactivate the enzyme; this setpoint was reached after 1 hour and was maintained for 15 minutes to have a complete deactivation.

The pulp was then let drain inside a sheet with a mesh size of 1 µm and washed with deionized water till neutral pH. After, using a centrifuge at 10000 rpm for 10-15 min (keeping the pulp inside the sheet to avoid loss of fibers) the non-bonded water was removed. This procedure was necessary because a pulp much more concentrated than 2% wt is needed to allow its processing inside an extruder.

Figure 2.5: The 15 L enzymatic reactor full of hemp pulp suspension at 2% wt.

2.3 *Defibrillation process: Twin-Screw Extrusion*

2.3.1 The extrusion process

A twin-screw extruder (TSE) with a barrel diameter of 16 mm and a length/diameter ratio (L/D) of 45 was used to produce hemp MFC at high solid content (model: Thermo Scientific™ HAAKE™ Rheomex PTW 16 OS).

The device is equipped with a system for the control of the temperature (using cold water circulation), which was set at 10°C.

The two screws, which are parallel and co-rotating, consist of kneading disks and conveying elements (see Fig. 2.6 and 2.7, FS = forward screw, LH = long helix) that can be removed and replaced to change the profile as desired. It is also possible to change the angle between each kneading disk (30°, 60°, 90°) and to make the disks form an helix in the same direction (F = forward) or the opposite (R = reverse) direction of the material flow rate inside the extruder.

Two kind of extrusion profiles were investigated for the production of MFC in this work. In Fig. 2.6 the profile “A” with 6 shearing zones can be seen, while the profile “B” with 5 shearing zones is presented in Fig. 2.7.

The profile A was very recently elaborated by Rol et al. (2020), while the B one was developed during the present work in order to provide a less aggressive shearing to the pulp: it can be noticed in Fig. 2.7 how one of the two “R30” shearing zones consisting of 9 kneading disks (present in the profile A, Fig. 2.6) was eliminated. The first shearing zone was also adjusted with the aim of providing a more gradual shearing to the incoming pulp, which is supposed to be not even partially fibrillated, and so more difficult to be processed without a high torque demand. The last shearing zone was modified in order to allow a possible addition of the PFA in the final part of the extrusion, that could increase the constraint inside the machine. The reason behind this procedure is the obtaining of a good mixing between the two components, fibers and polymer, and the avoiding of further steps to disperse the MFC in the resin (these idea could be implemented in future works).

During the extrusion, the rotational speed of the screws is increased gradually as long as the torque value increases: a higher rotational speed makes the torque value decrease, being the power required to extrudate the material constant and equal to the product of these two variables.

Using the profile A, a screws rotational speed of 1000 rpm was necessary in order to keep the torque value under 100 Nm; the device is in fact equipped with a safety system which stops the process when the torque reaches a value of 110 Nm. For the profile B, instead, 700 rpm were sufficient to have the same or lower value of the torque.

During the process, samples of the fibrillated material coming out of the extruder within 30 seconds were taken and weighed; in this way the flow rate of the product was estimated.

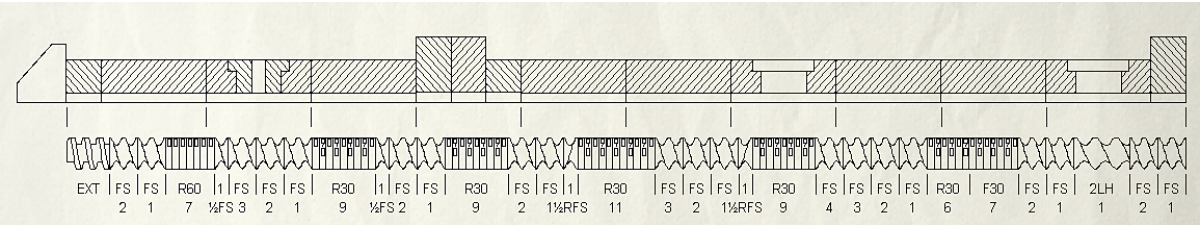

Figure 2.6: Extrusion profile A, 6 shearing zones.

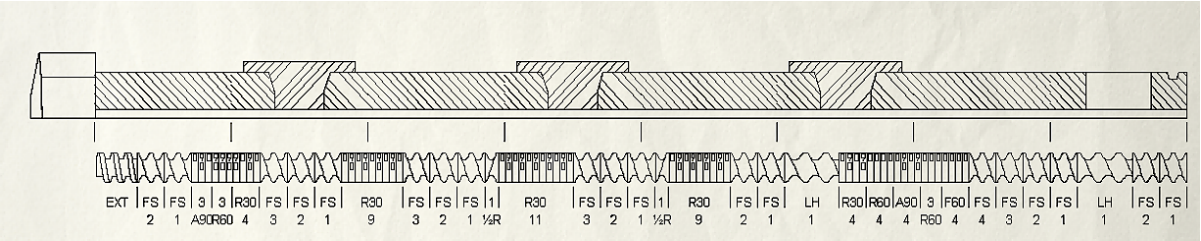

Figure 2.7: Extrusion profile B, less aggressive, 5 shearing zones.

2.3.2 Evaluation of the energy required for the extrusion

The specific mechanical energy (SME_D) demanded by each extrusion performed was calculated using the formula 2.1 (Rol et al., 2020):

$$SME_D = \frac{n \cdot T \cdot P_{max}}{Q_D \cdot n_{max} \cdot T_{max}} \quad (2.1)$$

In this formula T is the torque measured by the TSE software (in Nm), T_{max} is the maximum torque (130 Nm), n is the rotational speed imposed to the screws (rpm), n_{max} is the maximum rotational speed of the screws (1100 rpm), P_{max} is the motor power (7 kW) and Q_D is the mass dry flow rate (in kg/h), evaluated by the method described in the sub-section 2.3.1. and then modified multiplying that value by the dry content of the concerned MFC.

Given the oscillations of the torque during the extrusions, the value of T used for the calculations is an average value that it assumed within the 30 seconds of the measurement of the flow rate.

The SME_D was calculated for each pass of the material through the TSE and the values of the energies were added in case of more than one pass.

2.4 Characterization of MFC and pre-treated hemp pulp

Different test were done on the MFC produced by extrusion in order to determine the quality of the material. Some characterizations were carried out also on the enzymatically treated hemp pulp, for comparison.

The methods used are reported below, each sub-section corresponding to a specific test.

2.4.1 Measuring of the dry content

After each step of processing 3 samples for each batch were taken and weighted before and after drying in an oven at 105°C overnight. The dry content in percentage was calculated using the formula 2.2:

$$\%dry = \frac{weight\ before\ drying}{weight\ after\ drying} \cdot 100 \quad (2.2)$$

then an average of the three dry contents calculated (one for each sample) was used as the reference dry content of the material, necessary to be known for the following characterizations.

2.4.2 Turbidity of MFC-water suspensions

100 mL suspensions at 0,1% wt of dry content of MFC in deionized water were prepared.

The suspensions were let on the magnetic stirrer for at least two hours, then a further dispersion of the MFC was provided using an Ultra-Turrax® at 8000 rpm for 1 min.

The turbidity value (NTU) was measured using a turbidimeter (model: Aqualytic® Infrared AL250T-IR).

2.4.3 Preparation of hemp films

400 mL suspensions at 0,5% wt of dry content of MFC or enzymatically treated pulp in deionized water were prepared using the same procedure described in the sub-section 2.4.2. Suspensions were then treated with ultrasounds for 5 minutes in order to eliminate air bubbles produced inside the suspension by the stirring systems.

The suspensions were then vacuum-filtrated through a sheet former (model: Rapid Köthen, Fig. 2.8) and a nylon sieve with a mesh size of 1 µm, until no more water was visible on the surface of the sheet.

The sheets were dried under vacuum (below -0,8 bar) between two sieves and two sheets of paper to prevent adherence with the drying machine. The drying was conducted following the standard protocol, i.e. 85-90°C for 20 minutes (Rol et al., 2017) for the films produced from the enzymatically treated hemp pulp. In the case of MFC instead, applying the standard procedure the films were found completely broken. After several trials, good MFC films were obtained drying at 60°C for 30 min and then putting the films again inside the drying machine on the opposite side for other 3 minutes.

Afterward, each film was stored in a conditioned room at 23°C and 50% RH (Relative Humidity) for at least 48 hours before further characterizations.

The MFC films obtained with the just described method are commonly known as "nanopapers" (Rol et al., 2017).

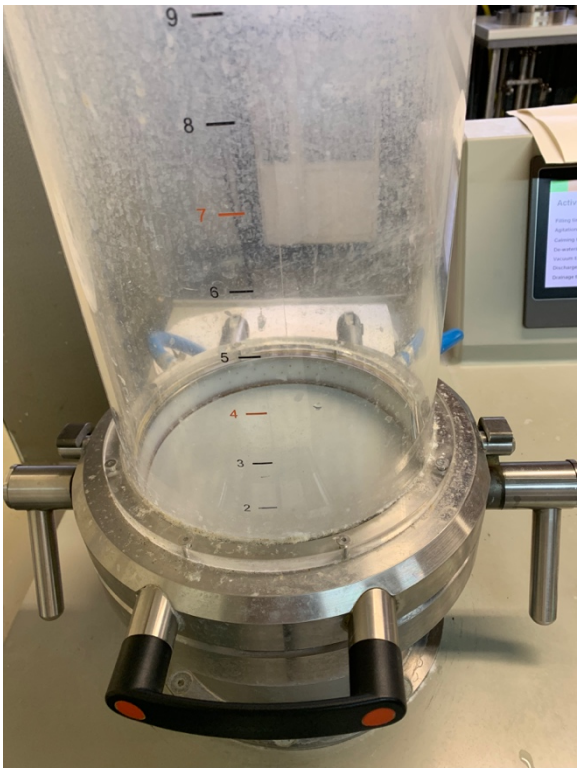

Figure 2.8: Vacuum filtration of a MFC-water suspension through a Rapid Köthen sheet former.

2.4.4 Transmittance of the films

The transmittance of the hemp films was measured by a UV-spectrophotometer (model: Shimadzu, UV-1800) using a wavelength of 550 nm as the incident light.

Rectangular specimens of 6,5 cm x 5 cm were cut from the nanopapers and analyzed at least 3 times in different zones. At least 2 specimens were cut from each film, to take into account the possible inhomogeneity.

2.4.5 Calculation of the grammage of the films

The grammage of a film's specimen is given by the ratio between its weight and its surface (g/m^2). To take into account the inhomogeneity of the prepared films, the grammage of each film was evaluated different times:

- on the intact sample, calculating the area of a disk with a diameter of 20 mm;

- on each rectangular specimen of 6,5 cm x 5 cm used then for the transmittance test.

The weighing and grammage calculation were performed on every film prepared, then the average grammage for each type of film was evaluated and it is reported in Tab 3.4.

2.4.6 Tensile tests

The mechanical properties of the films were determined performing tensile tests on films' stripes of 15 mm of width and at least 100 mm of length. At least 3 stripes were cut from each film.

The apparatus used for all the tests was an Instron 5965 equipped with a load cell of 5 kN (Fig. 2.9). Each sample was tested at a cross-head speed of 10 mm/min.

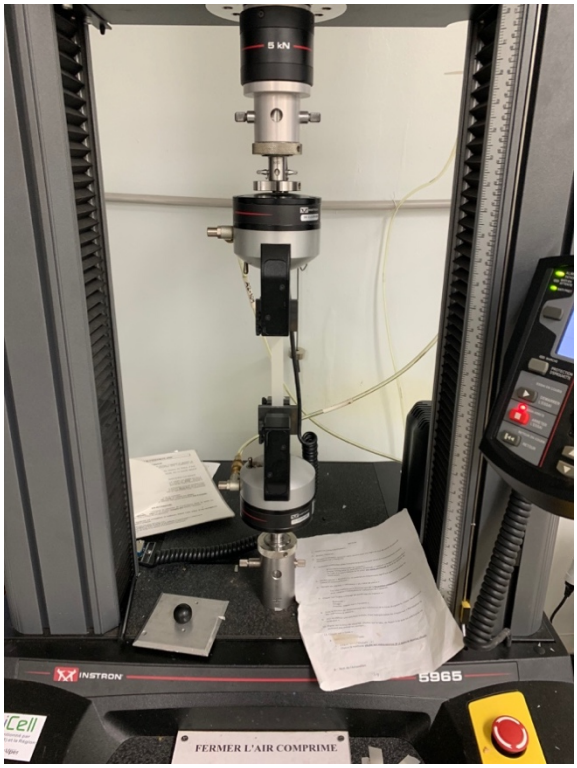

Figure 2.9: Instron 5965 machine for traction tests equipped with a 5kN cell load.

2.4.7 Optical microscopy analysis

100 mL suspensions at 0,5% wt of dry content of hemp MFC in deionized water were prepared using the same procedure described in the sub-section 2.4.2.

100 mL suspensions at 0,5% wt of dry content of hemp pulp before and after pre-treatment were prepared letting them on the magnetic stirrer for at least 2 hours.

A drop of the suspension was put on a microscope slide by a Pasteur pipette, then a drop of methylene blue was added to color the fibrous elements and make them visible. Another glass slide was placed on the sample before inspection with an optical microscope.

The images were taken at 50x, 200x and 500x magnification using a Carl Zeiss Axio Imager M1 optical microscope (in transmission mode) equipped with an AxioCam MRc 5 digital camera. At least 3 images for each magnification in different zones of the sample were taken for each specimen.

A 100 mL suspension of 0,1% wt of dry content of non-pre-treated hemp pulp in deionized water was prepared putting it on the magnetic stirrer for at least 2 hours. Then it was analyzed with the same microscope at 50x of magnification in order to have an idea of the length of the original fibers.

2.4.8 Morphological analysis

The morphological characteristics of hemp MFC were investigated using a MorFi® analyzer.

40 mg of dry matter was added to 1 L of deionized water, the 0,004% wt suspension was stirred with a magnetic stirrer for at least 8 hours, until no agglomerate was visible.

The system is equipped with a scanning camera (resolution of 5 μm) able to detect the elements present inside the very diluted suspensions. A computer is connected to the machine and a software keeps track of every single measurement and provides the results in real time. The software needs to distinguish the scanned elements between fibers and "fines"; these latter are fine cellulosic particles (diameter maximum 76 μm) which are generated during the common papermaking processes like pulping and bleaching (primary fines) and refining (secondary fines) (Fischer et al., 2017; Odabas et al., 2016). A value of 200 μm was set as the limit length of fines in the machine software: in this way only the elements with an higher length were considered as fibers, while all the others as fines.

The measurements were repeated 3 times for each sample and the average values are reported.

2.4.9 Crystallinity Index

X-ray diffraction (XRD) spectra were used to calculate the crystallinity index (CI) of the hemp fibers after each processing step and compare it with the CI of eucalyptus fibers.

To obtain the spectra a PANanalytical X'Pert PRO MPD diffractometer equipped with an X'celerator detector was used, generating the X- rays with a copper anode (Kα radiation λ = 1.5419 Å). The measuring range was 2θ=5−56° with a step of 0.067°, the counting time per step was 3.2 s.

The CI (%) was calculated from the XDR spectra according to the peak height method, using the formula 2.3:

$$CI = \frac{\left(I_{002} - I_{am}\right)}{I_{002}} \cdot 100 \quad (2.3)$$

where I_{002} is the intensity of the main crystalline peak at 2θ between 22° and 24° and I_{am} is the intensity of the non-crystalline diffraction at 2θ around 18° (Marrot et al., 2013; Rol et al., 2017; Terinte et al., 2011).

2.5 Preparation of the 3D-printing paste

2.5.1 Formulations

Among the produced hemp MFCs mechanically tested so far, the one with the highest elastic modulus was chosen to be incorporated to the resin, i.e. the one with a concentration of 33,85% wt, passed two times through the extruder's profile B.

Five different formulations were investigated varying the amount of hemp MFC; the detailed quantities of each component in the pastes are reported in Tab. 2.1.

Hemp MFC was used as rheology modifier and possible reinforcing element, poly-furfurylalcohol resin (Furolite™) as matrix and 2-hydroxyethylammoniumnitrate as catalyst, necessary to promote the crosslinking during the curing step.

The three components were mixed using a planetary blender at its maximum speed.

Table 2.1 Formulations of the printing paste (% wt).

	1	***2***	***3***	***4***	***5***
Hemp MFC	5%	10%	20%	25%	35%
Furolite	90%	85%	75%	70%	60%
Catalyst	5%	5%	5%	5%	5%

2.5.2 Dispersion of MFC agglomerates inside the paste

Two different methods were tried to obtain a good dispersion of the MFC agglomerates inside the resin: stirring the paste by the use of Ultra-Turrax® at 12000 rpm for 10-15 minutes or passing it up to 6 times through a three-roll milling machine.

The three-roll milling machine can be seen in Fig. 2.10 and consists of a feed roll, a center roll and an output one which rotate in opposite directions. The end of the machine near the apron roll is provided with a blade for the removal of the processed material. The distance between the rolls can be regulated and was set at 1 mm, and also the rotational speed of the first and the last rolls can be fixed as preferred, and was set at the minimum possible.

This method is commonly used in the ink and paint industry to disperse pigments inside very viscous liquids; the operating principle relies on the shear and impact forces

produced by the rotation of the cylinders to break the aggregates into primary particles (Ng et al., 2019).

Fig. 2.10: Processing of the printing paste with the three-roll milling machine.

The aspect of the paste at 35% wt of MFC before any pass, after 1 pass and after 3 passes through the machine was analyzed with the aid of a binocular magnifier (ZEISS SteREO Discovery V20 with an AxioCam ICc 5). For each sample, a thin layer of paste was placed on a Petri dish, the dish was covered with its cap and put under the magnifier.

At least three pictures were taken per each specimen in different zones at 7,5x of magnification; the most relevant are reported in Fig 3.13.

2.5.3 Rheology tests

The rheological behavior of the paste was tested with an Anton Paar MCR 302 rheometer using two parallel plates (Fig. 2.11). A gap of 1 mm between the two plates during the measurements was set.

For each test, a sample of paste of sufficient amount to completely cover the surface of the upper plate was put on the lower plate.

Some tests were done to compare the behavior of the pastes with different quantities of MFC (from 0 to 20% wt): the shear rate was gradually increased from 0,1 to 10^3 s^{-1}, then reversely decreased; the viscosity and the shear stress were measured every second.

A particular test was performed on the pastes deemed visually printable, at 25 and 35% of MFC (Fig. 3.16), in order to see their capability of recovering the viscosity: firstly the samples were sheared at 100 s^{-1} for 1 minute, then left to rest for 1 min (shear rate ≅ 0 s^{-1}) and finally the shear rate was varied between 0,1 s^{-1} and 500 s^{-1} every 60 seconds for 4 times, making each test last in total 5 minutes. The first two intervals of variation of the shear rate are done only with the aim of preparing the pastes and having them at the same conditions before starting the real testing, therefore the resulting curves are reported starting from the third interval (Fig. 3.16).

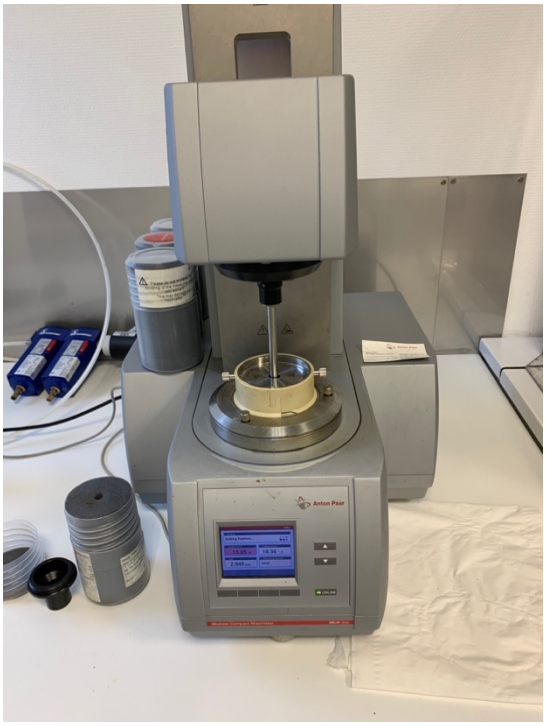

Figure 2.11: The Anton Paar MCR 302 rheometer during a test on the paste.

2.5.4 Printing test

Because of its very high viscosity, the paste, normally stored in the fridge, was kept at room temperature for at least 12 hours before printing.

The paste at 35% wt of hemp MFC was employed for printing tests, using a Leapfrog 3D printer (Model: 3D Creatr, Fig. 2.12) provided with a modified head. This printer, originally designed for the FDM printing process using common thermoplastics, such as PLA filaments, had been previously modified in order to allow the printing of cellulose pastes. The head of the printer is visible in Fig. 2.13b: the material can be deposited thanks to the presence of an extruder (1) to which a syringe (2) is connected: after that the syringe has been filled with the paste, it is placed in a designated cavity (3) (hooked up with the extruder) and the pneumatic air system (4) is activated, so that the material can be pushed through the syringe and the nozzle.

The nozzle used for this work has a diameter of 0,76 mm and the pressure of the compressed air used for the pneumatical pushing was between 2 and 4 bar. A thickness of 0,5 mm was imposed for the layers. An extrusion speed of 500 mm/min was tried. The infill percentage was set to 100% and each layer was printed in a direction orthogonal to

the previous one, alternating horizontally and vertically printed layers (angle of 90° between the direction of two adjacent layers, see Fig. 2.13a). The software "Simplify3D®" was used to control the printing process and adjust the printing parameters from a computer connected to the 3D printer.

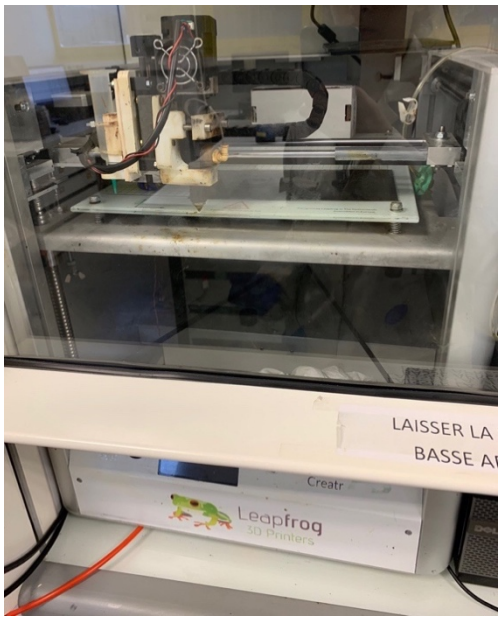

Figure 2.12: Leapfrog 3D printer, model: 3D Creatr – equipped with a modified head.

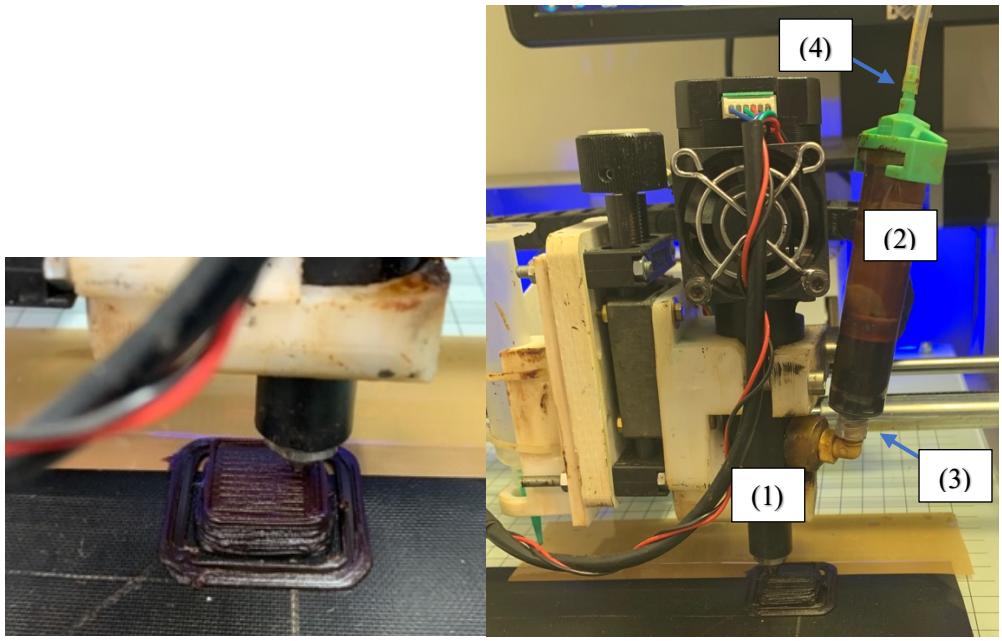

Figure 2.13: Printing trial – (a): 2cm x 2cm cube; (b): modified head of the 3D printer.

The object chosen for testing the printability of the hemp pastes was a 2cm x 2cm cube. The cube model (shown in Fig. 2.14) was downloaded from the "Thingiverse" database.

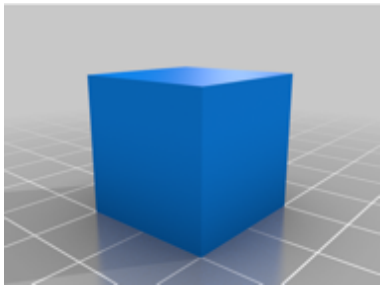

Figure 2.14: 2cm x 2cm cube model (downloaded from the “Thingiverse” database).

3 Results and Discussions

3.1 Pre-treatment of the pulp

The SR degree of pulp samples taken from the Valley beater every 10 minutes and the corrected values derived using the correction curves of Fig. 2.4 are reported in Tab. 3.1. The samples with a dry weight lower than 2 g presented a corrected value of °SR obtained following the respective correction curve which was higher than the pure experimental one. On the contrary, dried samples heavier than 2 g gave a lower corrected SR degree.

The kinetic of refining for a full load of a 22 liters beater is reported in Fig. 3.1, where each value represented with a dot on the plot is the average of the two corrected values obtained from the two samples (A and B) taken at the same refining time.

As it can be seen in Fig. 3.1, it took about 50 minutes to reach 80°SR starting from around 50°SR. However, it can be mentioned that the time required to attain 80°SR is less for partial loads: indeed, during a second run of 15 liters of pulp, 30 minutes were enough to reach 80°SR. This can be explained by the fact that, either with a partial or full load, the same amount of material passes in the same interval of time through the bed plate and the beater roll, and so, if the total amount of matter inside the valley beater lower, it takes less time to have it all processed. Basically, the refined flow rate is the same, but the material is less, so the time required to refine it all will be lower.

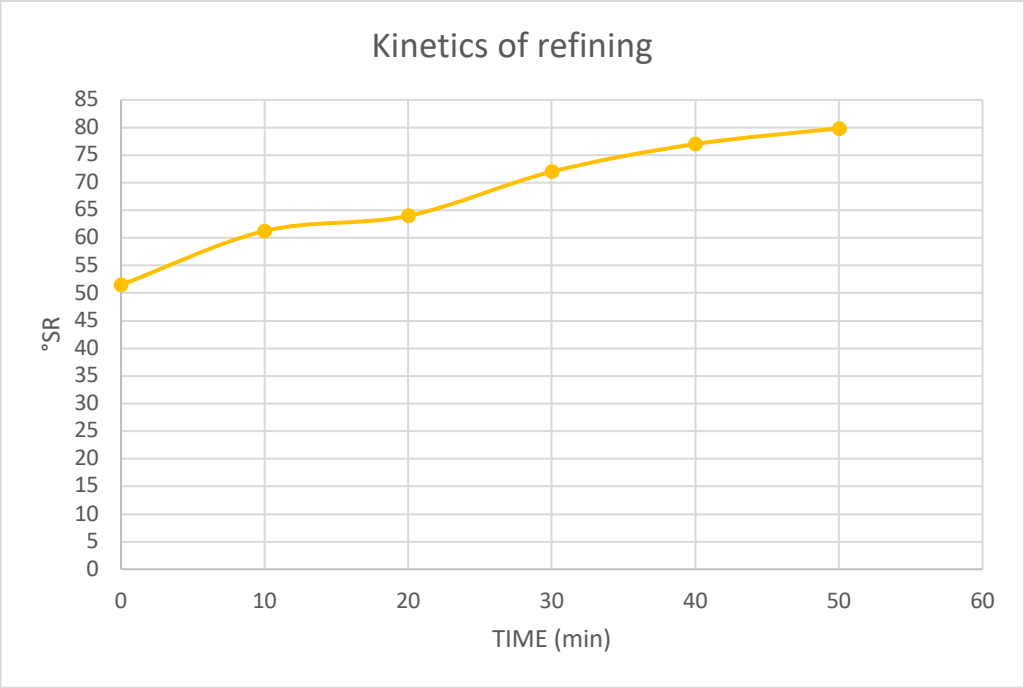

Figure 3.1: Evolution of the Schopper-Riegler degree of refining of hemp pulp at 2% wt using a fully loaded (22 liters) Valley beater.

Table 3.1: Values of the SR degree of the samples taken from the Valley beater every 10 minutes during the refining.

TIME (min)	°SR (sample A)	°SR (sample B)	°SR corrected (sample A)	°SR corrected (sample B)
0	55	52	51	52
10	61,5	63,5	60	62,5
20	66,5	66,5	64	64
30	73	76	71	73
40	77	77	75	78
50	81	81,5	79,9	80

It is important to underline that an initial value of °SR around 50 indicates that the starting pulp was pre-refined, in fact a normal initial value for raw pulp is around 20°SR.

After the enzymatic treatment and the centrifugation, a dry content between 29.2 % wt and 35% wt was reached; this was measured in accordance with the standard protocol illustrated in the subsection 2.4.1.

The yield of the entire pre-treatment, calculated with the formula 3.1, was between 88% and 91%.

$$yield\% = \left(\frac{weight\ before\ refining \cdot 2\%}{weight\ \text{after centrifugation} \cdot \%dry} \right) \cdot 100 \tag{3.1}$$

In formula 3.1 the % dry is calculated as described in subsection 2.4.1.

As discussed in chapter 1, the role of the two pre-treatment steps is of making the fibrillation easier, thus decreasing the energy demand, and of improving the quality of the MFC produced (Heiskanen et al., 2012a; Rol et al., 2020).

3.2 Analysis of the fibrillation through TSE

A first extrusion trial was carried out employing the profile A (Fig. 2.6), which provides a very high shearing, using a first batch of pre-treated hemp pulp at 35% wt of dry content. This profile has been demonstrated to be really performant in the fibrillation of eucalyptus pulp at an initial dry content of around 20% wt (Rol et al., 2020). However, the initial dry content of the hemp pulp of the present work was much higher and the more the material is concentrated, the higher will be the constraint inside the extruder during the process. For this reason, it was not possible to perform a complete extrusion using this profile: the extruder is in fact equipped with a safety system which stops the process when the torque inside the device reaches a value higher than 100 Nm. Only a small amount of MFC was obtained from this first extrusion trial, being not possible to process the entire batch of

pre-treated material because of several blocking of the system. Indeed, the torque tended to systematically increase and the process was stopped and restarted many times without being successfully completed.

With the use of profile B, instead, the extrusion was successfully completed without any blocking or interruption: two batches of pre-treated hemp pulp, with an initial dry content of 29,2% wt and 32,5% wt, respectively, were fully processed (the dry content of these two batches was adjusted around 30% wt in order to facilitate the extrusion and have a lower SME_D). Some of the fibrillated material was passed again through the extruder with the aim of understanding how the quality of the MFC could change with more than one pass.

In Tab. 3.2 the key parameters of the extrusion process (already introduced in subsection 2.3.2) are presented. As it can be noticed, during the extrusion performed with the profile B, it was possible to keep the torque at the same or lower value than in the case of profile A with the use of a lower rotational speed of the screws. Moreover, the dry flow rate of the outcoming material was higher too. This results in a much lower energy demanded by the process, quantified by the SME_D values. In the case of 2 passes through the extruder (profile B), both the SME_D required by each pass and the sum of the two (Tot SME_D) is reported; as can be noticed, even repeating the extrusion, the energy spent for the fibrillation is significantly lower when the profile B is used.

Table 3.2: Key parameters of the extrusion process; the data are given for each extrusion performed.

	35% - 1p (A)	**29,2% - 1p (B)**	**29,2% - 2p (B)**	**32,5% - 1p (B)**	**32,5% - 2p (B)**
n (rpm)	1000	700	700	700	700
$T_{average}$ (Nm)	78	70	70	75	78
Q_D (Kg/h)	0,11	0,41	0,86	0,44	0,44
SME_D (Kwh/Kg)	34,6	5,82	2,80	5,89	6,17
Tot SME_D (Kwh/Kg)			**8,62**		**12,06**
Dry content after extrusion	35 %	-	29,75 %	33,85%	34,5%

If compared to the value of above 15 kWh/kg of the SME_D required to produce MFC from enzymatically treated pulp using a grinder (Rol et al., 2017), the present TSE process (employing the profile B, Fig. 2.7) allows to spend less energy with the additional advantage of having a much more concentrated MFC (2% wt Vs. 29,75-34,5% wt).

Very recently Rol et al. (2020) demonstrated that the quality of the MFC, produced by TSE from enzymatically pre-treated eucalyptus pulp at a dry content of around 20% wt, reaches a plateau when a SME_D = 3-3.5 kWh/kg is provided. They also claimed to obtain a good quality MFC with just one pass through the TSE (same equipment of the present work) using the profile A (Fig. 2.6), with a SME_D = 2.1 kWh/kg. The SME_D presented in

Tab. 3.1 instead oscillate between 5.82 and 6.17 kWh/kg for 1 pass and between 8.62 and 12.06 kWh/kg (higher values for more concentrated MFC) when 2 passes are done. Anyway, is important to underline that the MFC produced in the present work is more concentrated, therefore requires higher values of torque to be extruded. Moreover, the hemp fibers are usually longer than the eucalyptus ones: as already mentioned in chap.1 (subsection 1.3.2) the shortest hemp fibers have a length which is not lower than 2 mm (Marrot et al., 2013), while the longest eucalyptus fibers don't even reach this value (Morais et al., 2019). A confirmation to the fact that the hemp pulp used in this work is made by long fibers can be found in Fig. 3.2 and Fig. 3.3, where respectively a photograph of a torn sheet of raw pulp and a picture recorded using the optical microscope are reported. In both figures it is clearly possible to understand how the fibers exceed 2 mm, and in Fig. 3.3 a fiber of around 5 mm can be seen. Talking about this, it is right also to clarify that two different kinds of pulp with the same °SR don't have necessarily the same mean fibers length (Bartalev et al., 2013), being the SR test based on the drainability of the fibers, which is improved during the mechanical refining by a combination of external fibrillation, formation of fines and cutting of the fibers (Motamedian et al., 2019).

Besides this, the eucalyptus pulp was refined up to 90°SR by Rol et al. (2020) before being enzymatically treated, while the hemp pulp of this work only up to 80°SR. In conclusion, both the degree of refining and the fibers length should reasonably affect the facility of processing through TSE (Heiskanen et al., 2012a), being the shorter and thinner fibers supposedly easier to be fibrillated. In support of this, one can notice how the second pass of the pulp at 29,2% wt of initial dry content through the TSE (see Tab. 3.2) produces an higher flow rate of MFC and consumes a lower SME_D than the first one. This can be explained by the fact that the material has been already extruded one time and is supposed to be made by shorter and thinner elements which are mostly fines and microfibrils, and in fact it requires a lower torque to be processed. The same behavior is not observed with the pulp at an initial dry content of 32,5% just because, together with the fibrillation degree, also the concentration of the material increases and it reaches a value in this case close to 35%, causing a consequential rise of the torque needed to extrude the material with the same rotational speed of the screws.

Furthermore, the higher crystallinity of hemp pulp (here demonstrated in the subchapter 3.2) with respect to the eucalyptus is expected to make the fibrillation even harder (Alila et al., 2013); an explanation of this can be found in chap.1 (subsection 1.3.2).

Starting from these premises, is possible to say that the production by TSE of hemp MFC at around 30% wt (or above) is supposed to be more difficult both in terms of processing and of energy required then the production of eucalyptus MFC at 20% wt.

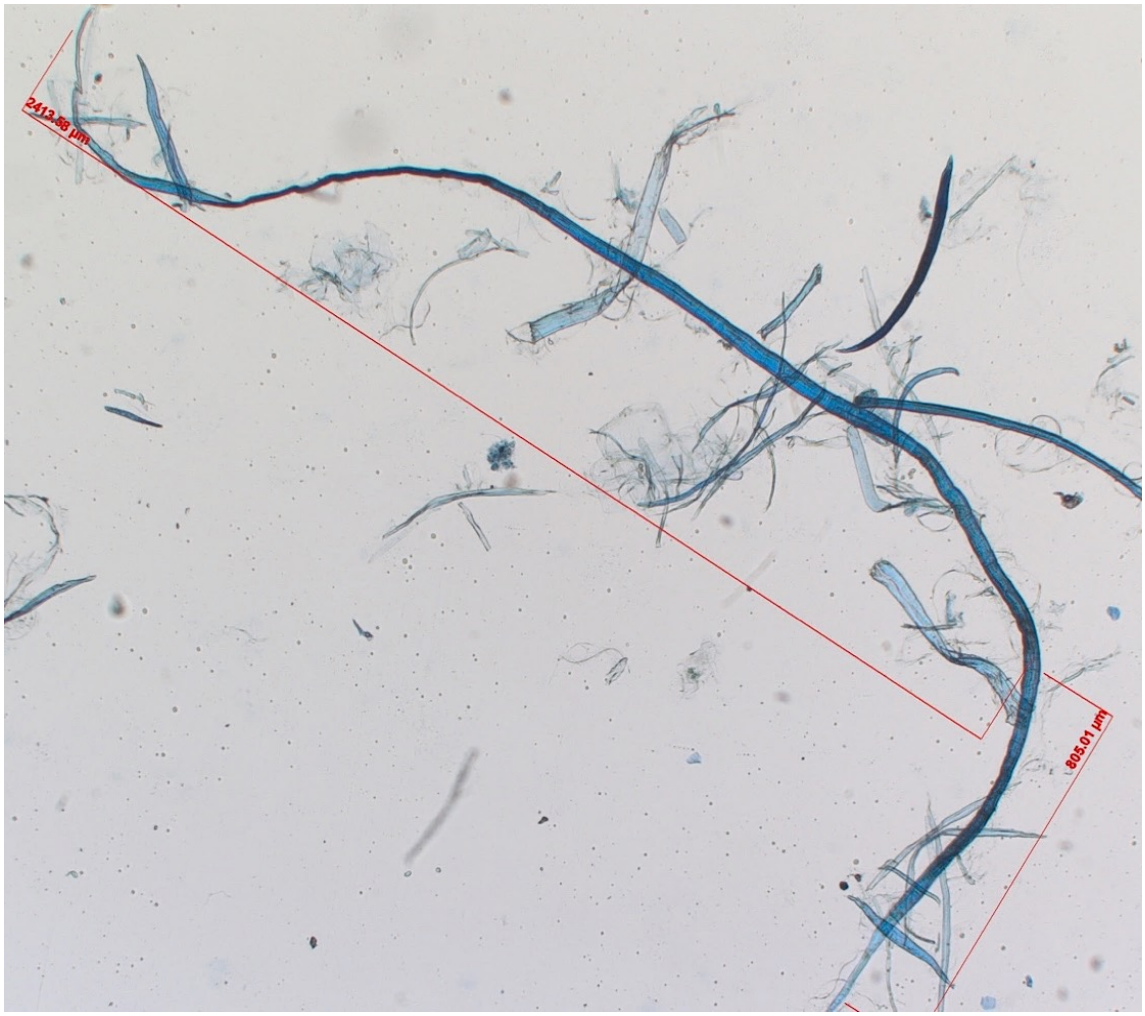

Figure 3.2: The length of a raw hemp fiber seen under the optical microscope at 50x of magnification.

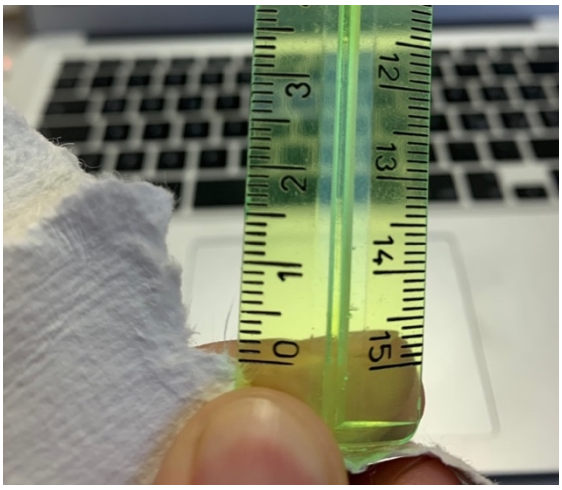

Figure 3.3: The length of a raw hemp fiber coming from a torn sheet of pulp.

Another remarkable fact is that the dry flow rates of all the outcoming MFC produced with the profile B are higher than the 0,36 kg/h reported in the previously mentioned study

by Rol et al., (2020) with the use of profile A. However, this values are influenced by the dry content of the MFC, which is higher in the case of hemp: the humid flow rate of eucalyptus MFC reported by the same authors is 1,8 kg/h, generally higher indeed than the ones obtained in the present work, which oscillates around 1,3 kg/h.

Concerning the dry content of the material after the extrusion, reported in Tab. 3.2, the measure was considered necessary because the cooling system was not able to keep the temperature around the setpoint of 10°C, especially in the middle part of the extruder, where the highest shearing is provided. This problem was observed particularly during the extrusion with the profile B, with a temperature that reached 65°C in the middle part of the extruder; this did not happen with the use of profile A, with a maximum temperature of 30°C in the same zone, just because the extrusion did not last enough time. For this reason, in the case of profile A, the final dry content was assumed to be the same as the initial one. The others % dry instead increased significantly after the extrusion, meaning that either a certain evaporation or at least a "squeeze" of the pulp occurred during the process, but no clogging of the extruder was observed.

It is also reasonable to state that no degradation of the material occurred, being the temperatures of degradation of the various components far enough from the one reached. In fact, bleached hemp fibers should start to be degraded at a temperature close to 300°C, thanks to the reduction of the hemicellulose and lignin content in favour of cellulose made by the bleaching process; however, also the latter two components usually don't start their degradation before 200°C (Pacaphol and Aht-Ong, 2017).

The cooling system, although not perfectly working, is considered anyway necessary in order to avoid a very important rise of the temperature, with a consequent further increase of the concentration of the material that could cause, prior to degradation, the clogging of the apparatus (Ho et al., 2015).

3.3 Quality and characteristics of the produced MFC

The quality of the MFC produced by TSE and the properties of the hemp pulp before the extrusion were investigated thanks to several techniques, according to the available literature (Ho et al., 2015; Rol et al., 2020, 2018, 2017).

Firstly, the CI of the raw, enzymatically treated and extruded hemp were obtained from the related XRD spectra with the method described in chap. 2 subsection 2.4.8. The same analysis was performed on three samples of eucalyptus which had been previously subjected to the same steps of processing.

The results are reported in Tab. 3.3 and the values are compared. As it can be noticed, hemp is intrinsically more crystalline than eucalyptus, even more so taking into account that its raw pulp was pre-refined and at 50°SR, while the eucalyptus was around 20°SR: the mechanical treatment indeed is supposed to produce a decrease of the CI (Van Hai et al., 2013). Besides this, hemp's CI increases even more (in proportion 7,7% Vs. 3% of increase) than the eucalyptus one after the enzymatic hydrolysis. The general increase of CI after this treatment is anyway expected because the enzymes employed, namely the endoglucanase, attack the amorphous zones of the fibers (Missoum et al., 2013).

Anyway, the crystallinity decreases significantly after the extrusion through the profile A: precisely there is a reduction of 13,4% for the eucalyptus and of 22,4% for the hemp. This difference can be associated to the different concentration of the two pulps before the extrusion, and, consequently, the higher torque and SME_D to which the hemp is subjected,

especially using the profile A. In fact, the eucalyptus pulp was at around 20% wt of dry content before being introduced inside the TSE: this is because the concentration of this kind of pulp typically doesn't reach an higher value, although centrifugated in the same way of hemp, being more hydrophilic: this is a confirmation of the fact that the eucalyptus fibers are generally shorter and thinner than the hemp's ones, and, having an higher specific surface, they have also an higher number of external OH groups.

Table 3.3: A comparison of the CI of eucalyptus and hemp at each step of processing

	CI - Hemp (35%)	**CI - Eucalyptus (20%)**
Raw	76,1 %	70%
Ref-Enz	82,5 %	72,2%
MFC (A)	64 %	62,5%
MFC (B)	?	?

The average characteristics of the films obtained with the different kind of MFC and with the enzymatically treated hemp pulp are reported in Tab. 3.4.

In Fig. 3.4 is possible to see a MFC's nanopaper produced without putting the suspension in ultrasonic bath before the vacuum filtration: as it can be noticed, many white dots are visible. These dots disappeared with the use of ultrasonic bath, suggesting that they were probably caused by air bubbles that are consistently formed during the stirring processes, especially with the employment of the Ultra-Turrax®.

At least two good quality films were produced both from enzymatically treated pulp and from each kind of MFC obtained using the extrusion profile B, while only one with the MFC obtained using the profile A. In this latter case in fact, the amount of fibrillated material was very low and not enough for more nanopapers production. Examples of the nanopapers produced with the MFC obtained using the profile B are reported in Fig 3.5.

Figure 3.4: A nanopaper prepared without putting the MFC suspension in ultrasonic bath before the vacuum filtration.

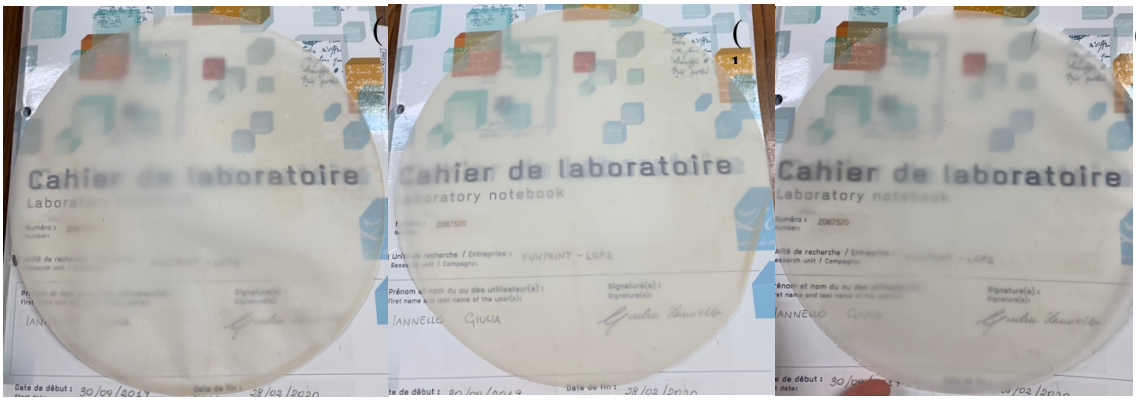

Figure 3.5: Nanopapers made by the MFC produced with the use of the extrusion profile B – (a): 29,2% - 2p; (b): 32,5% - 1p; (c): 32,5% - 2p.

The time required for each vacuum filtration necessary to produce a film was between 1/2 an hour and 3 hours depending on the degree of fibrillation: that means the better the quality of the MFC, the longer the filtration. This seems reasonable if we think about the fact that the fibrils have an higher specific surface than the original fibers and so an higher number of available hydroxyl groups that lead to an enhanced hydrophilicity (Ho et al., 2015).

Table 3.4: Properties of the produced films.

	Ref-Enz	**35% - 1p (A)**	**29,2% - 2p (B)**	**32,5% - 1p (B)**	**32,5% - 2p (B)**
Transmittance (%)	0,61 ± 0,05	11,52 ± 0,14	4,62 ± 0,19	7,83 ± 0,18	12,3 ± 0,5
Grammage (g/mm^2)	64,8 ± 4,1	58,2 ± 0,7	67,7 ± 6,2	66,3 ± 0,4	70 ± 1
Thickness (µm)	96 ± 6	64 ± 4	76 ± 0,005	64 ± 3	72 ± 5
Young's Modulus (GPa)	4,44 ± 0,25	3,99 ± 1,1	5,87 ± 0,24	6,65 ± 0,24	?
Elongation at break (%)	0,77 ± 0,19	0,458 ± 0,07	0,61 ± 0,12	0,28 ± 0,07	?
Tensile strength (MPa)	19,8 ± 1,33	14 ± 2,3	29 ± 6,8	15,6 ± 2,94	?

As it's possible to notice in Tab. 3.4, the films produced with non-fibrillated pulp have a transmittance close to 0 %, while this property increases with the processing inside the extruder. The transmittance is strictly correlated to the transparency of the nanopapers, which is due to the fact that tightly packed nanosized elements do not scatter the light; the higher is the fibrillation degree of the MFC, the more transparent will be the related film (Chinga-Carrasco, 2013; Rol et al., 2018).

Comparing the MFC obtained with 1 or 2 passes from the pulp at 32,5% wt of initial dry content, it can be seen how the second pass improves the transmittance of the nanopapers. But having a look at the MFC produced from the pulp at a lower dry content (29,2% wt – 2p (B)) it seems that the 2 passes didn't ensure the same degree of fibrillation of the pulp at 32,5% wt, leading to a transmittance even lower than the sample extruded just one time (32,5% - 1p (B)). This can be again explained by the higher shear that a more concentrated pulp causes inside the extruder, which is also demonstrated by the values of the torque and SME_D reported in Tab. 3.1, higher indeed in the case of the 32,5% wt pulp. Essentially, giving more energy to the material means enhancing the fibrillation (Rol et al., 2020). The same conclusion can be deduced looking at the mechanical properties of the films: the highest Young's Modulus and the low strain at break and tensile strength suggest how the behavior of the more concentrated MFC is less ductile, being more fibrillated and so reasonably more crystalline (Ho et al., 2015; Kukle et al., 2013; Wang et al., 2007).

An additional proof is given by the comparison of the average thickness and grammage of the two kinds of nanopapers: while the grammage is almost the same, the thickness is 12 µm higher for the samples "29,2% - 2p (B)" than for the ones "32,5% - 1p (B)". This can be due to the fact that these last nanopapers, being made by more fibrillated MFC, are constituted by thinner elements than the other ones.

The values of the mechanical properties of the two-times extruded MFC at the highest dry content (32,5% - 2p (B)) are missing because of the interruption of the research work (see

the introductive chapter for more explanation), but the behavior just illustrated is expected to be even more accentuated than in the case of 1 pass, as it can be deducted from the highest transmittance that this MFC presents (even presenting the highest grammage).

The mechanical behavior of the different kinds of material is also highlighted in Fig. 3.6, where some of the traction curves resulting from the tests are reported as example: the light ductility observable in the non-fibrillated sample (Fig. 3.6a) basically disappears with the increase of the fibrillation degree, and the curves get closer to the straight lines, the slope of which represents the elastic modulus.

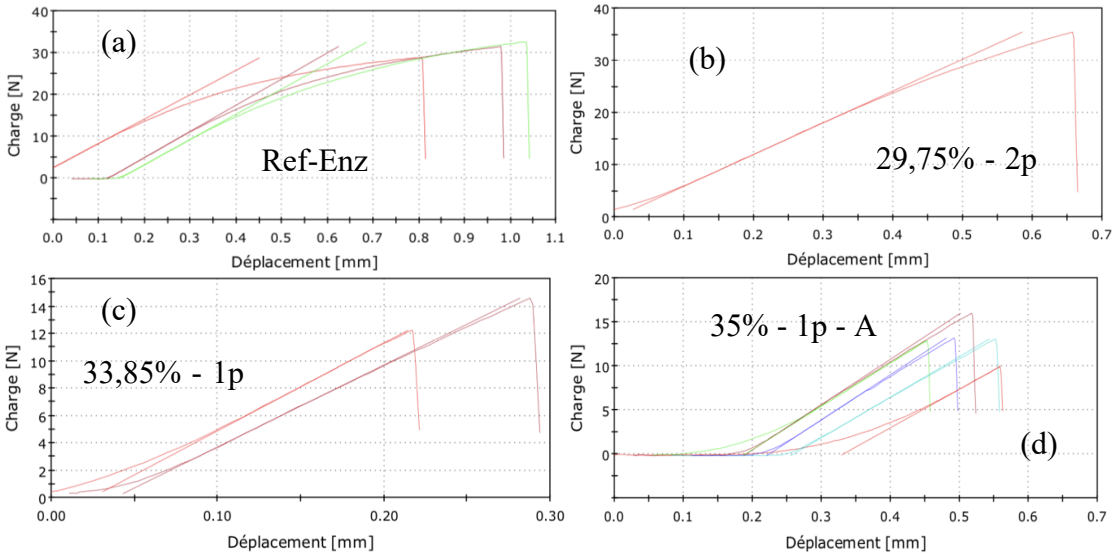

Figure 3.6: Some of the traction curves are reported (as example) for the different kinds of materials (déplacement = displacement; charge = load).

In general, the values of the Young's Modulus obtained in this study are higher compared to the ones reported by Ho et al. (2015), but lower than the ones obtained by Rol et al. (2020), even if the just cited missing value (the modulus of the sample 32,5% - 2p (B)) is supposed to be promising. The transmittance of the nanopapers at 550 nm is also generally lower compared to what the latter authors reported, but it's important to precise that they measured this property on casted films with a grammage of 45 g/m^2 , while the grammage of the nanopapers of the present work is about 50% higher.

A separate argumentation is needed for the MFC produced using the extrusion profile A. The Young's Modulus of the corresponding nanopaper is even lower than the one reported for films made by non-extruded pulp. Moreover, the standard deviation of more than 1 GPa proves the inhomogeneity of the material due to the instability and discontinuity of the extrusion performed with that profile. Anyway, the value of the strain at break induces to think that a certain fibrillation occurs. Also the transmittance is quite good, even if it is necessary to notice that its grammage is much lower than the ones of the other nanopapers. So, having a look at how much the CI decreased after passing the hemp pulp only one time through the profile A (Tab. 3.3) and also at the tensile strength that is the lowest reported, it seems right to suggest that a such aggressive shearing coupled with a dry content of 35% wt, partially de-structured the crystalline regions of the hemp fibers with a negative impact on the mechanical properties (Ho et al., 2015).

The turbidities (NTU) of 0,1% wt suspensions of the different MFCs in water are reported in Tab. 3.5. This property is an index of the fibrillation degree of the material, in fact the higher is the amount of residual fibers, the higher will be the turbidity; on the contrary, the smaller elements make it decrease (Chinga-Carrasco, 2013; Rol et al., 2018).

According to the available literature, the values of turbidity are usually higher for the MFC produced by TSE rather than by other processes. In this case they are also higher than the value of 397 ± 23 NTU reached by Rol et al. (2020) extruding one time a pre-treated eucalyptus pulp (around 20% wt dry) through the profile A (Fig. 2.6). These results, in addition to the ones already discussed, suggest that the same degree of fibrillation reported by these authors was not achieved. Indeed, considering the CI in Tab. 3.3, a higher Young's Modulus than the eucalyptus is expected from a more fibrillated hemp pulp. Nevertheless, this goal is not easy to be reached, since it has been demonstrated that a good percentage of amorphous components could facilitate the fibrillation (Alila et al., 2013).

The turbidities obtained are however in accordance with the entire already exposed argumentation, confirming that an additional pass through the extruder improves the fibrillation degree for the pulp at an initial dry content of 32,5% wt, but it is not enough to have the same result for the pulp at 29,2% wt. The lowest turbidity belongs to the suspension made by the MFC produced with the profile A, and this also proves that its poor mechanical properties are not due to inadequate fibrillation.

Table 3.5: Turbidities (NTU) at 0,1% wt dry content of suspensions MFC-water.

35% - 1p (A)	**29,2% - 2p (B)**	**32,5% - 1p (B)**	**32,5% - 2p (B)**
448,5 ± 13	660,4 ± 14,5	564,6 ± 13,8	462,4 ± 9,1

The three kinds of MFC produced using the profile B were analyzed by the MorFi® apparatus. It is important to underline that this type of analysis is not able to detect the nanosized elements because of a minimum resolution of 5 μm. However, it is useful to evaluate the number and the morphology of residual fibers and fines which can give an idea about the different degree of processing of the MFC (Rol et al., 2020, 2018).

The results given by the MorFi® are presented in Fig. 3.7 and summarized in Tab. 3.6. From the first line of the table it is possible to see how the MFC with the best quality (32,5% - 2p) has the highest number of fines and the lowest number of residual fibers; these few remaining are still quite thick and long, as it can be noticed from the fibers length and width distribution (Fig. 3.7a,b), while in the case of the fines, the shortest lengths prevail in this MFC (Fig. 3.7c). On the contrary, the MFC with the worst quality (29,2% - 2p) has still a significant amount of residual fibers, although most of them have the lowest lengths and widths (Fig. 3.7a,b), and its fines are generally longer than the ones of the other two samples. The "32,5% - 1p" sample presents instead intermediate characteristics, like halfway stands its quality. These results clearly demonstrate how better properties of the MFC are obtained thanks to the higher degree of fibrillation that a more processed material reaches. Trends illustrated in Fig. 3.7 are in accordance with the mean fibers length and width and with the fines length which can be found in Tab. 3.6. Even if the fines content of the "29,2% - 2p" sample one is slightly higher than the value of the "32,5% - 1p", it is good to take into account that this last sample can contain

actually more nanosized elements which are not detected by the MorFi's camera. The difference in fibrillation is however well underlined by the fibers contents.

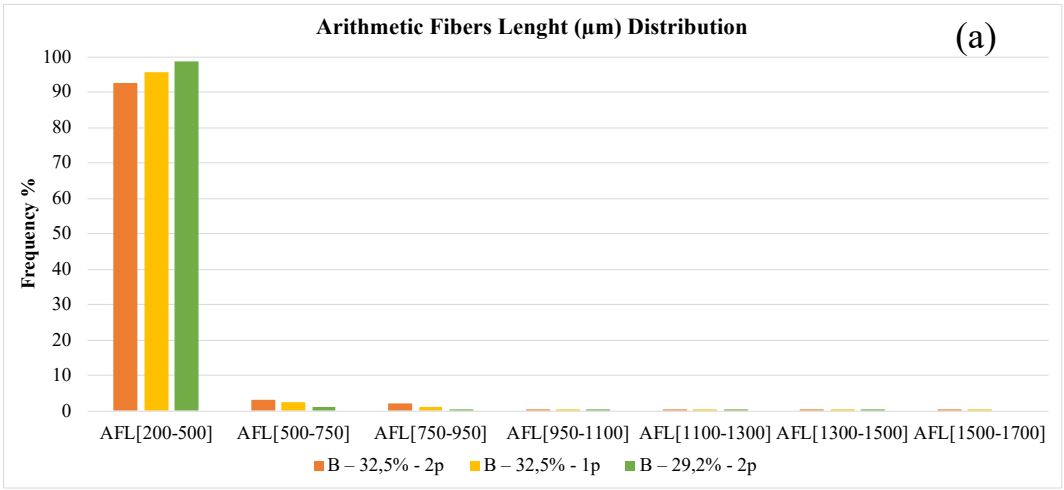

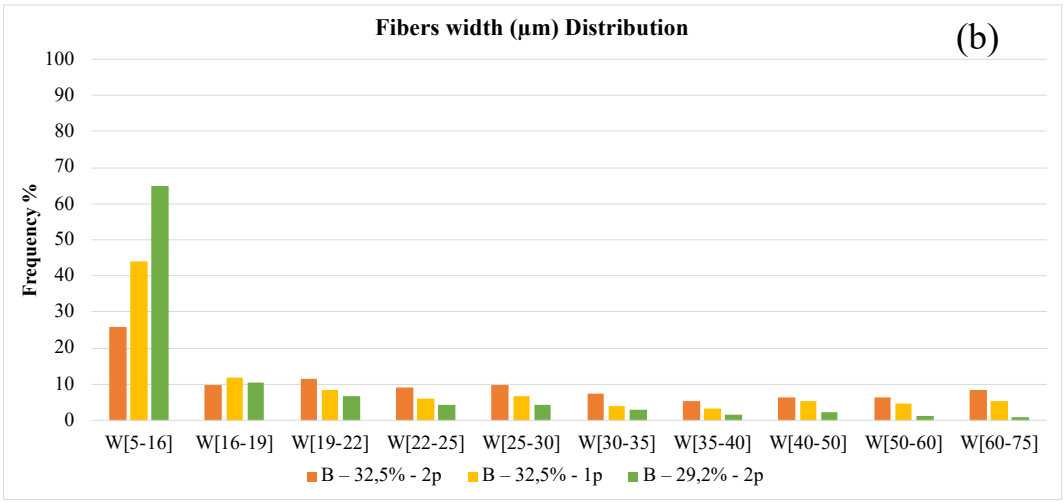

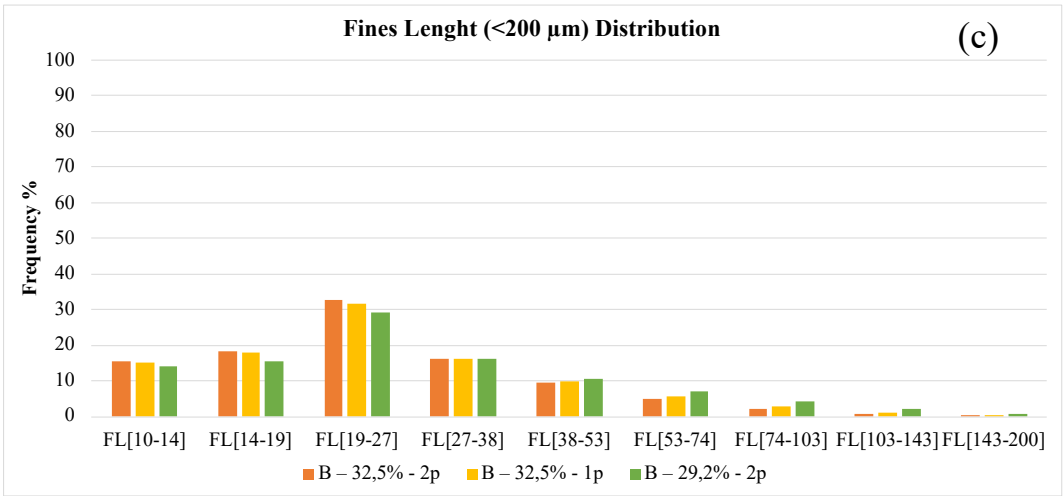

Figure 3.7: Distribution of the arithmetic fibers length (a), fibers width (b) and fines length (c) of different MFCs analyzed by the MorFi.

Table 3.6: Key results of the MorFi® analysis.

	B – 32,5% - 2p	**B – 32,5% - 1p**	**B – 29,2% - 2p**
Fiber content (millions/g of pulp)	0,11	0,27	1,45
Fines content (millions/g of pulp)	3577,26	3216,66	3236,35
Mean arithmetic fiber length (μm)	303,67	282,33	273,00
Mean fiber width (μm)	28,17	23,17	16,20
Mean fine length (μm)	27,33	28,67	32,33

The most representative pictures captured by optical microscopy are reported in Fig. 3.8 to 3.11. Even if the optical microscopy is not able to furnish a global visual of the morphological characteristics of the material (Chinga-Carrasco, 2013), the images can anyway be helpful to understand how the processing changes the aspect of the fibers.

In Fig. 3.8 the effect of the pre-treatments on the hemp pulp is evidenced: the treated fibers appear shorter and externally fibrillated compared to the raw ones thanks to the coupling of mechanical refining and enzymatical hydrolysis (Motamedian et al., 2019; Siqueira et al., 2010). From Fig. 3.9 to 3.11 is possible to understand how the aspect of the material changes completely after being passed through the TSE. The different MFCs obtained are compared at various magnifications, and the images are in accordance with what has been discussed so far: some big elements are still present in the sample "B - 29,2% - 2p" and in Fig. 3.11b even a partially fibrillated fiber can be distinguished. In the sample "B - 32,5% - 1p" few residual fibers can be noticed, but their amount is reduced with an additional pass through the TSE, as the pictures related to the sample "B - 32,5% - 2p" show. Moreover, the microscope analysis confirms the fact that the MFC produced using the profile A has a good degree of fibrillation, which is not responsible of the poor mechanical properties.

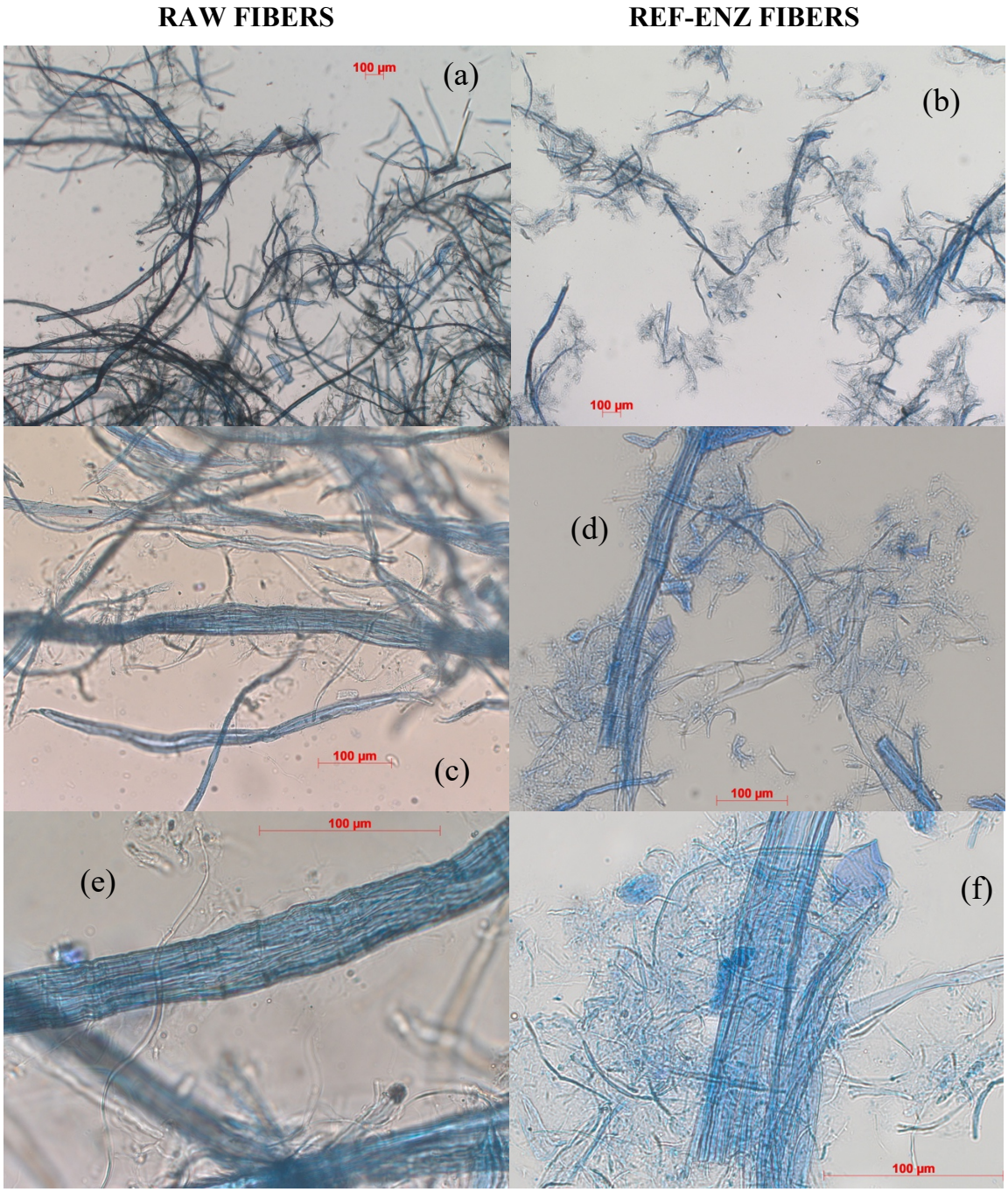

Figure 3.8: Hemp raw and pre-treated fibers are compared with the optical microscope at different magnifications: 50x (a) and (b), 200x (c) and (d), 500x (e) and (f).

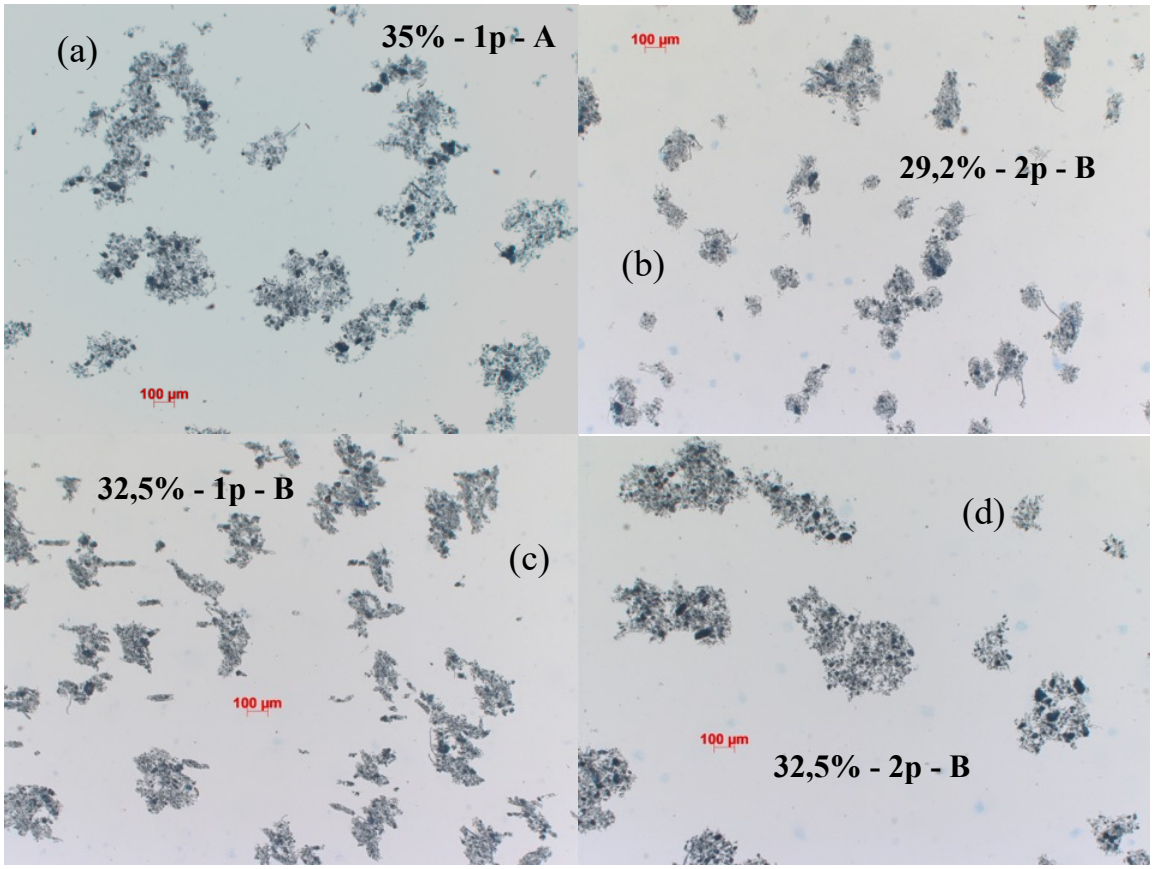

Figure 3.9: The different MFCs produced are compared with the optical microscope at 50x of magnification.

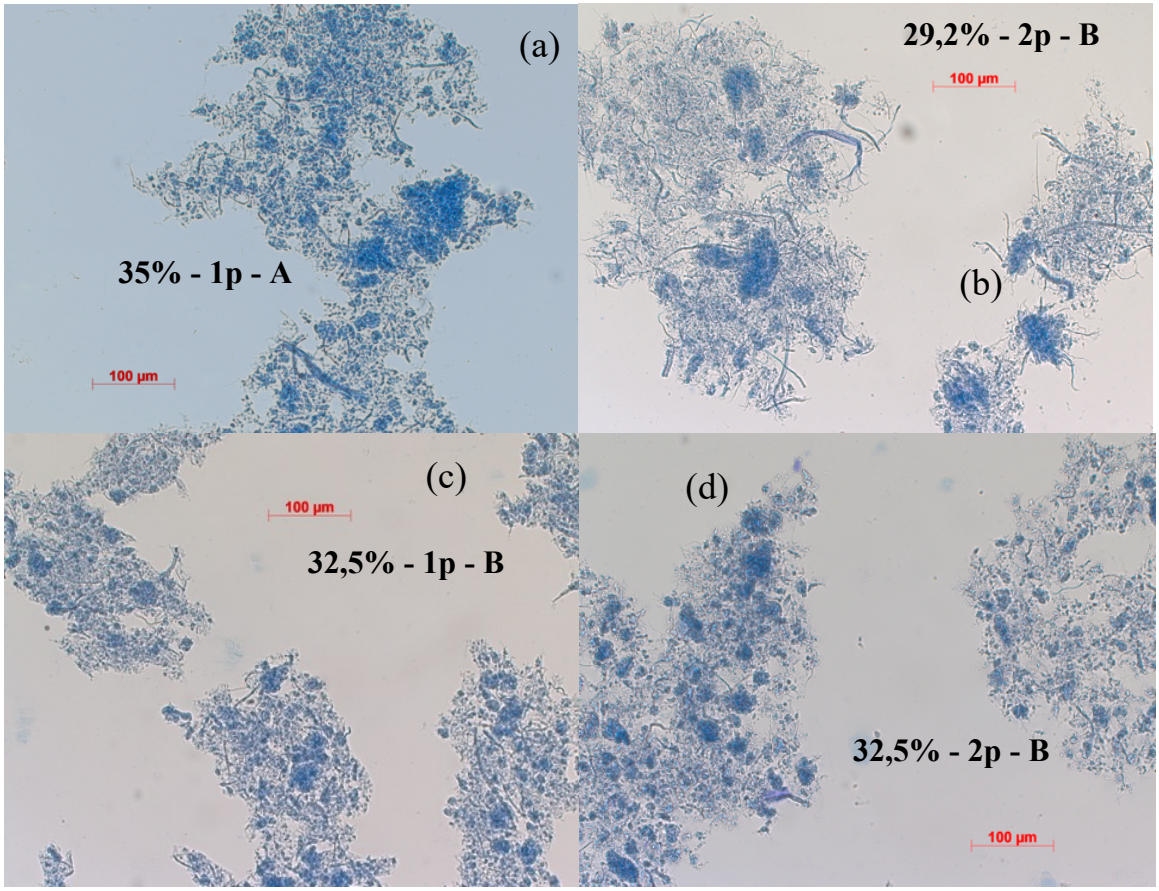

Figure 3.10: The different MFCs produced are compared with the optical microscope at 200x of magnification.

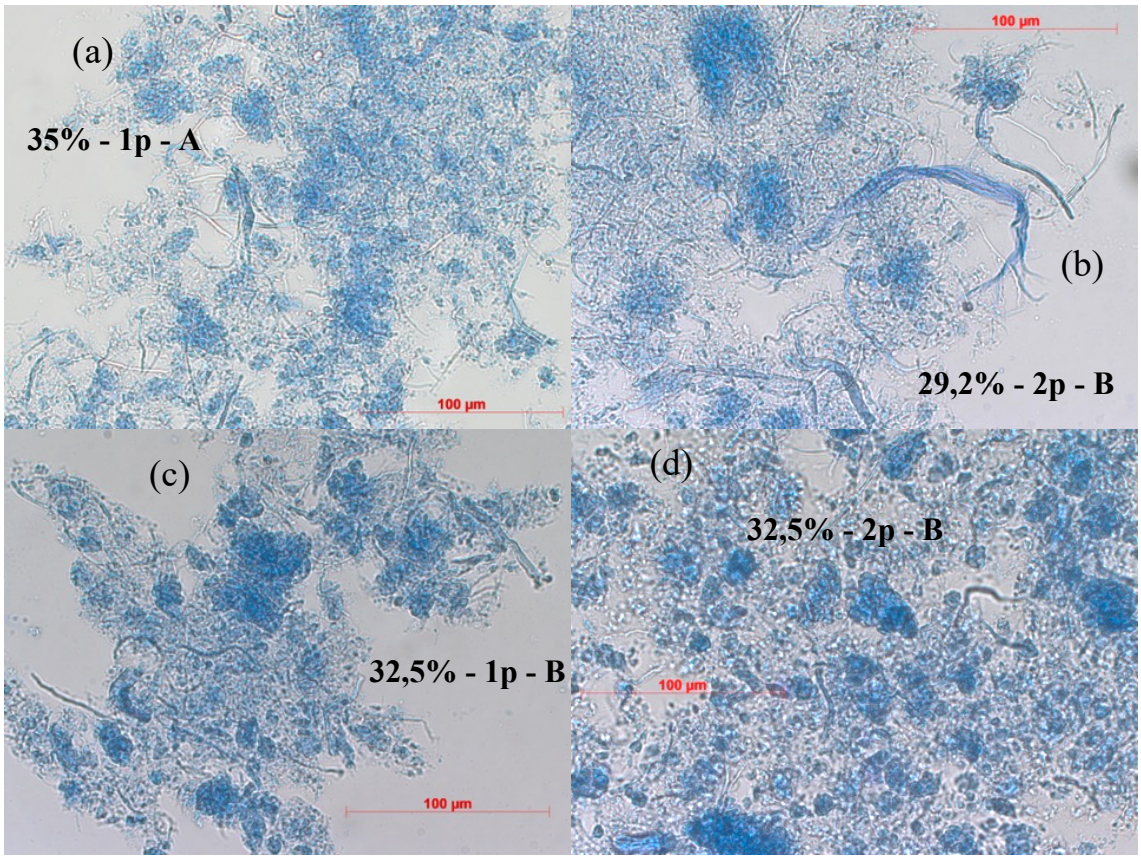

Figure 3.11: The different MFCs produced are compared with the optical microscope at 500x of magnification.

3.4 The printing paste

Since the mixing with a planetary blender was not sufficient to have a good dispersion of the MFC agglomerates inside the resin, two different methods (illustrated in chap. 2 subsection 2.5.1) were tested.

The Ultra-Turrax® high-speed mixer was effective only with up to 20% wt of MFC, while at higher concentrations the method turned out to be inefficient to finely disperse the fibrils: even using a nozzle with a diameter of 1 mm, the 3D printing was unfeasible because of the clogging of the apparatus.

Therefore, a three-roll milling machine was employed for the pastes with a MFC content of 25% and 35% wt, thus obtaining much better results that are presented in Fig. 3.12 and 3.13.

Even with the naked eye, many MFC agglomerates can be seen in the sample which had not been passed yet through the three-roll machine (Fig. 3.12a), but their quantity noticeably decreased in both pastes (Fig. 3.12a,b) in a gradual manner after different passes. The effect of this treatment is also visible in Fig. 3.13, where the aspect of the paste at 35% wt of MFC is seen under a binocular magnifier after different number of passes through the machine: it is easy to notice how the pressure between the cylinders favors the dispersion of the MFCs, even if 3 passes are not enough to make the paste completely homogeneous, leaving rather darker and lighter zones.

The secondary effect of this type of processing was a significant increase of the viscosity of the pastes as the natural consequence of a better dispersion of the microfibrils, that

gradually improved after each pass. Before being passed through the rolls, the paste consisted only of a resin with many roughly spherical particles inside (Fig. 3.12a), which were destroyed during the processing, letting out the microfibrils.

The change in the paste visual aspect and viscosity is clearly shown in Fig. 3.12 and it occurred for both the formulations, even if a higher viscosity was achieved with the more concentrated paste. When comparing the two samples after 4 passes, it can be clearly seen how the paste at 35% of MFC (Fig. 3.12b) has different rheological properties than the one at 25% and it is also less shiny. The difference is obviously due to an higher presence of microfibrils, which supposedly start to form a network inside the PFA matrix involving their outward hydroxyl groups.

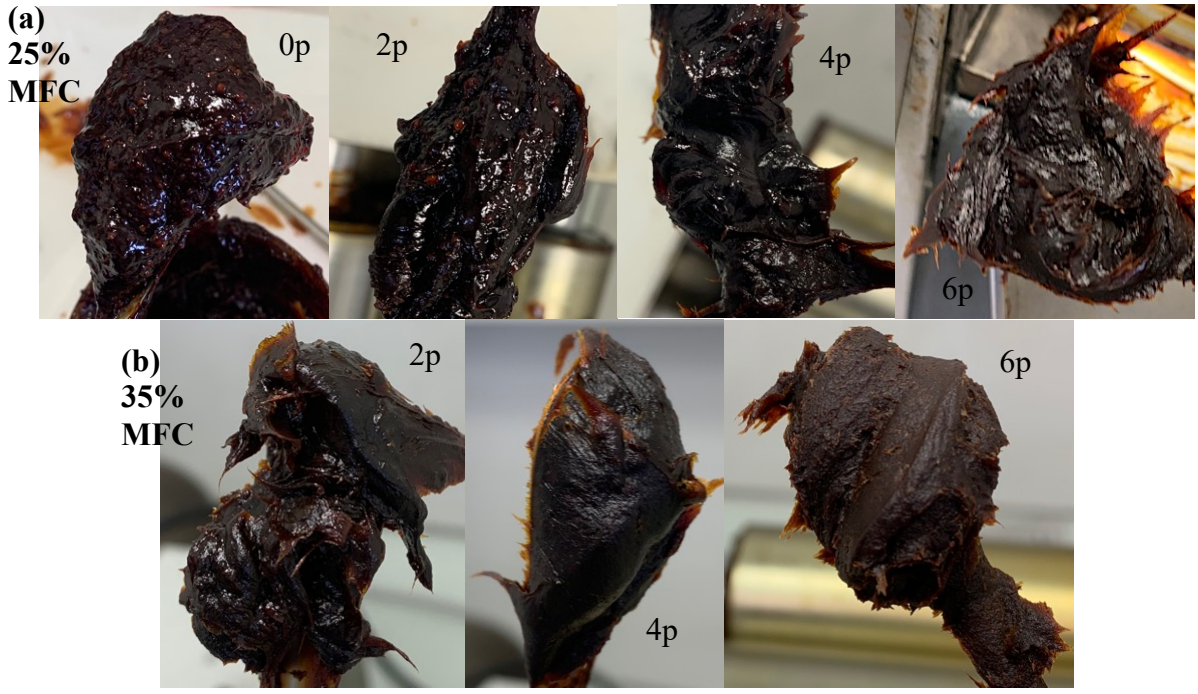

Figure 3.12: The aspect of the two highly concentrated pastes after different number of passes through the three-roll milling machine.

The rheology of the pastes was further investigated with a rheometer, in order to understand if the addition of MFCs induces a thixotropic behavior in the PFA paste, which is fundamental for the 3D printing. In fact, the viscosity must decrease when a stress is applied, in order to allow the extrusion through the nozzle, and must be recovered after a while so that the printed layers can maintain a certain shape fidelity.

The MFC suspensions are known to have a pronounced shear-thinning behavior, which arises especially at high shear rates. At rest as well as at low shear rates, the microfibrils form a network (Martoïa et al., 2015; Schenker et al., 2018). Below a certain value of stress, namely the "yield stress", the MFC network is responsible for the viscoelastic behavior of the suspension: "viscous" thanks to the relative movement between the microfibrils which dynamically interact each other, and "elastic" because of the stretching of the single fibrils and the entire network when a stress is applied (Schenker et al., 2018).

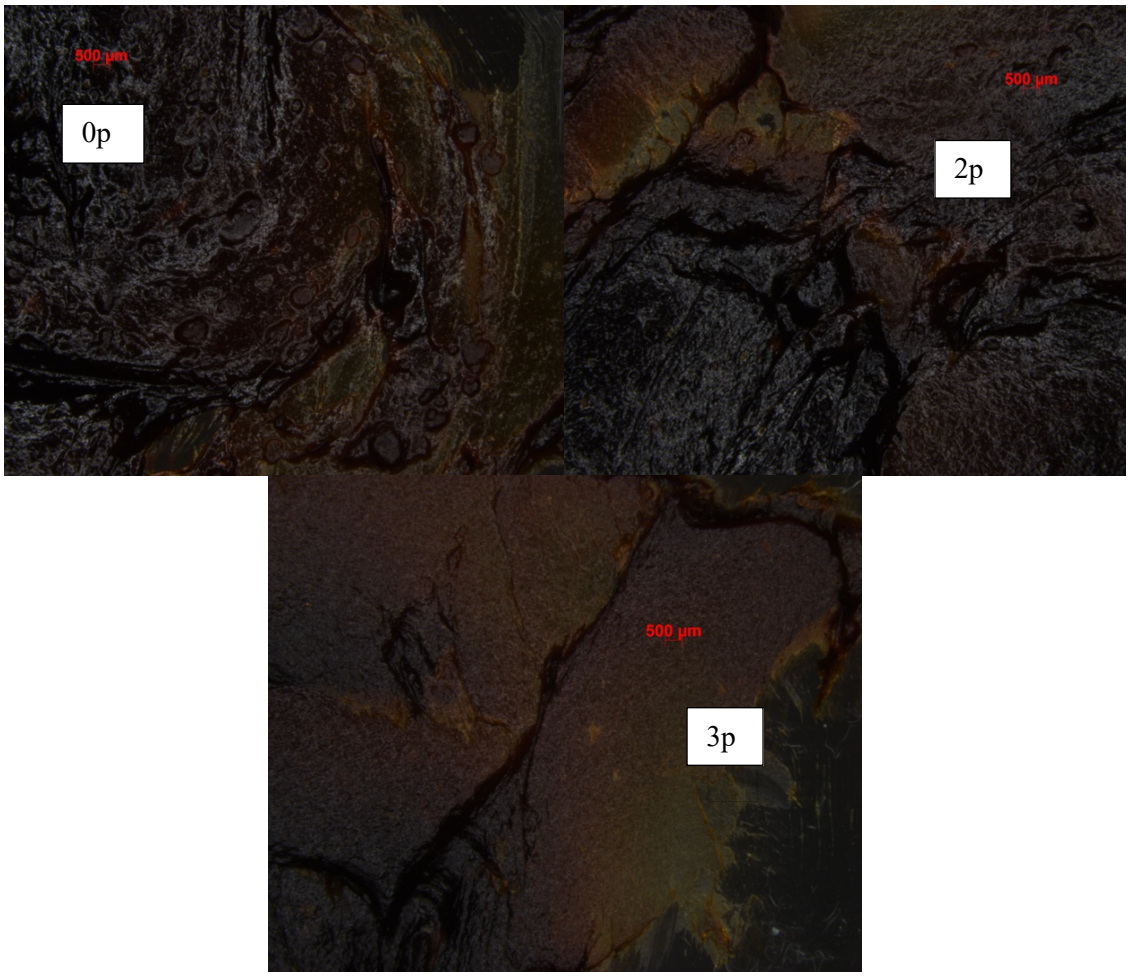

Figure 3.13: Changing of the aspect of the 35% MFC paste, seen under a binocular magnifier at 7,5x of magnification, after different number of passes through the three-roll milling machine.

In Fig. 3.14a the results of the tests conducted on the pastes containing up to 20% wt of MFC are illustrated. As it can be noticed, the pure PFA resin showed a Newtonian behavior, which turned to a thixotropic one even with the addition of only 5% of MFC; also the zero shear viscosity increased, as expected, each time that more MFC was added. The shear thinning behavior of the pastes is well demonstrated by the curves, which show a gradual decrease in viscosity as a consequence of the increasing shear rate. Moreover, every initial value of viscosity was fully recovered when the minimum shear rate of 0,1 s^{-1} was restored.

To provide a more rigorous characterization, the power-law model (also known as "the Ostwald-de Waele model") was applied to each viscosity curve (Fig. 3.14b). This model is useful to model the rheological behavior of fluids under shear and can be synthetized by the equation 3.2:

$$\eta = K \cdot \gamma^{n-1} \tag{3.2}$$

where K is the consistency factor and n is the power-law index, while η and γ are respectively the viscosity and the shear rate. A value of $n < 1$ represents a shear thinning behavior (pseudoplastic fluids), a value of n close or equal to 1 represents a Newtonian behavior, and $n > 1$ indicates instead a shear thickening behavior (dilatant fluids) (Ng et al., 2019).

The equation of each fitting curve is reported in Fig. 3.14b (same color of the corresponding real curve) and next to it one can find the R^2 value, which is an index of how close the real curve is to the fitting one. The values of the parameters of the power-law model derived from the equations, as long as the R^2 values, are also summarized in Tab. 3.7. It is possible to establish from the R^2 values that the model is not suitable for the pure PFA resin (R^2 = 0,36), while it starts to provide a very good fitting when a small amount of MFC, namely 5% wt, is added. At 20% of MFC the power-law seems to predict almost perfectly the behavior of the paste. The power-law indexes (n) reported in the table confirm that the pure PFA has a Newtonian behavior which shifts into a shear-thinning one with the addition of MFC. Then, the higher is the MFC content of the pastes, the more pseudoplastic is the fluid we are dealing with (lower n).

Table 3.7: Parameters of the power-law model for pastes at different % wt of MFC

	0% MFC	**5% MFC**	**10% MFC**	**20% MFC**
K	7,05	21,18	81,61	204,02
n	0,979	0,694	0,473	0,318
R^2	0,361	0,966	0,974	0,988

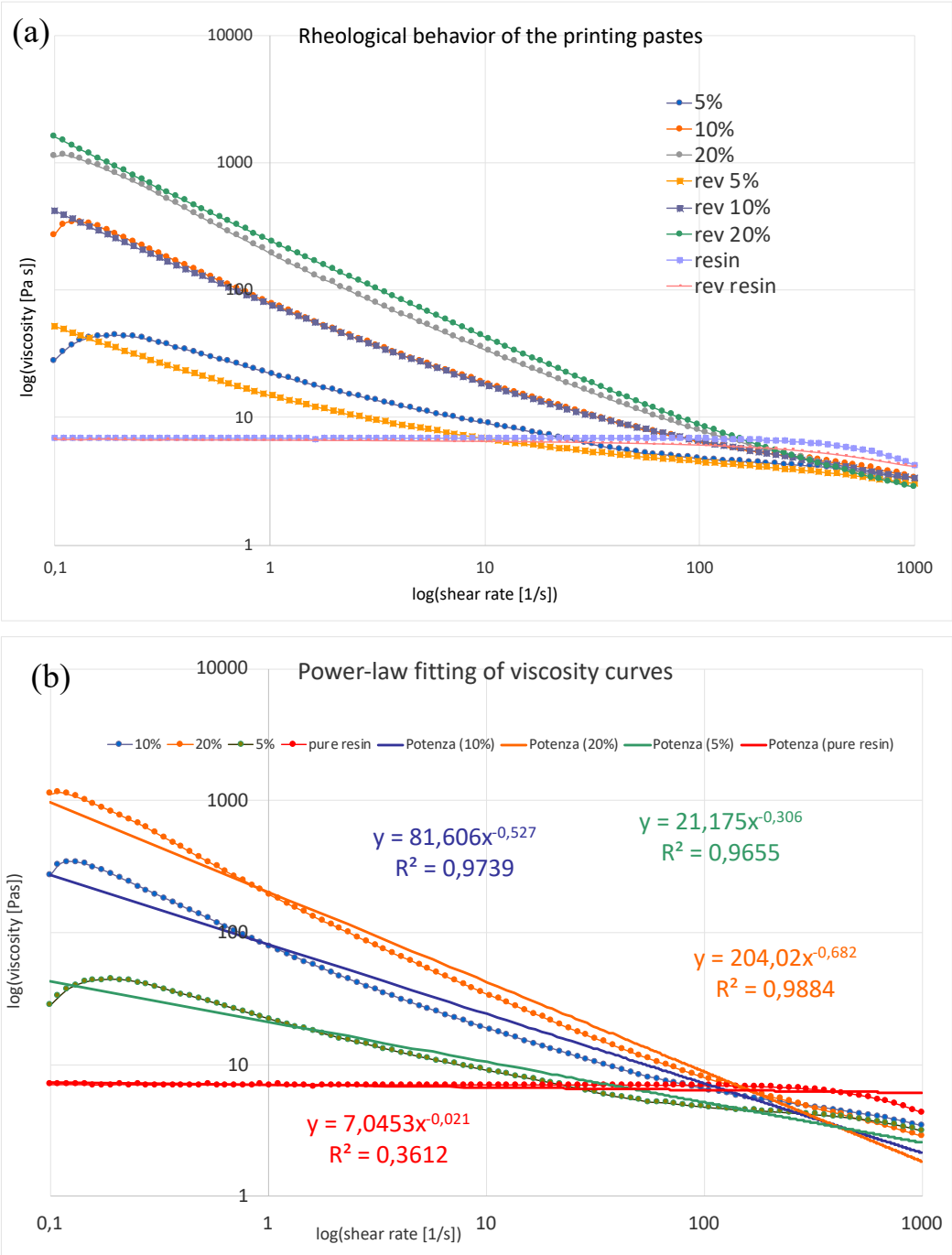

Figure 3.14: Rheological behavior of the printing pastes at different concentrations of MFC: comparison in log scale increasing and decreasing the shear rate (a); power-law fitting of the viscosity curves (b).

In Fig. 3.15 the evolution of the shear stress as a function of the shear rate is illustrated for the paste at the lowest content of MFC (as an example): also this graphic reveals the pseudoplasticity of the fluid, with a gradual decrease of the slope of the curve, namely the viscosity, as the shear rate is increased.

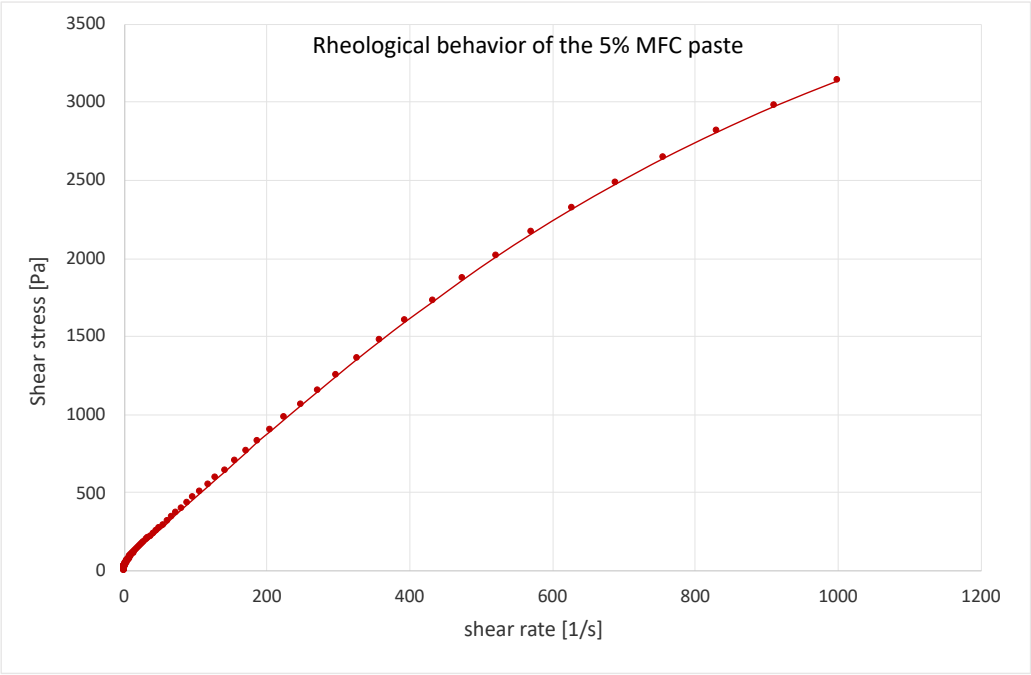

Figure 3.15: Rheological behavior of the 5% MFC printing paste: shear stress Vs. shear rate.

From 25% wt of MFC onwards, the paste had an aspect that induced to consider it printable. A particular test reported in Fig. 3.16 was performed in order to see the capability of these pastes of recovering their viscosity after the application of a step-shaped shear variation. In fact, even if a certain thixotropic behavior had been already demonstrated by the test reported in Fig. 3.14a, this different testing approach (Fig. 3.16) was considered useful because during a 3D printing process the shearing is not increased and decreased gradually, but instead it is applied constantly during the extrusion through a syringe and a nozzle and then immediately removed when the filament comes out. Therefore, a sort of simulation of this phenomenon was tried. Anyway, as it can be noticed from the related graphic, the intervals of 60 seconds were not long enough to make the test trustable: the plateaus of viscosity were never reached in any interval, so that its proper values were not determined in none of the two pastes. Moreover, looking only at what the curves suggest, it seems that the most concentrated paste (35% wt of MFC) is not able at all to recover its viscosity, while the behavior is just a bit better for the one at 25% of MFC, which however doesn't get close to the initial value and loses almost totally this capability after being sheared at 500 s^{-1} for the second time.

What happens is actually that, when the initial γ = 0,1 s^{-1} is imposed the microfibrils are gradually separated and, if the steady-state was reached, a new structure in which the MFCs continuously lose and recreate contact, stabilizing the viscosity, would had been formed (Martoïa et al., 2015). Instead, the subsequent shearing at 500 s^{-1} basically destroys the MFC network ($\eta \cong 0$ Pa s). The network was being rebuilt during the second interval at γ = 0,1 s^{-1} (t = 120-180 s), as the slowly increasing viscosities demonstrate, but the steady-state was not reached neither this time. Thus, completing the destruction of the network was even easier when the maximum shear was applied once more (t = 240-300 s), in fact the viscosities barely increased.

Concerning the slow kinetics of the 35%-MFC paste in recovering its viscosity, this can be explained by the fact that less strain is needed to create higher stress at this concentration: as well clarified by Schenker et al. (2018), increasing the number of fibrils

per unit volume means also increasing the fibrils contact points and so having a shorter distance between every contact point. The induced stress is greater, so a lower strain is necessary to break the contact and cause the yielding of the network. This could justify both the more marked slope of the first segment of the curve (compared to the other one), meaning that, despite the higher initial viscosity, the decreasing is faster, and the slower capability of recovering the viscosity. In addition, the formation of clusters of microfibrils could be present and more pronounced than in the other paste as consequence of their higher concentration. In fact, it was demonstrated by some other studies that high shear rates can lead to a sort of "flocculation" of the microfibrils, with the formation of clusters in which they are physically entangled. These "flocs" and the depleted parts inside the matrix (voids) grow with increasing shear rate up to a maximum, then their size decreases and the voids begin to be filled again (Schenker et al., 2018).

Furthermore, one must take into account that during these tests at high shear rates a phase separation can occur, with the formation of a film of PFA (poor of microfibrils) on the plates which acts like a lubricant, concealing so the real behavior of the paste.

In conclusion, because of the all just explained issues, more tests with a step-shaped shear variation (and maybe with other systems of measurement) are needed to obtain reliable results. Despite this, the plot of Fig. 3.16 can be useful to confirm that: (i) adding more than 20% wt MFC in PFA results in an additional increase of the viscosity of the paste (more than 4000 Pa s at $\gamma \cong 0\ s^{-1}$); (ii) a thixotropic behavior is still present, like suggested by the first part of the curves, characterized by a progressive decrease of the viscosity when the pastes are sheared from 0 to 0,1 s^{-1} (first interval, 0-60 s).

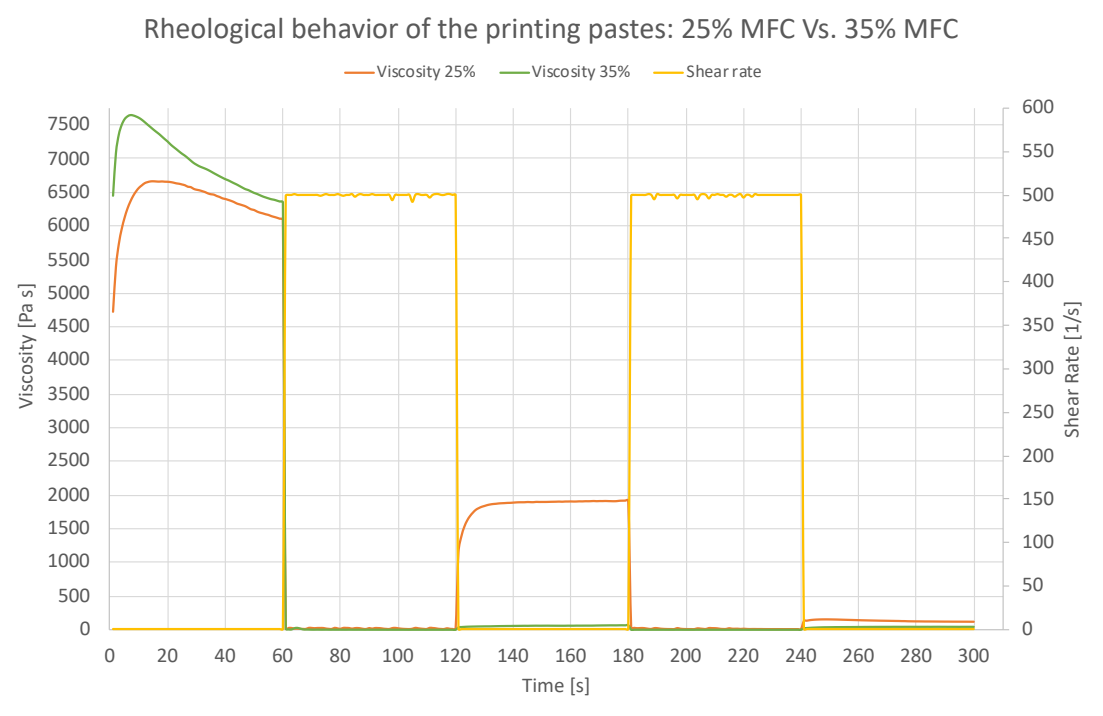

Figure 3.16: Tests of the ability of the printing pastes of recovering their viscosity after being subjected to a certain shearing.

A 3D printing test was tried with the paste at 35% wt of MFC content and no clogging of the nozzle was observed during the entire process, meaning that the use of the three-roll milling machine allows to achieve a degree of dispersion of the micro-fibrils inside the resin sufficient for this printing conditions.

Fig. 3.17 shows an extruded filament which appears to maintain well its shape, without any apparent swelling; this means that the stress state in it is below the so called “yield stress”, namely that any irreversible deformation occurred, and the filament behaves like an elastic solid (Thibaut et al., 2019). A reduction of the diameter is expected after an hypothetical curing because of the evaporation of water (contained both in the MFCs and in the PFA resin), but a measure is needed to state how much it could decrease.

The cube in Fig. 3.18 doesn’t show a well-defined shape. In particular, the appearance of the first layers can be due to an overflowing of material during the extrusion because of a maybe excessive pneumatic pressure of 4 bar imposed to push the paste through the syringe. Indeed, decreasing it to 2 bar could have improved the aspect of the last two printed layers, but, producing a lower flow rate, it could also have caused the breaking of the filament that can be noticed in Fig. 3.18b (Thibaut et al., 2019); an intermediate value of 3 bar should be tried. Furthermore, the distance of the nozzle from the worktop was not enough, since it pressed the filaments on the underneath layer while printing them and repeatedly touched the just extruded filament while printing the subsequent.

Moreover, the printing speed of 500 mm/min could have been too high: printing at lower velocity can allow a better settlement of the filament and adherence to the layer below, before the deposition of new material.

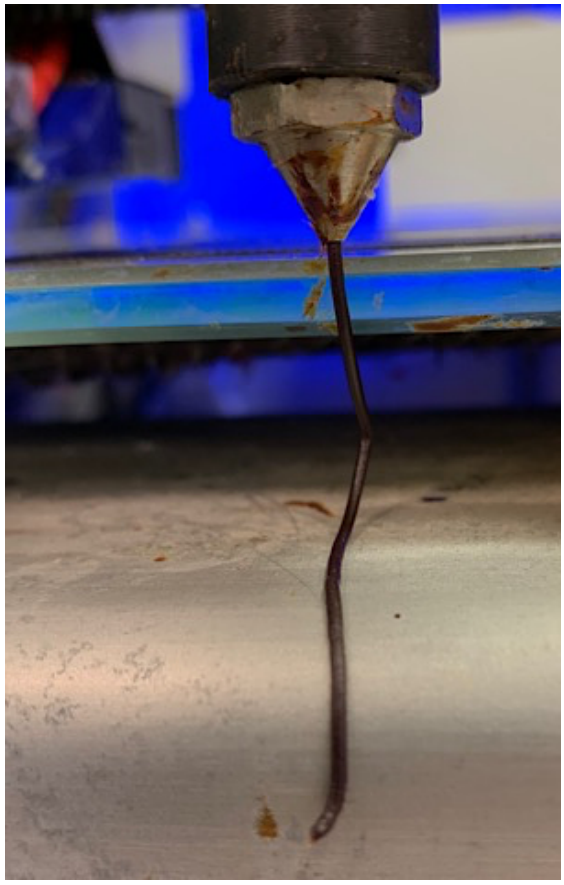

Figure 3.17: Printing of a filament of the paste containing 35% wt of MFC.

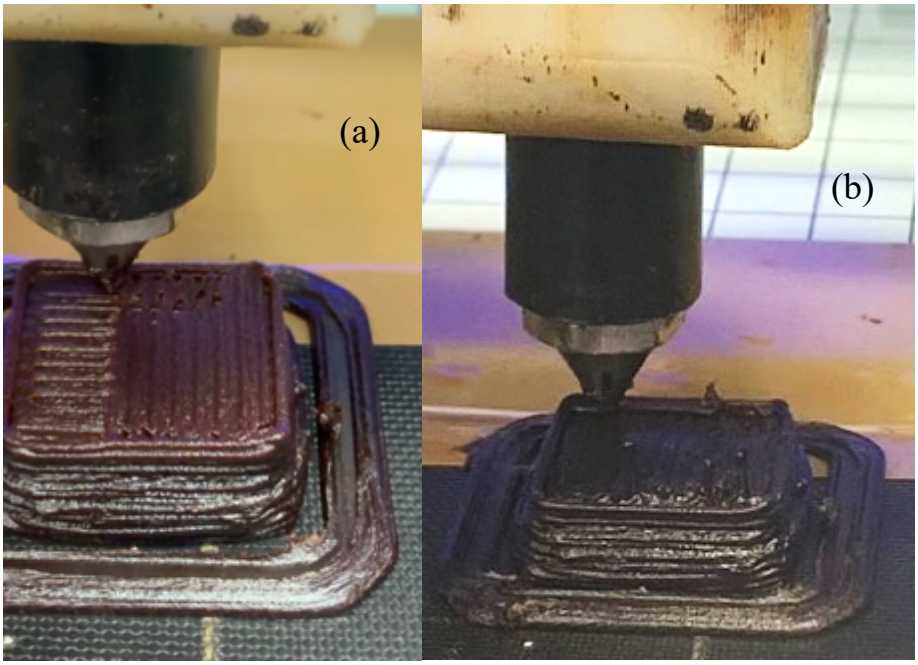

Figure 3.18: Printing of a 2cm x 2cm cube, the main problems are illustrated: deformation of the layers caused by the nozzle touching the filaments (a) and breakage of a printed filament (b).

After the first breaking of the filament, the (orthogonal) deposition of the others upon that was problematic and led to some instability in the structure, which although didn't collapse. However, it was not possible to cure the cube and so obtaining a resulting solid object because of an unexpected interruption of the work (closure of the laboratories for sanitary emergency, Covid-19).

Since the composite was not cured, the resulting mechanical properties could not be investigated. Anyway the pure PFA matrix is supposed to be quite weak, with values of the Young's modulus reported in the literature barely higher than 2 GPa (Deka et al., 2013; Linganiso et al., 2014), therefore an improving of the strength is expected with the addition of MFC. Moreover, it must be considered that the rheological characteristics of the resin (already discussed in this work) don't allow the 3D printing of an object by DIW, so the addition of a rheology modifier is necessary. The substances commonly employed to fulfill this goal are usually just powders, the presence of which in the matrix doesn't improve its mechanical properties, but makes them worse; that is also why the use of MFCs is encouraging.

It is also important to underline that the elastic modulus of the single microfibrils is generally much higher compared to the one of the films produced with MFC: the first value can be between 120 and 200 GPa (Biron, 2017; Iwamoto et al., 2009), while the second one usually is not much higher than 20-21 GPa, even for the MFC produced with the Masuko's grinder (Rol et al., 2017). Therefore, the values of the mechanical properties reported in Tab. 3.4 for the hemp nanopapers cannot be considered as representative of the strength of the single microfibrils, which should be evaluated by the help of other techniques (Iwamoto et al., 2009).

It is so clear why not even a theoretical estimation of the Young's modulus of the final composite, for example based on the weighted average of the ones of the two components, could be provided. Furthermore, the printing process should produce an alignment of the

fibrils caused by the extrusion through the nozzle (Wang et al., 2018), and the mechanical properties are expected to be higher if the direction of traction is parallel to their orientation: in fact the elements perpendicular to the charge direction are not load-bearing in the composite structure (Ramamoorthy et al., 2019). So, the way the filaments and the layers are printed can influence the resulting mechanical properties of the final object, and these could be higher than the ones of an hypothetical just casted sample (so certainly also than the theoretical predicted values). On the contrary, either a not sufficient dispersion of the MFC agglomerates inside the paste or a very weak interfacial adhesion between the microfibrils and the matrix could lead to actual mechanical properties poorer than the theoretical ones. In fact, if the cited interface is too weak, this will tend to break very soon, before the stress is even transferred to the nanofibers (Pin et al., 2014).

4 Conclusions

The final objective of the present work was the mechanical characterization of the produced composite, with the aim of evaluating to what extent hemp MFCs can reinforce the PFA matrix: as already explained, this last step was not taken.

Nevertheless, different goals were achieved throughout the research, even if additional work is required to perfect the results.

Indeed, an highly concentrated (>30% wt) and good quality MFC was successfully produced with the use of a low energy consuming method (i.e. Twin-Screw Extrusion): this is promising in the perspective of a diffused industrial-scale production of MFC, which has not been achieved yet.

Moreover, the use of hemp as starting pulp is interesting in terms of the possible mechanical properties of the resulting MFC as well as in terms of sustainability and costs of the plant cultivation.

Despite this, further studies are required to find the most suitable screws' profile and operative parameters for the extrusion of the selected pulp. Indeed, more experiments are needed to evaluate the perfect amount of energy to be provided to the chosen pulp, sufficient to fulfill its fibrillation, but not so high to damage the crystallinity of the fibers. Then, the use of a flow simulation software (Rol et al., 2020) could be a powerful resource in the estimation of the best profile able to provide, with only one pass through the extruder, the desired amount of energy. In fact, the improvement of the quality of the produced MFC after a second pass through the extruder suggests that the profile developed in the present work is not capable to complete the fibrillation process with only one pass, and there is no evidence that this goal was accomplished neither with the second one. Designing the required profile with the help of a simulation software can finally allow to obtain the best possible quality of MFC from the pulp, with also the advantage of an high productivity and a low SME consumption (because in that way we could both avoid to supply any excess of energy and to perform more than one pass).

Concerning the printing paste, even if the three-roll milling method apparently gave good results in terms of dispersion of the microfibrils inside the PFA, this additional step of processing could be avoided with the direct injection of the resin inside the extruder. This injection is allowed by the equipment used in the present work, and should be provided in a specific part of the extruder (probably its last section) in order to not affect the fibrillation of the pulp and resulting, at the same time, in a good mixing of the two components. By the way, this procedure should be tested to decide its feasibility and additional work would be needed to find the most adequate extrusion parameters, taking into account the presence of the resin.

Furthermore, a proper rheological test should be carried out in order to evaluate the actual capability of the paste of recovering its viscosity after being subjected to a certain shear rate. In particular, when applying a step-shaped shear variation, longer intervals of shearing and resting are necessary to make the test trustable. Then, knowing how long does it truly take for the paste to reach its original viscosity, the most suitable printing speed could be adjusted.

Anyway, it was demonstrated that the single printed filaments maintained well their shape, revealing so that a sufficient value of viscosity was recovered just after their extrusion through the nozzle. This fact allows to state that the prepared paste (35% wt of

MFC) used for the printing test performed is absolutely printable, but obviously more printing trials are needed to find the best process parameters and so obtain a well-defined final object.

In conclusion, the results obtained so far suggest that there is not any significant obstacle which could impede the production of a fully bio-based composite made by hemp MFC and PFA. Therefore, any additional research required to perfect this goal should be carried out with the awareness that the purpose is anything but unattainable, and a future without petrol-based materials could be closer than one can imagine.

Bibliography

Alila, S., Besbes, I., Vilar, M.R., Mutjé, P., Boufi, S., 2013. Ind. Crops Prod. 41, 250–259.

Bartalev, S., Ershov, D., Loupian, E., Tolpin, V., 2013. Web-service VEGA for operational satellite monitoring of forest resources. pp. 15–22.

Berto, G.L., Arantes, V., 2019. Int. J. Biol. Macromol. 127, 637–648.

Bhatnagar, A., Sain, M., 2005. J. Reinf. Plast. Compos. 24, 1259–1268.

Biron, M., 2017. 6 - Renewable Alloys, Compounds, Composites, and Additives, in: Biron, M.B.T.-I.A. of R.P. (Ed.), Plastics Design Library. William Andrew Publishing, pp. 371–436.

Chinga-Carrasco, G., 2013. Micron 48, 42–48.

Crossley, R.J., Schubel, P.J., Stevenson, A., Moreira, M., 2012. ECCM 2012 - Compos. Venice, Proc. 15th Eur. Conf. Compos. Mater. 24–28.

Dai, L., Cheng, T., Duan, C., Zhao, W., Zhang, W., Zou, X., Aspler, J., Ni, Y., 2019. 3D printing using plant-derived cellulose and its derivatives: A review. Carbohydr. Polym.

Davis, A.Y., Zhang, Q., Wong, J.P.S., Weber, R.J., Black, M.S., 2019. Build. Environ. 160, 106209.

Deka, H., Misra, M., Mohanty, A., 2013. Ind. Crops Prod. 41, 94–101.

European Industrial Hemp Association, 2017. Yearly average prices of technical flax and hemp short fibres 2003-2017.

Fischer, W.J., Mayr, M., Spirk, S., Reishofer, D., Jagiello, L.A., Schmiedt, R., Colson, J., Zankel, A., Bauer, W., 2017. Polymers (Basel). 9.

Guigo, N., Mija, A., Vincent, L., Sbirrazzuoli, N., 2010. Eur. Polym. J. 46, 1016–1023.

Guvendiren, M., Molde, J., Soares, R.M.D., Kohn, J., 2016. ACS Biomater. Sci. Eng.

Van Hai, L., Park, H.J., Seo, Y.B., 2013. Palpu Chongi Gisul/Journal Korea Tech. Assoc. Pulp Pap. Ind. 45, 27–33.

Håkansson, K.M.O., Henriksson, I.C., de la Peña Vázquez, C., Kuzmenko, V., Markstedt, K., Enoksson, P., Gatenholm, P., 2016. Adv. Mater. Technol. 1, 1600096.

Heiskanen, I., Backfolk, K., Vehviläinen, M., Kamppuri, T., Nousiainen, P., 2012a. Process for producing microfibrillated cellulose.

Heiskanen, I., Harlin, A., Backfolk, K., Laitinen, R., 2012b. Process for the production of microfibrillated cellulose in an extruder and microfibrillated cellulose produced according to the process.

Ho, T.T.T., Abe, K., Zimmermann, T., Yano, H., 2015. Cellulose 22, 421–433.

Hull, C.W., 1984. Apparatus for production of three-dimensional objects by sterolithography.

Iwamoto, S., Kai, W., Isogai, A., Iwata, T., 2009. Biomacromolecules 10, 2571–2576.

Kaczmar, J.W., Pach, J., Burgstaller, C., 2011. Polimery/Polymers 56, 817–822.

Kukle, S., Gravitis, J., Grave, L., 2013. Conf. Pap. Mater. Sci. 2013, 1–5.

Linganiso, L.Z., Kumar, R., Anandjiwala, R.D., 2014. J. Biobased Mater. Bioenergy 8, 299–

307.

Machado, G., Leon, S., Santos, F., Lourega, R., Dullius, J., Mollmann, M.E., Eichler, P., 2016. Nat. Resour. 07, 115–129.

Markstedt, K., Mantas, A., Tournier, I., Martínez Ávila, H., Hägg, D., Gatenholm, P., 2015. Biomacromolecules 16, 1489–1496.

Marrot, L., Lefeuvre, A., Pontoire, B., Bourmaud, A., Baley, C., 2013. Ind. Crops Prod. 51, 317–327.

Martoïa, F., Perge, C., Dumont, P.J.J., Orgéas, L., Fardin, M.A., Manneville, S., Belgacem, M.N., 2015. Soft Matter 11, 4742–4755.

Missoum, K., Belgacem, M.N., Bras, J., 2013. Materials (Basel). 6, 1745–1766.

Morais, F.P., Bértolo, R.A.C., Curto, J.M.R., Amaral, M.E.C.C., Carta, A.M.M.S., Evtyugin, D. V., 2019. Mater. Lett. X 4, 100028.

Motamedian, H.R., Halilovic, A.E., Kulachenko, A., 2019. Cellulose 26, 4099–4124.

Ng, L.W.T., Zhu, X., Hu, G., Macadam, N., Um, D., Wu, T.C., Le Moal, F., Jones, C., Hasan, T., 2019. Adv. Funct. Mater. 29.

nova-Institut, 2019. European Production of Biocomposites.

Odabas, N., Henniges, U., Potthast, A., Rosenau, T., 2016. Prog. Mater. Sci. 83, 574–594.

Pacaphol, K., Aht-Ong, D., 2017. J. Clean. Prod. 142, 1283–1295.

Partanen, A., Carus, M., 2019. Reinf. Plast. 63, 317–321.

Pereira, P.H.F., De Freitas Rosa, M., Cioffi, M.O.H., De Carvalho Benini, K.C.C., Milanese, A.C., Voorwald, H.J.C., Mulinari, D.R., 2015. Polimeros 25, 9–22.

Perez, R.F., Fraga, M.A., 2014. Green Chem. 16, 3942–3950.

Pin, J.M., Guigo, N., Mija, A., Vincent, L., Sbirrazzuoli, N., Van Der Waal, J.C., De Jong, E., 2014. ACS Sustain. Chem. Eng. 2, 2182–2190.

Pohl, T., Bierer, M., Natter, E., Madsen, B., Hoydonckx, H., Schledjewski, R., 2011. Plast. Rubber Compos. 40, 294–299.

Pranger, L., Tannenbaum, R., 2008. Macromolecules 41, 8682–8687.

Ramamoorthy, S.K., Åkesson, D., Rajan, R., Periyasamy, A.P., Skrifvars, M., 2019. 14 - Mechanical performance of biofibers and their corresponding composites, in: Jawaid, M., Thariq, M., Saba Fibre-Reinforced Composites and Hybrid Composites, N.B.T.-M. and P.T. of B. (Eds.), Woodhead Publishing Series in Composites Science and Engineering. Woodhead Publishing, pp. 259–292.

Rol, F., Belgacem, M.N., Gandini, A., Bras, J., 2019. Prog. Polym. Sci. 88, 241–264.

Rol, F., Karakashov, B., Nechyporchuk, O., Terrien, M., Meyer, V., Dufresne, A., Belgacem, M.N., Bras, J., 2017. ACS Sustain. Chem. Eng. 5, 6524–6531.

Rol, F., Petit-conil, M., Banvillet, G., Meyer, V., Bras, J., 2018. J. Mater. Sci. 53, 12604–12615.

Rol, F., Vergnes, B., Kissi, N., Bras, J., 2020. ACS Sustain. Chem. Eng. 8, 50–59.

Schenker, M., Schoelkopf, J., Gane, P., Mangin, P., 2018. Cellulose 25, 961–976.

Siqueira, G., Bras, J., Dufresne, A., 2010. Polymers (Basel). 2, 728–765.

Siró, I., Plackett, D., 2010. Cellulose 17, 459–494.

Stephens, B., Azimi, P., El Orch, Z., Ramos, T., 2013. Atmos. Environ. 79, 334–339.

Terinte, N., Ibbett, R., Schuster, K.C., 2011. Lenzinger Berichte 89, 118–131.

Thibaut, C., Denneulin, A., Du Roscoat, S.R., Beneventi, D., Orgéas, L., Chaussy, D., 2019. Carbohydr. Polym. 212, 119–128.

Turbak, A.F., Snyder, F.W., Sandberg, K.R., 1983. Microfibrillated cellulose. 4,374,702.

Unwin, J., Coldwell, M.R., Keen, C., McAlinden, J.J., 2013. Ann. Occup. Hyg. 57, 399–406.

Vartiainen, J., Lahtinen, P., Kaljunen, T., Kunnari, V., Peresin, M.S., Tammelin, T., 2015. O Pap. 76, 57–60.

Voet, V.S.D., Strating, T., Schnelting, G.H.M., Dijkstra, P., Tietema, M., Xu, J., Woortman, A.J.J., Loos, K., Jager, J., Folkersma, R., 2018. ACS Omega 3, 1403–1408.

Wang, B., Sain, M., Oksman, K., 2007. Appl. Compos. Mater. 14, 89–103.

Wang, Q., Sun, J., Yao, Q., Ji, C., Liu, J., Zhu, Q., 2018. Cellulose 25, 4275–4301.

Xu, W., Wang, X., Sandler, N., Willför, S., Xu, C., 2018. Three-Dimensional Printing of Wood-Derived Biopolymers: A Review Focused on Biomedical Applications. ACS Sustain. Chem. Eng.